Numerical modeling of settlement and deformation behavior of wooden pile reinforced railway embankments on peat foundation soils

Sandra Abena Agyeiwaa

A Thesis

In

The Department

of

Building, Civil, and Environment Engineering

Presented in Partial Fulfillment of the Requirements

for the Degree of Master of Applied Science (Geotechnical Engineering) at

Concordia University

Montréal, Québec, Canada

July 2023

CONCORDIA UNIVERSITY

School of Graduate Studies

This is to certify that the thesis prepared

By: Sandra Abena Agyeiwaa

Entitled: Numerical modeling of settlement and deformation behavior of wooden pile reinforced railway embankments on peat foundation soils

and submitted in partial fulfillment of the requirements for the degree of

Master of Applied Science (Civil Engineering)

complies with the regulations of the University and meets the accepted standards with respect to originality and quality.

Signed by the final Examining Committee:

_____ Chair

Dr. Ciprian Alecsandru

_____ Examiner

Dr. B. Li

_____ Examiner

Dr. Ciprian Alecsandru

_____ Supervisor

Dr. A. M. Zsaki

Approved by _____

Dr. S. Samuel Li Chair of the Department

_____ 2023 _____

Dean of Faculty *Dr. M. Debbabi*

ABSTRACT

Numerical modeling of settlement and deformation behavior of wooden pile reinforced railway embankments on peat foundation soils

Sandra Abena Agyeiwaa

A number of rail embankments in Canada are constructed on land surfaces covered by organic soils such as peat. Peat soils are known to exhibit enormous deformation potential owing to their excessive water content with low strength. Because of this, railway embankments built on peat experience reoccurring problems of settlement and deformation. Consequently, this increases the cost of maintenance and impedes the safety and stability of a slope under moving freight train conditions. Thus, to stabilize the peat under the railway embankment, this research modeled the behavior and evaluated the effectiveness of driven wooden piles as a method of stabilization. Employing the finite element shear strength reduction (FE-SSR) method, the development of excess pore water pressure and settlement of 2-dimensional models are investigated thoroughly. Using the Biot's consolidation theory, a coupled model providing an in-depth understanding of the mechanism of development of excess pore water pressure and stress essential for understanding the development of settlements is considered. Key factors such as geometric characteristics of the slope, wooden piles (length, diameter, and spacing), and freight train speeds were conducted through a series of parametric studies to ascertain their effects on embankment failure. A sensitivity analysis was introduced to individually investigate each parameter of the wooden piles and its effect on slope stability. Adopting a minimum factor of safety of 1.3, slopes with different geometric parameters and wooden piles, and maximum safe train speed is required to ensure the adequate performance of slopes considering the high compressibility nature of peat. The results illustrate that a slope with 2H:1V slope inclination exhibits a larger degree of settlement and deformation and a considerable increase in pore water pressure under a high-speed train load. Details of the maximum allowable speed a train can use, given the geometric parameters of the slope, railway embankment height, and wooden piles are finally presented in this study for safe freight train performance.

ACKNOWLEDGEMENT

My sincere thanks go to God almighty who makes everything possible. I would like to express my deep gratitude to my supervisor, Dr. Attila Michael Zsaki, for his support, patience, and the opportunity to join his group. His professional guidance helped me finish my research project to fulfill my study aim. I cannot say thank you enough for his tremendous help.

I am also very grateful for the help provided by Dr. Reginald Hammah for his encouragement and advice to advance in my academic and professional career. This work would not be possible without the endless love and support both in the study and life of my husband, Kwabena Ofori. My gratitude also goes to my family for their firm support.

Finally, I would like to acknowledge the financial support that was provided by Dr. Attila Michael Zsaki through ENCS/GCS FRS fund to help me successfully complete the research work.

Table of Contents

List of Tables

List of Figures

List of Symbols

ap	=	unit toe resistance of pile
A	=	bearing area of cross tie (in.^{2}) or (mm^2)
ABP	=	average ballast pressure (psi) or (MPa)
$A\mathrm{S_i}$	=	area of pile segment
c	=	cohesion (kPa)
D	=	wheel diameter (in.) or (mm)
D_{bs}	=	distance along ballast surface from center line
DF	=	distribution factor of axle load carried by a single tie (%)
D_F	=	differences in FS value
$\mathrm{D_s}$	=	design speed
d	=	assumed pile length (m)
E	=	Young's modulus (MPa)
$\mathrm{E_L}$	=	embankment load
e	=	void ratio
FS	=	factor of safety
IF	=	impact factor (%)
k	=	hydraulic conductivity (cm/s)
k_{s}	=	earth pressure coefficient
$\mathrm{L_e}$	=	effective pile length (m)
L_{o}	=	influence length of an axle load or adjacent axle loads (km)
P	=	applied load (kN) or (lbf)
Q_{s}	=	sum of skin friction
S	=	pile center to center distance
$\mathrm{S_T}$	=	settlement of ballasted track on soft soil
u	=	pore pressure
V	=	train speed (km/h) or (mph)
ν	=	Poisson's ratio

γ	=	unit weight of material (kN/m^3) or (kg/ m^3)
ϕ	=	friction angle (°)
σ	=	normal stress (kPa)
σ'	=	effective stress (kPa)
σ	=	inner stress (kN/m^2) or (kPa)
τ	=	shear strength (kPa)

CHAPTER 1 INTRODUCTION

1.0 Background of the Study

The economic growth of every country is irreplaceably connected to its transportation system even in advanced economies (Trimbath 2010). Transportation Infrastructure plays a key role in socio-economic development, therefore, making it a fundamental pillar in globalization because of its intensive use of infrastructure.

Being one of the safest, most dependable yet affordable modes of transport, railway transport continuously experiences increasing demand in its operation. To perform this purpose efficiently, there is a need for improvement in its construction and maintenance techniques. In light of this, more emphasis should be placed on their overall stability, maintenance, and serviceability during the design and construction phase of rail lines to meet up with recent technical standards.

Design as well as the construction of the railway track and foundation will consider structural performance, environmental conditions, and geotechnical challenges among others. The main geotechnical set-backs with regard to safety requirements, loading conditions, and geometry of railway embankments, in addition to the scope of geotechnical investigation needed to make a well-informed recommendation on a final design guide (Bogusz and Godlewski 2019).

Recent modernization and development in railway infrastructure construction require the need to understand slope stability and foundation settlement. This will eliminate or minimize deterioration and failure of railway embarkment to meet standardized design with prolonged serviceability of rail tracks. Skempton (1996), reports that embankment failures happened both during and shortly after embankment construction in the course of railways expansions in the 1800s. Taking this into account, the prerequisites to be factored in when building a permanent way will include estimating the magnitude of settlement, evaluation of slope stability, ballast performance, suitable materials to use in construction, rail geometry, and maximum axle load capacity.

In as much as rail tracks are most often laid in meandering routes in rocky and mountainous topography, these routes may be located within undesirable soft and organic soils such as peat. Several challenges associated with permanent ways situated in deposits of weak soils adversely affect the shear strength of the soil causing progressive foundation failure. It is therefore

appropriate to appreciate and acknowledge the dynamic response and settlement behavior of compressible soils. Soil improvement or stabilization is a necessary technique to employ in mitigating failure and excessively large settlements due to embankment construction.

1.1 Problem Statement

In recent years, attempts to stabilize excessive and differential settlement of structures in organic soils have intensified, however, deformational obstacles persist (Wheeler et al. 2016). It is recognized that the predominant geotechnical features to be considered prior to, during, and after the construction of earth structures are soil settlement, bearing capacity of the soil, and slope stability.

Soil settlement is in three phases comprising; immediate, primary and secondary settlement with organic soils displaying a significant amount of secondary settlement through creep due to the high amount of organic content. Organic soils generally do not exhibit reliable engineering properties and often have poor drainage which tends to be unstable. Peats are organic soils that show varying compressible behavior as compared with other types of soils in two ways. First, the compression of peat is much more extensive than that of other soils. Second, the creep portion of settlement plays a more significant role in predicting the total settlement of peat than of other soil types (Kazemian et al. 2004).

Peatland covers approximately 13% of the land mass of Canada (Peat Moss Associations in Canada 2020) thereby hosting a majority of peatland worldwide. The most extensive Canadian peatland is located in the northern area even though they exist in all provinces. However, significant deposits occur in the Atlantic provinces, southern Québec, Ontario, and Manitoba. Railway tracks over peat subgrades can experience large ground deformations, increased pore-water pressures, formation of pumping holes, and pumping of fines during the passage of trains, which can lead to accelerated track deterioration and risk of derailment (Wheeler et al. 2016).

The construction or modernization of a railway line requires a risk assessment and consideration of possible issues in a design (Bogusz and Godlewski 2019). Again, Bogusz and Godlewski (2019), recommend that in regard to geotechnical engineering, these issues are mostly: the stability of embankments and the prediction of settlement of railway tracks. According to Zien and Elgasim (2014), the design and building of high embankments set up on weak and compressible soils i.e., low shear strength and excessively large settlements creates a number of problems in relation to

their safety and stability. Instability results when the shear strength of soil is not sufficient to support the loads applied to it. Embankment deformation is also attributed to excess moisture in subgrade soil and the development of ballast pockets. Briggs et al. (2017) affirm that the construction of primitive railway embankments was empirical and was not modeled to suit present-day soil mechanics concepts (Harrison 1881).

In view of the aforementioned shortcomings in railway embankments on peatlands associated with settlement and deformation, this research seeks to explore the suitability and effectiveness of the use of wooden piles as a method of stabilization of peat under railway embankments.

1.2 Research Hypothesis

The key hypotheses of the research are:

- Peats are labeled as geotechnically problematic soils which show high compressibility as well as low shear strength that contributes to the poor performance of structures constructed over them.
- Suitable ground improvement technique adopted to stabilize flexible soils relies on the vertical and lateral extent of soil, cost, and practicality of the method, structure to be built, availability of stabilizing material to be used, and effectiveness of the technique.
- The mode of failure for railway embankments is dependent on construction material, construction method, and subgrade material.
- Considering the compressibility of the solid phase and the existence of the gas phase as well as the development of pore water content, it will be appropriate to use Biot's three – dimensional consolidation theory to model the deformation behavior of peat.

1.3 The Objective of the Research

The main aim of the proposed research is to model the behavior and evaluate the effectiveness of driven wooden piles under railway embankments. The shortcomings associated with the settlement and deformation behavior of wooden pile-supported railway embankments on peat foundation

soils will be identified for continuous and future improvements. However, the objectives of the proposed study seek to:

- Recap the use of the finite element method to model the organic foundation for peat soil, embankment, and wooden piles.
- Discover the main causes of slope and foundation failure under the railway embankment.
- Unveil guidelines derived for the maximum allowable train speed as a function of the settlement and consolidation process.
- Application of the worst drainage conditions (undrained conditions) for coupled (groundwater flow and stress) analysis on slope stability and summarize its performance and key trends.
- Recommend practical standards and measures for the construction of an effective and efficient railway system in peatlands with respect to the number and location of wooden piling to be installed.
- Assess the effectiveness of wooden piles as a function of controlling settlement of the rail, particularly in the light of increased loading due to extra tonnage hauled by the modern railways

1.4 Methods of the Analysis

This thesis adopts assumptions, and model parameters together with the methodology that represents the majority of situations in attaining justifiable research. In summary, the assumptions methodology that is set up and considered in the model consists of:

1. The use of Rocscience's RS2 (Rocscience Inc. 2019) to simulate a two-dimensional finite element method (FEM) based model.
   Model parameters (such as the dimension of railway embankments, slope inclination ratios, soil properties, loading due to trains, etc.) that govern the model's behavior are compiled to develop representative models. This is followed by conducting a set of parametric studies with the RS2 software.

2. Parametric study

   Three scenarios that entail a parametric study of the influence parameters will be investigated. This considers an assumed 3 horizontal to 1 vertical and 2 horizontal to 1 vertical slope inclination railway embankment. The first scenario studies the behavior of an embankment slope without piles constructed on an organic soft peat foundation. Scenario two looks into the effect of supporting the embankment with wooden piles. To derive the allowable maximum safe train for safe performance on the rail, scenario three examines the influence of moving train load condition.

3. Analysis of FEM models

   The method of analysis used in evaluating the effectiveness of wooden piles under railway embankments as a function of determining the maximum allowable train speed on a stable slope is the finite element shear strength reduction (SSR-FEM) method. Additionally, a coupled model using Biot's consolidation theory will be considered to assess the development of pore water pressure and stress.

1.5 Purpose of the Study

The objectives outlined in this research are intended to emphasize reoccurring slope and foundation failure under railway embankments in Canadian peatlands. Compared with other soils, peat is known to have low strength, excessive water content, and a high potential for deformation when subjected to structural loading. The purpose of this research is, therefore, to contribute to a blueprint for further investigation with the prospect of improving the settlement behavior of wooden piles in a peat environment.

1.6 Significance of the Research

The importance of this research work is attributed to its findings and recommendations. This will add to the already existing knowledge on foundation instability as well as slope stability using analysis and validation of FEM models to predict organic soil settlement under railway

embankments. This contributes to understanding the load transfer mechanism from rails to ties, from ties to ballast, sub-ballast, and subgrade to determine the load due to passing trains.

1.7 Structure of the Thesis

This research thesis is organized into six chapters and described as follows:

Chapter 1 presents a general overview of the whole study. It entails background information identifying the need for the research. The chapter clearly defines the research knowledge gap to be addressed, a set of objectives, and the purpose of the study. The hypothesis, scope, and significance of the research are also highlighted in this chapter.

Chapter 2 reviews previous and recent literature on slope stability using the Limit Equilibrium Method (LEM), slope stability using FEM (using the Shear Strength Reduction concept), foundation instability under embankments (bearing capacity) using FEM, and settlement (consolidation) of soils - organic soils, in particular, using FEM in railway construction. Within this chapter are appraisals on the load due to passing trains, using wooden piles as foundation support was analyzed based on numerical modeling using FEM.

Chapter 3 explains the research methodology adopted and explicitly details the significance of the methodology used, the parameters, the models created with FEM, the choice of software used, and the tested hypotheses.

Chapter 4 presents the creation of the numerical models used for the studies.

Chapter 5 discusses the data analysis, findings, results, and presentation.

Chapter 6, the final chapter is made of conclusions deduced from the study. The summary and recommendations are also stated in this chapter

CHAPTER 2 LITERATURE REVIEW

2.0 Introduction

Within this chapter are reviews of some existing, published, and unpublished available literature on theoretical and empirical modeling of railway embankments on peat soil with an emphasis on slope stability using the LEM / FEM. Salient areas such as foundation instability under embankments (bearing capacity) using FEM are also addressed in this context.

The challenges associated with the construction and settlement of civil engineering structures on peatlands are further discussed in this chapter. Within this section are themes concerning the consolidation of soils, particularly organic soils - using the FEM. Furthermore, load due to train traffic, load transfer mechanisms from rails to ties, from ties to ballast, sub-ballast, and subgrade are also scripted.

2.1 Peatlands and Peats Soils

Soils with a high content of organic matter such as decaying or decayed living matter that contains carbon and inorganic minerals are defined as organic soils. According to Kroetsch et al. (2011), the Canadian System of Soil Classification categorizes wetland and upland organic soils into an organic order which comprises soils that progressively grew from materials that mainly consist of accumulated remnants of plant tissues. Organic soil is usually referred to as “peat,” if fibrous plant residues are still conspicuous (Galloway et al. 1999).

Peat is a kind of special soil material rich in organic matter, usually more than 75%, and therefore requires a better understanding of its geotechnical responses due to its problematic nature. The Canadian Wildlife Federation identifies three types of peatlands: fens, bogs, and swamps with mostly fens and bogs dominating Canadian wetlands. Except for deserts and the arctic region (Deboucha et al. 2008), they are notably found in various parts of the world.

In Canada, about 76% of the wetland is classified as peatland with these zones dominating the boreal region, Prairie Provinces, and Hudson Plains according to the Canadian System of Soil Classification (CSSC). Again, every province in Canada has wetland organic soils which are generally noted as (unfrozen) peatland soils. Figure 2.1 depicts a schematic view of the location of peats in Canada.

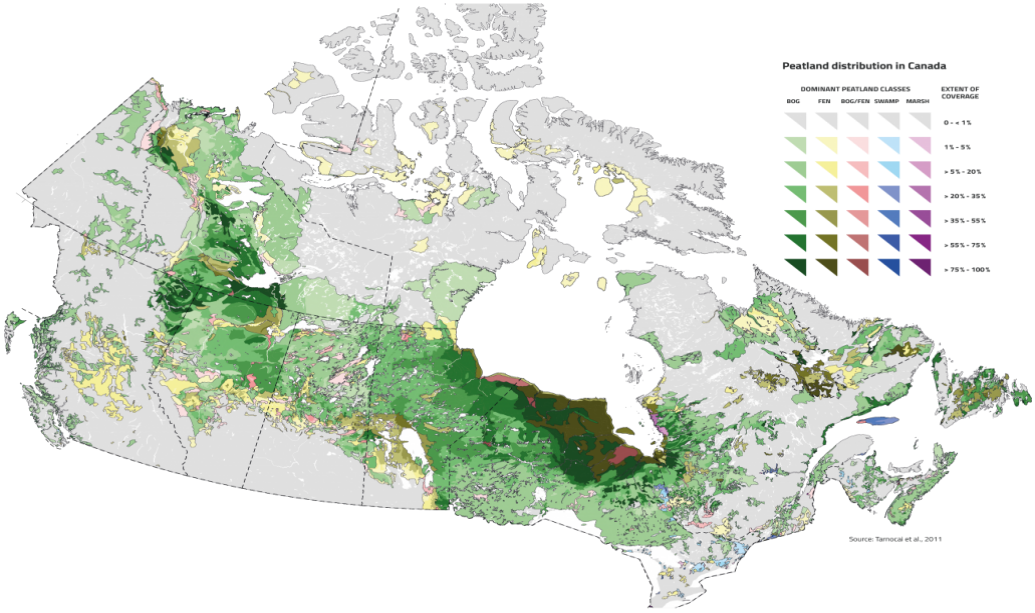

Figure 2.1. Distribution of Canadian Peatland (Canadian Sphagnum Peat Moss Association (CSPMA) 2011)

2.1.1 Properties of Peat

Peat soils are uniquely visually recognized due to their dark brown to black color and accompanying organic odor. Osman (2017) states that many peat soils are submerged as well as vulnerable to subsidence. Tagged as geotechnically troublesome soils, peats show certain unique characteristics that distinguish them from other organic soils thereby requiring special considerations for construction over them. In connection with geotechnical engineering practices, peat is undoubtedly designated as a material with high compressibility and low bearing capacity and therefore regarded as undesirable as a foundation material suitable for construction work (Zainorabidan and Wijeyesekera 2008). An entry point knowledge of the physio-chemical and mechanical properties of peat is essential in assessing its suitability for the construction of engineering structures.

2.1.1.1 Physiochemical Properties of Peat Soil

Physical and hydraulic properties reveal the physio-chemical properties and characteristics of peat. Kalantari (2013) urges engineers to the Von post field system of peat classification which groups peat materials on their level of decomposition. The higher the organic content of the peat soil, the

higher the water content, compressibility, permeability, and void ratio. It is known that peats have high water retaining capacity and this is exhibited more in fibrous peat as compared to granular peat.

Rezanezhad et al. (2016) explain that the movement and retention of water are closely related to the physical properties of peat, and consequently to the degree of decomposition and soil compaction. Osman (2017) documented those peats located in the Northern Hemisphere display a characteristic increase in the rate of decay with a decrease in water content.

2.1.1.2 Engineering Properties of Peat

Peat is mainly characterized by portraying low stability, and low bearing capacity partly due to high water table and high compressibility, adversely resulting in a high settlement, and low specific gravity.

In addition to the above-mentioned engineering properties, peats are known to have a low bulk density that is close to the density of water which reflects high soil porosity and compaction. The two most outstanding reasons for the growing interest in understanding and recognizing the engineering behavior of peat in Canada is a result of increased northern development which discourages the removal of extensive coverage of peaty soils due to the cost involved and urban explosion in the southern region of Canada (MacFarlane 1969).

2.1.2 Consolidation of Peat Soil

Sing et al. (2008) propose that compressibility is one of the principal mechanical properties of peat to be studied. This is because the non-negligible compressibility behavior of peat is largely due to high organic material constituent (Yang and Liu 2016). Hashim and Islam (2008) state that due to its long-term consolidation behavior, peat creates critical problems in the construction field even when a moderate load is applied. Ibrahim et al. (2014) give a compressibility range for peat as being between 0.19-1.5. Kazemian and Huat (2009) claim through observation the possible development of tertiary compression in peat after primary consolidation and secondary compression.

2.1.3 Peat as Foundational Material for Engineering Structures

The ability of soil to support load defines its bearing capacity. Johari et al. (2016) conclude by labeling peats which have a range between 5-20 kPa, as low bearing capacity. During the construction of a foundation, it is imperative to assess the underlying soil for its bearing capacity and settlement behavior. This will give an insight into the characteristics of the soil to overcome this hindrance in eliminating bearing capacity failure (Ibrahim et al. 2014). According to McHenry and Rose (2012), bearing capacity is an indicative measure of a soil's strength whereas its modulus defines its elastic deformation per applied load intensity. A survey conducted by the Transportation Safety Board of Canada (2007) showed that punching shear failure triggered derailment under the influence of axle weight, tonnage, and train speed on the track laid on a peat foundation.

2.1.4 Deformational Characteristics of Peat

Razali et al. (2013) describe peat as soil with low shear strength with values ranging between 5–20 kPa. According to Long (2005), earlier reports concluded that peat soils demonstrate cohesive shear strength nature ($\phi = 0$).

In geotechnical engineering practices, there are three components of settlement: elastic (immediate) settlement, primary consolidation settlement, and secondary consolidation settlement. It has been analyzed that, there will be variations in the amount of primary consolidation in peat at various locations but most often, there is an overall estimation of 50 percent settlement with regard to total settlement (Munro 2004). Secondary consolidation settlement often takes place in organic soils because of the adjustment of the soil fabric of grains reflecting a creep-like phenomenon.

Due to the remarkable nature of secondary consolidation on peaty grounds, it is imperative to use it in determining settlement (Hayashi et al. 2016). According to Kazemian and Mohayedi (2014), in estimating the total settlement of peat it is indispensable to factor in the creeping nature of the soil. Yang and Liu (2016) stated that when peat is compared to other standard geotechnical materials, it displays dissimilar deformational behavior due to the presence of a high amount of organic matter.

2.2 Rail Transport Systems

According to Dostál and Adamec (2011), the high capacity and speed of rail transport gives it a significant edge over other modes of transportation and is deemed the most environmentally friendly. Pyrgidis (2016) further describes its demographical competence as extensive since it can traverse across greater distances regardless of the community (urban, suburban, peri-urban, regional, and interurban) with approximate distance coverage for both passengers and freight.

2.2.1 Status Quo of the Railways of Canada

In recent times, the significant contribution of the rail sector to the Canadian economy cannot be overlooked (Railway Association of Canada 2016). Notwithstanding that, the literature reveals that most Canadian track infrastructure collapse is associated with railway embankment failure situated on glaciolacustrine peat. Since a larger fraction of Canadian rail lines were constructed during the 1800s and built along rivers or across marshy areas where peat is present, Railway Track Safety Rules (TSR) conducts frequent track inspections to better understand, identify, and remediate roadbed stability – a related risk which could cause a derailment. Most rail lines constructed on peatlands experience stability problems due to excessive deformation as peat is highly compressible and has low shear strength (De Guzman and Alfaro 2017). Due to this, safety issues and an increase in maintenance costs are of great concern. A detailed derailment analysis by the Transportation Safety Board of Canada (TSB) in 2005 following the 1999 and 2000 accidents in the marshy area of the Grande Plée Bleue, near Saint-Henri-de-Lévis near Quebec City, revealed that rail track constructed on saturated peat soils experiences exponential settlement and intensified compressibility as a result of increased cyclic loading (Transportation Safety Board of Canada 2007).

2.2.2 Engineering Construction of Rail Tracks

Transfer of static and dynamic forces from rail traffic loads takes place through a sequence of components to the foundation (Pyrgidis 2016). It becomes mandatory to take into consideration the basic design, construction, and maintenance parameters of a railway track structure which is broadly categorized into Superstructure and Substructure (Amorim Cork Composites 2018). Chakrabarti et al. (2013) present a successive component from top to bottom of the railway track architectural framework as ballast layer under sleeper, sub-ballast capping (SBC) layer, transition

layer (750mm thickness below SBC), general embankment, and prepared foundation. The track superstructure is a multi-layered system consisting of rails, sleepers, fastenings, elastic pads, ballast, and sub-ballast with its subgrade, and the formation layer being the main components of a railway track substructure (Pyrgidis 2016). Figure 2.3 presents a graphical illustration of the railway track components.

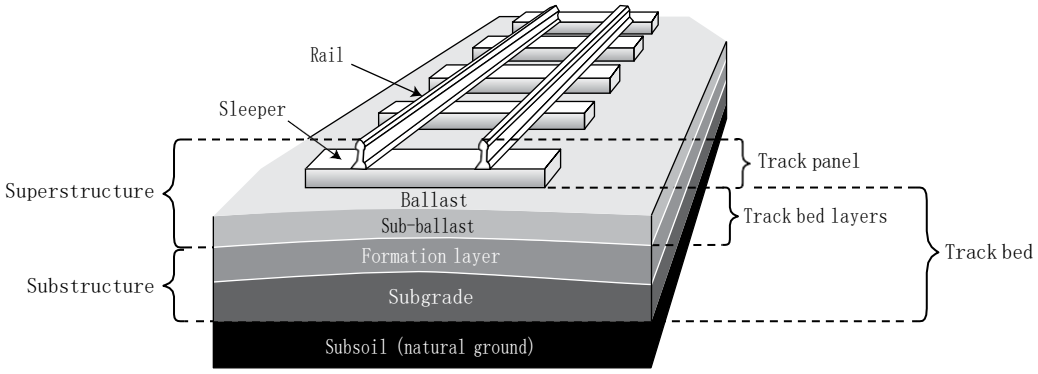

Figure 2.3. Railway Track (Pyrgidis 2016)

The ballasted track is described by the National Academies of Sciences, Engineering, and Medicine (2012) as a component of the track structure consisting of tie plates or fastenings, cross ties, and the ballast/sub-ballast bed supported on a prepared subgrade. Documentation by the Transportation Safety Board of Canada (TSB) (2007) reveals that most rail lines in Canada are ballasted track systems. This is often characterized by coarse aggregate (gravel) dominating a larger part and fine granulate (silt and sand) occupying a smaller fraction. To prevent failure of subgrade in addition to minimizing the extremely high amount of track deformity which is brought about by the continuous motion of the train's heavy axle load calls for the need to correctly design ballasted railway foundation using error-free estimation of presumed granular layer thickness (Sayeed and Shahin 2017). Sayeed and Shahin (2017) reflect on the importance to add traffic parameters such as wheel spacing, traffic tonnage, and train speed during the design method since they have a consequential impact on the track performance. Again, Doyle (1980) adduces that the strength of the individual constituent elements of the track needs to fulfill some specifications to meet up with the standard railway track design practices.

It is noted that the choice of a particular track system considers the axle loads, expected maximum speed, minimal cost involves in total service life, low maintenance cost, and the construction of tracks. Additionally, it is explained that the sleeper distributes the vertical load of the wheels in

the transversal direction of the track to the ballast. It also secures the fastening system and anchorages the superstructure to the ballast preventing lateral and longitudinal movements.

According to Anbazhagan et al. (2012), the railway track ballast is a uniformly-graded coarse granular material extracted from locally crushed rocks such as granite, limestone, or basalt which is placed above the sub-ballast and below the rails. This allows for the distribution of loads from the sleepers to the sub-ballast. A ballast additionally functions to resist lateral, vertical, and longitudinal forces enacted on the sleepers by providing stability, resilience, and energy absorption to the track. This facilitates drainage, reduces traffic-induced stresses, and enhances maintenance operations (Burrow et al. 2007). The blanket layer also called the sub-ballast is made up of adequately compacted sand and gravel that distributes the load and further serves as protection from ballast particles to the substructure's upper surface (Giannakos 2010). The subgrade forms part of the ballasted track foundation and is described as the top-most section of the earthworks on which the superstructure rests and is identified as the weakest and most inconsistent component of the track structure.

2.2.3 Deformational Phenomena of Rail Track on Peat Deposit

The two main characteristics that define railroad subgrade and soil performances are deformation and strength – expressed as a measure of bearing capacity or undrained shear strength parameters (McHenry and Rose 2012). Freitas de Cunha (2013) mentions that the differential settlement of rail is greatly influenced by the subgrade which consequently affects rail deflection and track response. Subgrade failure of a track on saturated peat areas is susceptible to shear plane failure hence developing punching failure as a result of cumulative and permanent settlement (Transportation Safety Board of Canada 2007). Figure 2.4 shows the formation of a shear plane due to the realignment of peat fibers as it distorts from developing incremental permanent settlement under the railway track. According to Esveld (2001), the greatest amount of stress within the track transpires between the rail and wheel with an estimated value equal to or greater than 30kN/cm^2. To prevent subgrade progressive shear failure and track plastic deformation, Sayeed and Shahin (2017) propose the provision of a sufficient granular thickness between the sleeper and subgrade surface. The collapse of a track on a peat deposit could be sudden as the distortion of peat fibers are difficult to observe (Transportation Safety Board 2007). A typical illustration of vertical rail track deformation on peat embankment is shown in Figure 2.5.

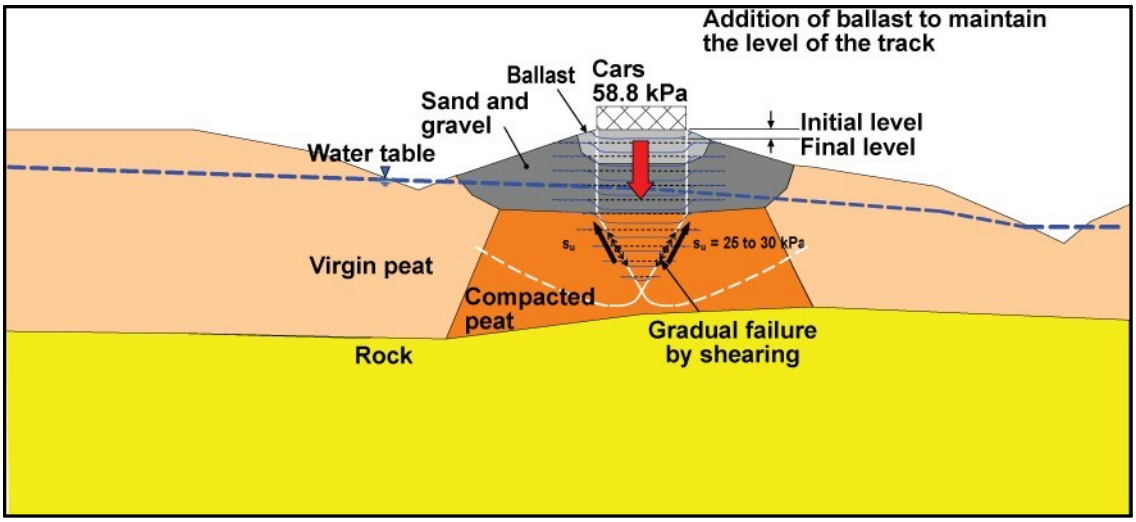

Figure 2.4. Shearing failure by punching developed as a result of increased permanent settlement due to loads from passing trains (Transportation Safety Board 2007).

Figure 2.5. Vertical deformation of railway track constructed on a highly compressible peat (De Guzman and Alfaro 2017).

Poor subgrade and drainage conditions could lead to ballast fouling, ballast pockets, pumping of soil fines through the ballast, and slope stability failure (McHenry and Rose 2012). It is recommended that to reduce track structure deformation, resilient fastenings, and compatible pads to clips should be employed during construction. Also, regular railway inspections to evaluate

track surface conditions are effective to monitor track settlement under peat deposits (Transportation Safety Board of Canada 2007).

2.3 Design and Construction of Railway Embankments on Peat Deposits

Railway traffic load, the geometry of railway embankments, and geotechnical conditions are the major influencing factor required for the design framework to guarantee the safety and reliability of a railway embankment (Bogusz and Godlewski 2019). In order to put up safe, stable, and serviceable embankments on peat lands, Munro (2004) recommends engineers overcome engineering obstacles by putting proper measures in place as well as effectively managing their engineering properties to achieve a long-term settlement. In-depth knowledge and understanding of the differences between undrained and drained conditions of the embankment material and subsoil are needed for the proper designing of the railway infrastructure, especially with the loading conditions (Bogusz and Godlewski 2019).

2.3.1 Railway Embankment Geometry

Residual deformation, settlement, and lateral displacement are usually experienced by the earthworks and ballast which adversely affects the deterioration of the geometry of the track (Giannakos 2010). The two most prominent factors that reduce riding quality and increase maintenance costs are subgrade progressive shear failure and excessive plastic deformation of the track (Sayeed and Shahin 2017). McHenry and Rose (2012) conclude that geometric complications could be directly impacted by subgrade conditions. Thus, this thesis adopts a ballasted railway track since it represents a typical North American railway system.

2.3.2 Track Drainage

Track drainage is effectuated by a surface and sub-surface drainage system. Proper drainage is essential to prevent excess water from reducing the bearing capacity and shear resistance of the formation soil. Track formation failure occurs as a result of inadequate track drainage leading to weakening and subsequent collapse when saturated. When planning the drainage system, all drains need an adequate gradient to allow the free flow of the water collected. One of the drainage problems associated with embankments is water ponding at the embankment base. This may result

in slips causing saturation of the embankment base, consequently leading to further consolidation and settlement of the embankment. The stability and longevity of a track depend primarily on the ability of water to be expelled and kept away from the track bed.

2.3.3 Load Distribution Mechanism on the Track

The train load is distributed to the track and subgrade through the contact points of the wheel and rail. Figure 2.6 shows a load transfer model that assumes the distribution of uniform vertical stress in the substructure. The effectiveness of the load transmitted to the ballast through the sleeper depends on the elasticity of the sleeper, ballast geometry as well as the degree of compaction under the sleeper.

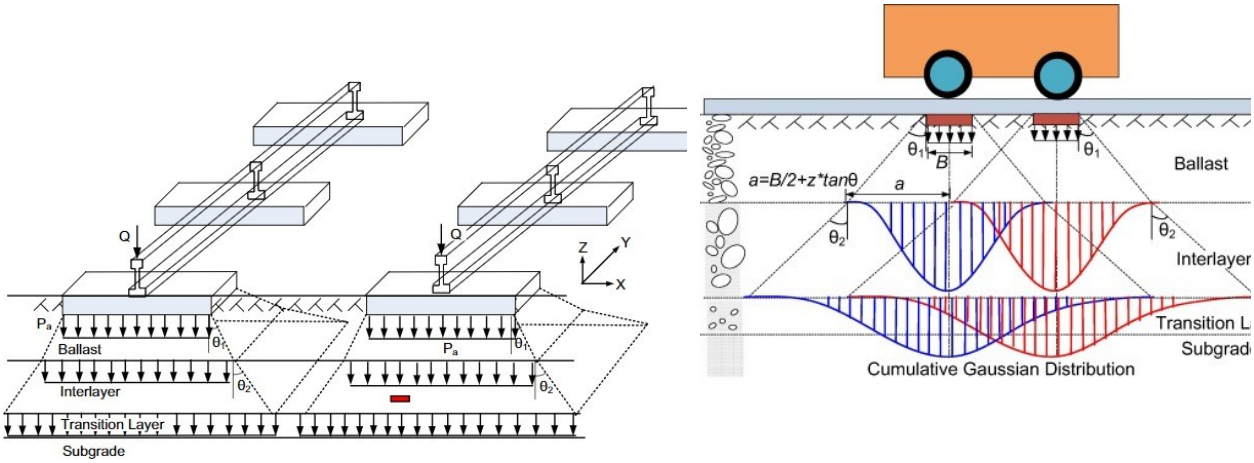

Figure 2.6. Load spread model (Zhang et al. 2016).

The formula used to transform dynamic loading to static loading is given by the equation (AREMA 2010):

$$P_v = P(1 + \theta) \qquad \text{Eqn (2.1)}$$

where P_v is the vertical dynamic load, P is the static load, and θ is calculated from Eq 2.2 (AREMA)

$$\theta = \frac{d_{33}v}{100d_w} \qquad \text{Eqn (2.2)}$$

Where d_w is the wheel diameter in inches, d_{33} is the wheel diameter of 33 inches, v is the train speed in mph.

2.3.4 Foundation Instability under Railway Embankments on Peat

To prevent foundation and side slope failure, stable embankments need to be critically examined during the design and construction phase to yield adequate factors of safety (Munro 2004). Since peat varies in thickness, long-term settlement under embankments constructed on these deposits directly differs in comparison with areas underlain with other soils (Tan 2008). This phenomenon gives rise to local depression. Zaytsev (2014) documented that, elastic deformation from loads of passing and residual deformations from peat foundation uplifts are the typical deformations exhibited by the embankment on weak peat foundation. Experiments indicated that an increase in water table level affects the hydrostatic pressure of embankments with minimal effect on pore water pressure (Transportation Safety Board of Canada 2007). Due to the heavy weight emanating from the movement of rolling vehicles, a railway is constantly subjected to dynamic loads leading to an increase in axle load with traffic stresses (Ciotlaus et al. 2017). Railway embankment routed on peats experiences uncontrollable settlements which generate subgrade failure that affects railway line operation (De Guzman and Alfaro 2017). Studies revealed that intensified excess pore pressures developed in the center of peat and are dependent on the axle load and train speed (Transportation Safety Board of Canada 2007).

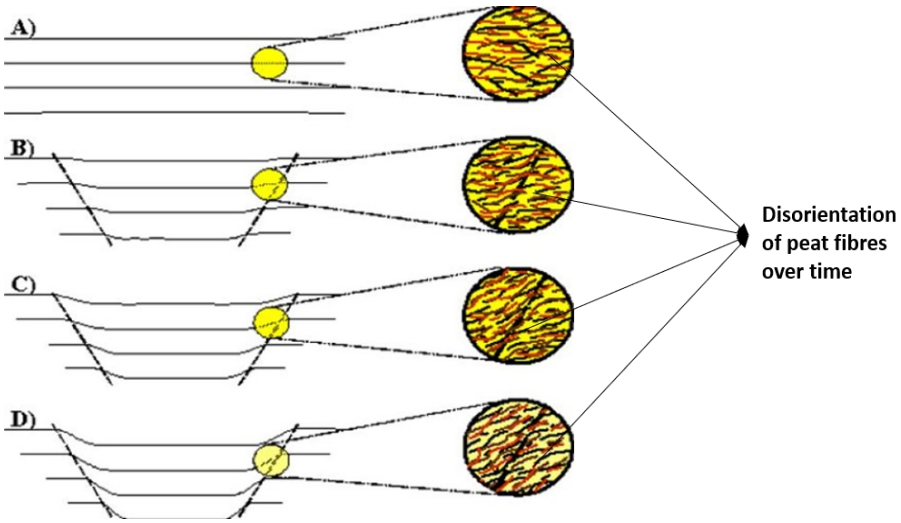

Figure 2.7. Evolution of settlement and distortion of peat fibers under a railway embankment when subjected to load (Transportation Safety Board of Canada 2007).

2.4 Performance of Railway Embankments

Unsatisfactory performance of embankments that results from unstable slopes, foundation instability, loading response, pore water pressure, the factor of safety (FS), etc. has to be regulated for reliable operation to eliminate catastrophic track foundation failure. Regarding a railway embankment, its performance is predominantly influenced by the prediction of the magnitude of settlement and its development with time. Accordingly, to effectively distribute loads to the foundation, a railway embankment constructed over soft deposits of organic soils requires stable supported slopes to reduce total and differential settlement. This section summarizes background information focusing on railway track settlement and stability as a performance indicator.

2.4.1 Stabilization of Embankment Slope on Peat Foundation

It is an accepted concept that slope ratios and the strength of the materials are the two most controlling factors that govern the design of slopes. In designing and constructing embankments, slope ratios of embankments are needed to ensure long-term stability. Yu and Sloan (1994) address the stability of embankments on soft foundations as a bearing capacity problem. Stabilizing railway embankments constructed on the poor subgrade to reduce vertical deformation and lateral displacement is achieved by increasing the foundation soil-bearing capacity strength. This problem arises as a result of the combination of vertical load applied by the embankment fill on the surface of the foundation and the outward shear stress originating from the horizontal stresses in the fill. The most important controlling factor to analyze the stability of slopes is the FS. In this thesis, typical railway embankment geometries of 2:1 and 3:1 slope ratios will be investigated as they are the dominant ones in North America.

2.4.2 The Need for Factor of Safety in Stabilizing Slopes

There are three (3) definitions for the FS. However, a FS is usually defined in terms of quantitative relation as the ratio of resisting forces to driving forces along a potential surface of failure. Gedney and Weber Jr. (1978) emphasizes the need to know that for a given slope, the FS is greatly dependent on data quality employed in the analysis and theoretically expresses that if the values of FS are less than one then failure is inevitable unless engineers are open-mindedly assured of the

precision of the quality of data used. Values greater or equal to one is an indicator of stability. Lu et al. (2013), after using the shear strength reduction FEM technique to predict the FS for reinforced piles for slope stability analysis, concluded that the method yields a significant result that helps to remediate failure. Table 2.1 summarizes factors of safety for various types of loading conditions for railway embankments on soft soils.

Table 2.1. FS for various types of loading conditions for railway embankments on soft soils

Source	Type of the model embankment	Loading capacity	FS
Esmaeili et al. (2013)	Non-reinforced	258.3 kN/m^2	1
	Reinforced	432.22 kN/m^2	1.303
Likitlersuang et al. (2018)	Non-reinforced	300 km/h	1.802
	Reinforced	300 km/h	1.547

2.4.3 Settlement of Railway Track

Post-construction settlement of railway track structure centers on both short-term and long-term processes that significantly affect the track geometry irregularity and track behavior. Most often, high-speed railway track differential settlement in typical soft soil regions is located in transition zones (e.g., reinforcement–embankment transition zones) as a result of structural and foundation differences (Zhou et al. 2020). Hendry (2011) reports an estimated accumulated settlement of 240 to 320 mm between 1996 and 2004 at the Lévis Subdivision (Saint-Henri-de-Lévis, Quebec) site. Again, Wang et al. (2014) also report a settlement rate of 3 -7 cm/year of geogrid-reinforced pile-supported embankments on collapsible loess in the case of a high-speed railway. The settlement of track embankments built on organic soils should avoid unacceptable differential settlement and subgrade failure during the construction and post-construction stages. Table 2.2. outlines the settlements of ballasted tracks for different loading in the design of high-speed railways.

Table 2.2. Settlement of ballasted track for different loading in the design of high-speed railways

Source	Description of the zone of settlement	S_b (cm)	D_s (km/h) / E_L (kPa)
Zaytev	Maximum S_T on center of embankment	6.0	80 kPa
(2014)	Embankment transitional zone	1.7	
Wang et al.	Reinforced embankment zone	10 .0	250 km/h
(2014)	Embankment transitional zone	5.0	
	Reinforced Embankment zone	5.0	300 to 350 km/h
	Embankment transitional zone	3.0	
Zaytev et al.	Embankment zone	127.5	80 kPa
(2018)	Maximum S_T along the axis of the embankment	135	80 kPa
Likitlersuang	Centre of the track	8.5	300 km/h
et al. (2018)			

*S_b = Settlements of ballasted track on soft soils, D_s = Design speed, E_L = Embankment load

2.5 Improvement Techniques for Peat Soils

Construction over peat could take place in two different ways: either through the complete removal of peat or through reinforcement of the peat to be able to give enough support to constructed structures on it (Ibrahim et al. 2014). Principal solutions for stabilizing embankments on peat foundations are stabilization using wooden piles or using concrete piles (Zaytsev 2014). Figure 2.8 illustrates the various combinations of supporting the construction of piles for peat soils. The long-term performance of piles is of great concern when dealing with peat soils as they display low strength, high compressibility, and significant creep behavior (Tan 2008). It is strongly required that soil improvement should be conducted on soft and consolidating soils as it is one of the possible settlement reduction methods for railways (Bogusz and Godlewski 2019). The soil – reinforcement interface properties are ranked as the most significant controlling variable influencing the behavior of the reinforced earth structure (Chai and Bergado 1993).

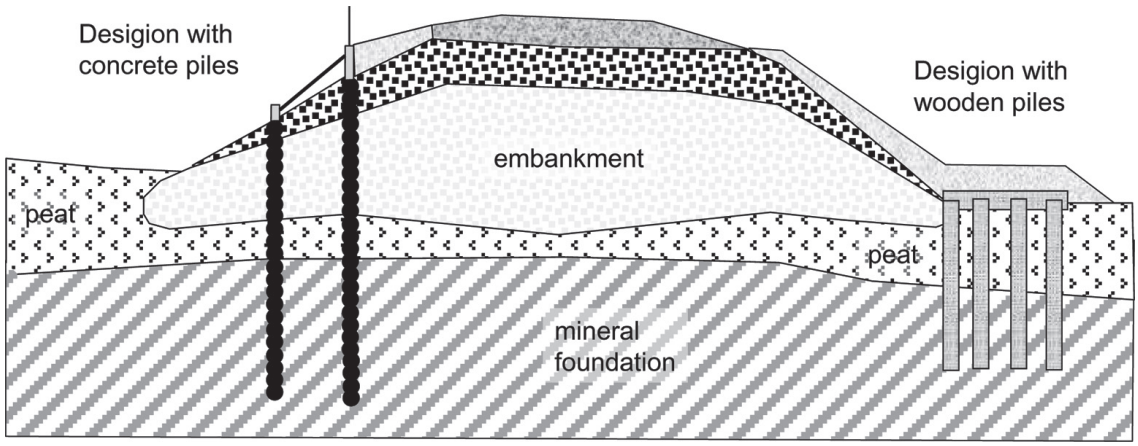

Figure 2.8. Scheme of principal solutions of stabilization of embankments on peat foundations (Zaytsev 2014).

2.5.1 Wooden Piles for Support on Peat Soils

The choice of pile type for a given foundation is dependent on a comparison of cost, stability under loading, long-term loading, pile length, and environmental factors (Grand 1970). Aside from being the most economical piling foundation system produced from a renewable resource; wooden piles are easy to transport due to their lightweight (Rollins 2012; Toprak et al. 2018). Grand (1970) adds to the fact that the use of wood as a pile material in areas with high water table is ideal as they are very adaptable to water owing to their resilience, wearing resistance, and ease of replacement. Since wood has prolonged and enhanced functionality underwater level it becomes essential for wooden piles to be operated at the water level (Toprak et al. 2018).

2.6 Design of Piles for Railway Embankments

Concrete piles are not suitable as stabilization materials due to their general unavailability in remote and inaccessible areas. Since timber is readily available in these areas, it can be used as piles to reinforce railway embankments constructed on peat in secluded areas that trains traverse. The use of timber piles as floating or frictional piles is mostly employed when embankments are constructed on a thicker layer of soft soils. They transfer external loads from traffic and embankment through the frictional resistance force between the pile surface and adjacent soil. According to experimental results, the number of piles in the transverse direction to the axis of the

railway should be four rows of wooden piles to prevent the uplift of the peat foundation outside a model (Zaytsev 2014).

2.6.1 Design Code Requirement for the Design of Wooden Pile

The design criteria set forth for wooden piles in this thesis conform to the requirements of the National Building Code of Canada (NBCC) (2005) as recommended in the Canadian Foundation Engineering Manual (2007). Wooden foundation piling in Canada shall comply with CSA Standard CAN3-056-M79 (Round Wood Piles) and CSA Standard CSA CAN3-O86-M84 (Engineering Design in Wood). To achieve the minimum level of performance, the NBCC and Canadian Standards Association (CSA) propose that all design methods should have both strength and serviceability criteria to meet a satisfactory level of structural integrity. To fulfill the minimum performance, NBCC Clause 4.1.2 provides specified loads and effects to be taken into consideration during design.

2.6.1.1 Canadian Design Code and Standard

CAN/CSA-O86-01 enumerates specified tables, data, and methods for the engineering design of timber piles in Clause 11. It includes Clause 11.2 (Suitable treated and untreated timber piling materials for construction.), Clause 11.3 (Specified strengths for round timber piles), Clause 11.4 (modification factors for duration of load as well as service condition), and Clause 11.5 (Strength and resistance; transfer of all applied loads to supporting soil or rock). Additionally, the requirements and design procedures stipulated in the CSA Standard O86 series shall meet the requirements of CAN/CSA-O56. The following general requirement during the design of timber pile structures. Clause 4.1 (The size of the pile), Clause 4.2.1 (The diameter of the pile), and Clause 4.2.2 (The length of the pile).

2.6.2 Pile Dimension and Load-Bearing Capacity of Wooden Piles

The load-bearing capacity of piles is directly proportionate to their length. The capacity of the individual pile is calculated based on skin friction resistance provided by the selected length of the pile. With an increasing number of piles and decreasing pile spacing, pile length decreases with increasing pile points where the load is distributed to the soil within a pile group (Tien 1981).

Local settlement and failure are likely to occur when there are variations in the length of piles within the same pile group. Moreover, an increase in the length of the pile reduces pile settlement.

For cohesive soils, it is necessary to achieve an even distribution of load in greater areas when arranging piles in groups. The definition of the ultimate bearing capacity of a pile (Q_u) can be stated as the sum of the skin resistance (Q_S) and the toe resistance (Q_P) and represented mathematically as:

$$Qu = Qs + Qp = \sum fSiASi + qP\ Ap \qquad \text{Eqn (2.3)}$$

where fS_i is the unit skin friction on shaft segment i, ASi is the area of this pile segment, qP is the unit toe resistance, and Ap is the toe area.

2.6.2.1 Design of Piles Considering Negative Skin Friction (NSF)

The downward shear drags that act on the pile group as a result of the downward sinking of surrounding soil in response to soil consolidation and pore pressure drawdown results in the development of negative skin friction. In pile group installation, the development of negative skin friction is an important consideration in the case of a pile in soft soils. Instead of providing resistance, this mechanism imposes extra loads on the pile. The induced drag load can be quite large thereby reducing the pile load capacity and increasing the stresses as well as settlement in the pile group. From a geotechnical point of view, it should be added to the design load for assessing the stresses in the pile. Thus, per design principles, the structural strength of the pile, the settlement, and the long-term bearing capacity of piles are taken into account when considering the negative skin friction on the group effects. To estimate the magnitude of negative skin friction. According to Johannessen and Bjerrum (1965), negative skin friction is proportional to the effective overburden stress in the soil surrounding the pile. The magnitude of negative skin friction can be calculated using:

$$q_n = \beta\sigma'v = MKs \tan \varphi' \qquad \text{Eqn (2.4)}$$

Where β is the constant of proportionality and is called beta-coefficient, and it is a function of the earth pressure coefficient in the soil Ks, σ'v is the effective vertical stress tan φ' is the soil friction, δ' the effective wall friction angle and M is the ratio of the wall friction, expressed as:

$$M = \tan \delta'/\tan \varphi' \qquad \text{Eqn (2.5)}$$

2.6.3 Number of Piles and Configuration

Piles are usually installed in groups to effectively resist vertical, lateral, and uplift loads from superstructures. Again, the transmission of loads through challenging ground conditions and heavy structures is best diffused through pile groups. A study conducted on the load settlement behavior for varying pile numbers by Poulos (2006) found a linear increment relationship between the ultimate load-bearing capacity and the number of piles. When considering pile spacing, the bearing capacity of the group should be greater than the sum of the bearing capacities of individual piles (Transportation Research Board 1977). Raithel et al (2008) recommend the center-to-center distance (s) of the piles and the pile diameter d (pile caps) should be less than or equal to 3.0 m for static loads and less than or equal to 2.5 m for chosen as follows: heavy live loads when dealing with soft soils. Abebe and Smith (2010) suggest the following formula to compute pile spacing:

$$\text{End-bearing and friction piles: } S = 2.5 \cdot (d) + 0.02 \cdot L \qquad \text{Eqn (2.6)}$$

$$\text{Cohesion piles: } S = 3.5 \cdot (d) + 0.02 \cdot L \qquad \text{Eqn (2.7)}$$

Where: d = assumed pile diameter, L = assumed pile length, and S = pile center-to-center distance (spacing).

Pile configuration affects the bearing capacity, settlement, failure pattern, and load transfer mechanism of the pile group. In wooden pile design, challenges arise during the arrangement of the piles under railway embankments constructed on peat with respect to the number and location of wooden pilings to be installed (Zaytsev 2014). Typically, piles are arranged in rectangular or triangular patterns in practice. This thesis aims to give recommendations on the suitable pattern for railway embankment geometries of 2:1 and 3:1 slope ratios and to identify the appropriate number and location of wooden piling to be installed to control the settlement of the rail as well as consolidation of peat.

2.6.4 Settlement of a Pile Group in Peat Soils

Settlement of pile groups in cohesive soils may experience both immediate settlements and long-term consolidation settlements as well as develop secondary compression settlements over a period of time. For this reason, it is recommended to compute the settlement due to consolidation as well as the elastic settlement. This helps to predict the foundation deformation subjected to structural loads. Factors that affect pile group settlement are the L/d ratio (L = pile length; d = pile diameter),

s/d ratio (s = spacing between piles), and Ep/Es ratio (Ep= Young's modulus of the pile; Es= Young's modulus of soil). Figure 2.9 depicts a relationship between the number of piles on settlement and ultimate load capacity. For an analysis of an entire pile group, the FEM analysis is the most rigorous technique available for the estimation of pile group response. To examine the mechanisms of pile group behavior, 2-D FEM analysis will be employed to help create a reduced number of elements associated with the modeling and analysis in relation to the slope stability of a pile group. The capacity of a pile group is obtained by using an efficiency factor and calculated as:

Pile group capacity = Efficiency of the pile group * Single pile capacity * Number of piles

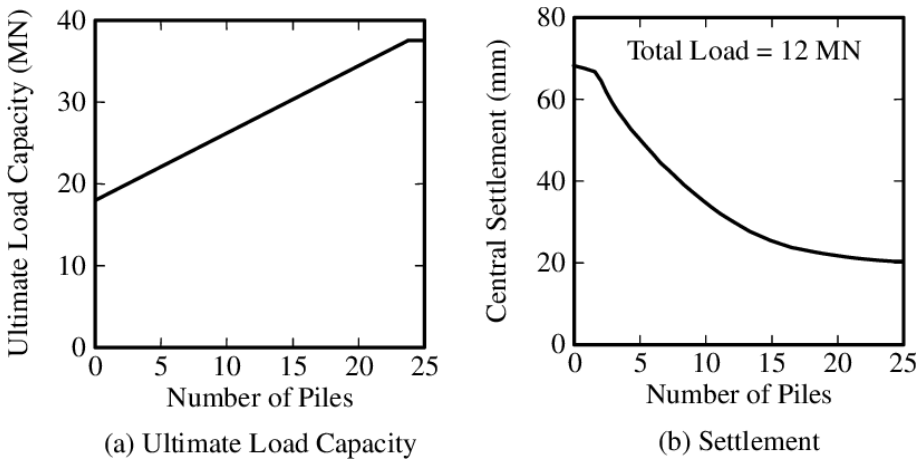

Figure 2.9. Effect of the number of piles and ultimate load capacity and settlement (Poulos 2006).

2.7 Evaluation of Slope Stability and Settlement of Piled Embankments on Peat

To understand the soil-structure interaction mechanism, there is a need to conduct an evaluation of the slope stability and settlement of piled embankments on peat to monitor failure. Moreover, repeated traffic (cyclic) loading causes progressive lateral and vertical deformation of ballasted rail tracks resulting in deviations in desired track geometry (Jiang and Nimbalkar 2019). In light of the aforementioned challenges, this research focuses on finding remediations by simulating a model that stabilizes embankments on peat foundations to deal with an excessive differential settlement and lateral sliding instability. Modeling of piled embankments under static load failure and settlement proved that support of the peat foundation with wooden piles is suitable for avoiding the deformation of the soil (Zaytsev 2014). To accurately define the processes involved in soil

failure in a piled embankment model, Zaytsev (2014) showed that both a physical model and a prototype need reinforcement of the foundation. Figure 2.10 shows the modeling of wooden piles used to assess locations of major deformations – slopes caving and uplift of peat foundations.

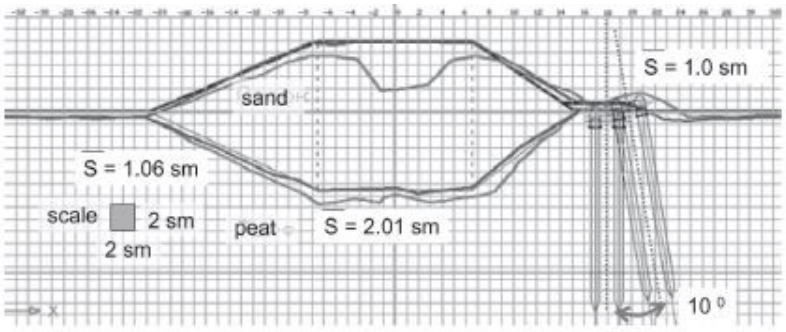

(a)

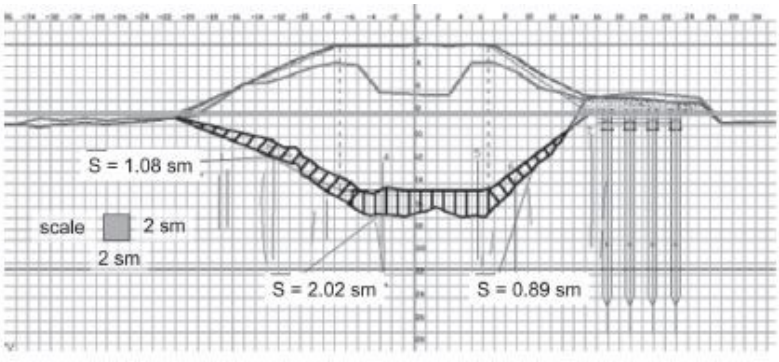

(b)

Figure 2.10. View after modeling with (a) two wooden piles (b) four wooden piles (Zaytsev 2014).

2.7.1.1 Wooden Pile Supported Embankment for Railway

In comparison with other soft soil improvement techniques, Chen et al. (2008) postulated that pile-supported embankments are more suitable in the sense that they exhibit minimal vertical and lateral deformation, rapid construction, and global stability. Thus, piled embankment presents itself as a more advanced resolution to dealing with railway embankments constructed over peat. This is because foundations erected on soft soils usually experience large differential settlement which becomes evident at the surface of the railway embankment (Quigley and Naughton 2007). The use of wooden piles as a method of stabilization in peat deposits in railway embankments could be attributed to their general availability in remote and inaccessible areas. A typical illustration of wooden piles for stabilizing railway embankments constructed on peat is shown in Figure 2.11.

Figure 2.11. The technology of wooden pile driving in railway embankments on Peat (Zaytsev 2014)

In conclusion, a railway embankment constructed on peat efficiently mitigates settlement, and vibration and showed improved total stability when wooden piles are used as a reinforcing method (Zaytsev 2014).

2.8 Numerical Modelling of Railway Embankments

According to Gupta et al. (2016), the method for analyzing the stability of slopes could be either a conventional, numerical, or neutral network. Explaining this in detail, Gupta et al. (2016) make clear that the numerical method of analyzing slopes is often chosen over the conventional forms of analysis. The preference for the numerical modeling technique is explained by Eberhardt (2003) in that it produces an accurately estimated result for a problem, unlike the conventional approach which is restricted to solving uncomplicated problems within the range of application. Fig 2.12 gives a breakdown of methods available for the analysis of slope stability. Numerical modeling simulates the time-dependent deformation and settlement of embankments (De Guzman and Alfaro 2017). Salunkhe and Bartakke (2017) enumerate the functions of numerical modeling as examining the impact of parameter variations, material deformation, and failure, enabling the

modeling of creep deformation, pore pressure, and dynamic loading. Despite the drawback of the numerical modeling technique in thwarting models to carry out further analysis of in-depth three-dimensional track performance, numerical simulation has proven to be a highly effective method of evaluating track performance as well as vibration propagation (Freitas de Cunha 2013). Again, Sabiti et al. (2007) iterate that, numerical modeling can account for all influencing parameters associated with the performance of piled embankments. Sayeed and Shahin (2017) state that the rapid development and application of numerical modeling methods aided by the recently advanced processing capacity of computers for the design of railway foundations is a result of its significant advantage over using most existing empirical and analytical approaches. Since the track serviceability condition is influenced by subgrade conditions, Freitas de Cunha (2013) stresses the need to assimilate track-soil reaction in any prediction model that seeks to simulate the track response. Numerical modeling of railway embankment settlement yielded results that revealed that the FS of an embankment is increased by approximately 30% and reduction of embankment crest settlement by 35% when reinforcement is used (Likitlersuang et al. 2018).

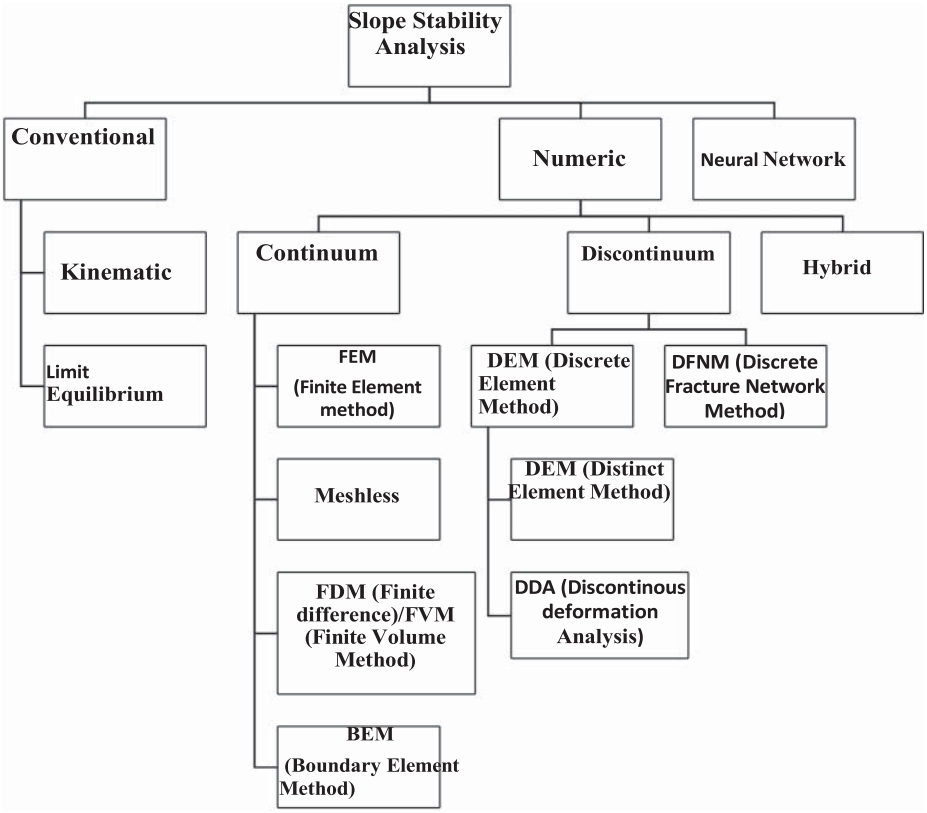

Figure 2.12. Flow chart indicating available methods for slope stability analysis (Gupta et al. 2016).

Numerical methods either based on traditional, analytical solutions or a more sophisticated approach like the FEM are used in performing stability analysis for design verification (Bogusz and Godlewski 2019). In contrast to laboratory and field investigations, numerical simulation presents a convenient and economical method for investigating the mechanical behavior of reinforcement and the surrounding components of track substructures (Jiang and Nimbalkar 2019).

2.8.1 Limit Equilibrium Method (LEM) for Analyzing Embankment Slopes

The LEM utilizes several analytical approaches dependent on the problem type (circular or non-circular) to be solved in order to yield precise results for the problem (Matthews et al. 2014). The technique requires specific assumptions for the interslice normal and shear forces, with dissimilarities between the various methods based on how the forces are assumed (Aryal 2006). The assumptions formulated to help resolve the interslice forces and the equilibrium equations lead to the generation of many alternative methods such as Bishop's, Fellenius, or Swedish method (Matthew et al. 2014).

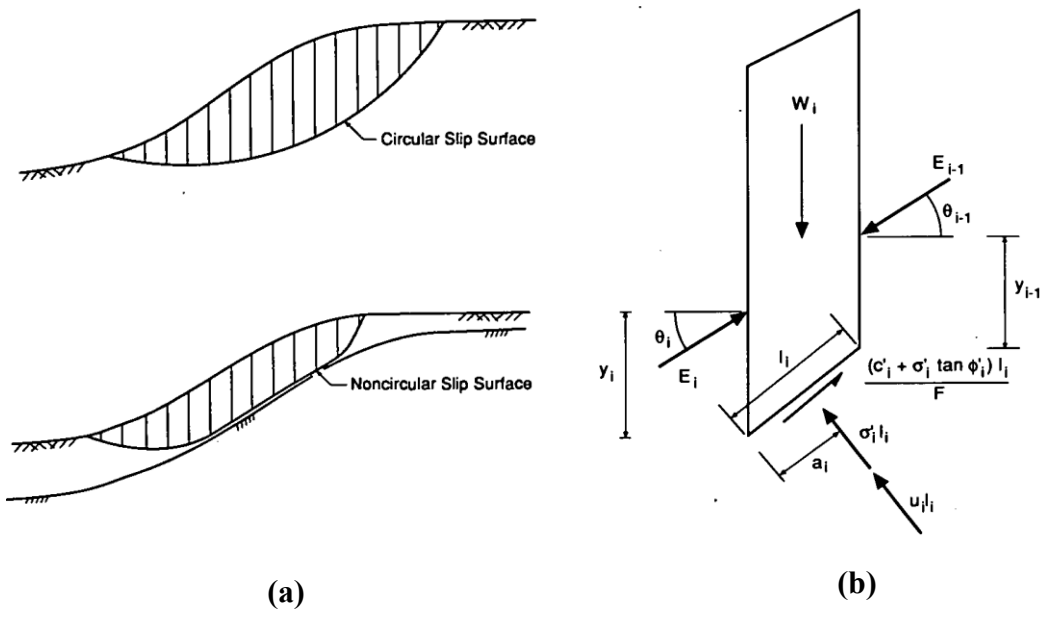

Figure 2.13. (a) Division of potential sliding masses into slices (slip surface is idealization of surface of rupture. (b) Forces acting on a slice (Duncan 1996).

LEM established mostly on force and moment equilibrium, are used in evaluating the stability of slopes and provide a direct measure of stability. To evaluate the stability of a slope with the limit

equilibrium technique, the first step is to calculate the FS. The mechanics of limit equilibrium analyses ensure the selection of a potential sliding mass and subdividing of the mass into a series of slices with consideration to the equilibrium of each of these slices by one of several possible computational methods (Duncan 1996). Figure 2.13 shows that the division of idealized slip surface potential sliding masses is of rupture and interslice forces. It is worth noting that different assumptions exist for different methods in determining the balance between equations and unknown forces even though some methods do not satisfy the conditions of force equilibrium.

2.8.2 Finite Element Method (FEM) for Analyzing Embankment Slopes

Constitutive models, data parameters and numerical techniques used for finite element analysis define how precise the results yielded would be when used for soft soils (Chai and Bergado 1993). Bogusz and Godlewski (2019) encourage the use of FEM where the preliminary computation of selected cross-sections turns out to be problematic. As a result of the complications associated with embankments on soft soils, the use of the finite element technique presents itself as a useful method for evaluation taking into consideration the construction process, and elastoplastic and time-dependent characteristics of soft grounds (Chai and Bergado 1993). In spite of FEM requiring the use of a large amount of data for its application, its dominant benefit includes being used as a design of reinforcement or in addition, to accurately predict failure surfaces without assumption but rather based on calculation (Bogusz and Godlewski 2019). Chai and Bergado (1993) outline three modes of incremental embankment load application when resorting to finite elements as a procedure for the numerical solution on soft grounds. The methods are laid out as surface loading applications, an increment of gravitational force in part or the whole embankment, or through a new embankment element layer placement. The use of FEM in embankment slope stability yields satisfactory predictions that simulate field measurements and provides rational explanations with field observation (Tan 2008).

However, Nakamura et al. (2008) highlight the limitations of the LEM and therefore suggest the use of the shear strength reduction finite element method (SSR-FEM) since it is able to resolve the LEM's limitation. The SSR-FEM slope stability technique, when in use for evaluation presents a gradual reduction in the soil shear strength until failure condition is achieved (Lu et al. 2013). Hammah et al. (2005) point out that, some of the advantages of SSR-FEM are the possibility to visualize the development of failure mechanism in addition to its applicability to predict stresses

and deformations of support elements, such as piles, anchors, and geotextiles. Providing a more insightful approach, Cai and Ugai (2000) recommend the use of the 3D elasto-plastic shear strength reduction FEM for the analyses of slope stability of reinforced piles or anchors in an established elasto-plastic FEM frame, simulating a zero-thickness elasto-plastic interface component between the soil-reinforcement interface.

The versatility of FEM yields successful and productive results for analyzing stresses and estimating movement in slopes, thus, requiring the understanding of the stress-strain behavior of the soil. The method has demonstrated its effectiveness and adequacy in evaluating track structure behavior based on a series of fundamental numerical simulations focusing on ballast behavior (Jiang and Nimbalkar 2019). The functionality of FEM, when used in slope deformation assessment, has been proven through experience when performed in conjunction with field instrumentation studies (Duncan 1996). Several researchers used FEM for modeling the behavior of slopes and to evaluate the effects of lateral loading on piled foundations. In the case of piled embankments, researchers concluded that the finite element analysis gives a reasonable representation of the actual behavior of a railway embankment. Carder and Temporal (2000) validate the use of the finite element technique in determining the magnitude of bending moments in the piled structure deduced from the limit equilibrium analyses. In planning instrumentation programs, the method could be valuable in locating areas where the largest movements would be expected to occur as well as the magnitude of movements (Duncan 1996). Additionally, the results of FEM are useful in interpreting instrumentation studies, the behavior of movements, and the provision of insightful details into the causes and significance of the measured movements. Jiang and Nimbalkar (2019) numerically simulated track structures by employing the finite element (FE) model to improve the comprehensive understanding of the reinforcement mechanisms of railway ballast. In summary, FEM is best at defining movements and stresses throughout a slope.

2.8.2.1 Modeling and Calculation of Slope Stability using FEM Approach for Embankments

The distinguishing characteristic of the FEM is the discretization of a body or region into smaller elements, on which the differential equations describe its behavior. FEM modeling depends on the integrated response of constitutive elements and considers a slope as a single entity (Gupta et al, 2016). In FEM analysis, the detected failure surfaces may not have a simple and regular shape as detected in LEMs (Koca and Koca 2020). FEM is widely used to incorporate discontinuity in a

model through joint elements with relaxed connectivity (Gupta et al 2016). Each element has nodal points which are mostly positioned at the element boundaries where the variables are assumed to be known. FEM operates on the principle of discretization of a fixed number of elements known as mesh and involves the interrelationship of forces, stress, strain, and displacements. More nodal points denote that an element has a more discretized body thereby having more unknowns and consequently yielding a higher accuracy result. Figure 2.14 shows a finite element model of a slope after discretization and mesh generation. The calculation of stress and deformation is performed for the nodes which link the sub-element without any assumption of the depth or location of the failure surface through an iterative solution process (Koca and Koca 2020). This enables the estimation of the failure surface from the incremental shear strain contours and plastic zones at the critical state.

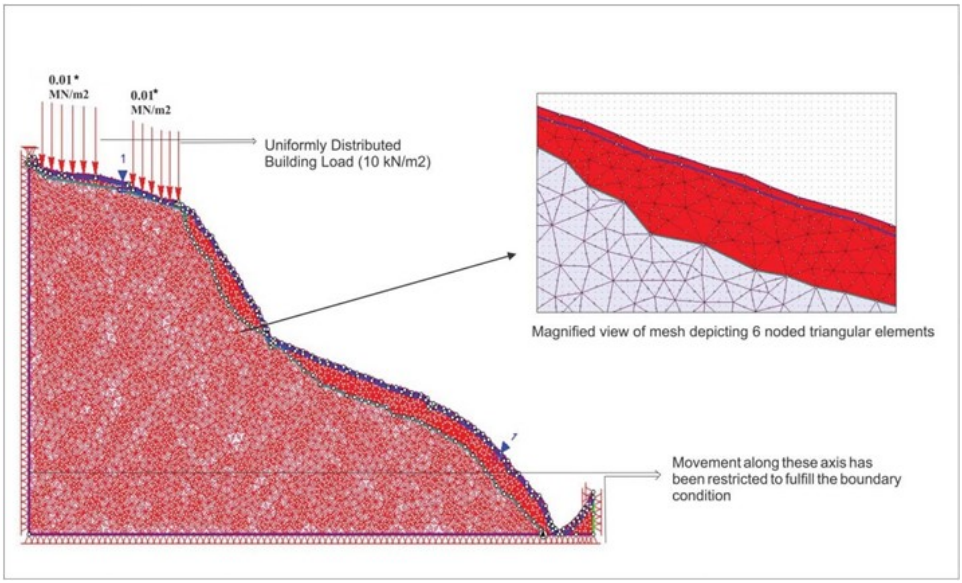

Figure 2.14. Finite element model of a slope after discretization and mesh generation (Gupta et al. (2016))

FE method is performed by solving for unknowns at the nodal points with shape functions describing the behavior of the element in between nodes (Lindberg 2020). The weak formulation of the differential equations defines the FEM. However, the weak formulation requires some mathematical manipulations from the strong formulation. The weak formulation is expressed mathematically as:

$$\int_{\mathrm{v}} (\mathrm{v}\widetilde{\boldsymbol{\nabla}})^{\boldsymbol{T}} \boldsymbol{\sigma}\, dV = \int_{S} \mathrm{v}^{\boldsymbol{T}} \mathrm{t}\, \mathrm{d}S + \int_{\mathrm{v}} \mathrm{v}^{\boldsymbol{T}} \boldsymbol{b} dV \qquad \text{Eqn (2.8)}$$

In equation (2.8), v denotes the weight vector, $\nabla\check{}$ is the approximate function, t is outer stress, and b is body forces.

The finite element discretization can start once the equilibrium equations are established in the weak formulation. According to Lindberg (2020), the weak formulation handles discontinuities without a change of expression. Additionally, the boundary conditions are well sorted out directly in the expression, which is the known part of the equation, the right expression in equation (2.8), unlike the strong formulation. Equation (2.9) is applicable to all constitutive models developed from a chosen constitutive relation. In this equation, internal and external forces should be equal to obtain equilibrium. Where σ is the inner stresses, *t* is the outer stresses and *b* is the body forces.

$$\int_{\mathrm{v}} \mathrm{B}^{\boldsymbol{T}}\, \boldsymbol{\sigma}\, dV - \int_{S} \boldsymbol{N}^{\boldsymbol{T}} \mathrm{t}\, \mathrm{d}S - \int_{V} \boldsymbol{N}^{\boldsymbol{T}} \boldsymbol{b}\, dV = 0 \qquad \text{Eqn (2.9)}$$

The nodes in the elements deform in conformity with the preferred material model. Within each element, there is a translation of strains developed in the nodes to stress points or Gauss points. During the solution procedure, there are load increments in small steps. The relation between the stress and the strain increments in the stress point can be mathematically expressed as

$$\dot{\sigma} = D_T\, \dot{\varepsilon} \qquad \text{Eqn (2.10)}$$

Such that D_T depends on the constitutive relation where D = Elastic material model and D^{ep} = elastoplastic material model.

2.8.2.2 Slope Stabilization with Piles based on SSR-FEM

The FEM adopts two techniques to evaluate slope stability: increasing the gravity load and the reduction of the strength characteristics of the soil or rock mass (Rabie 2013). The Shear Strength reduction method based on the finite-element method uses numerical simulation models to obtain FOS employing the Mohr-Coulomb failure criterion in an elastic-plastic behavior. The shear strength reduction technique searches for a stress reduction factor (SRF) value that brings the slope to failure. There is the possibility to increase the critical SRF number to show more than one slip surface. The shear strength reduced by a FS is deduced through sequential trials to adjust the friction angle (φ′), and the cohesion (c′) of a slope (You et al 2018). The shear strength reduction equation expressed in terms of the Mohr-Coulomb criterion is:

$$\frac{\tau}{FS} = \frac{c'}{FS} + \frac{\sigma' \tan \varphi'}{FS} \qquad \text{Eqn (2.11)}$$

In this expression, c' and φ' are reduced shear strength parameters that give values at failure and are expressed as:

$c' = \frac{c'}{FS}$ and $\varphi' = \arctan\left(\frac{tan_{\varphi}'}{FS}\right)$ with c′ being the reduced value of cohesion and φ′ the reduced value of internal friction angle. The SRF value is calculated based on the stress equilibrium for the mechanical behavior of the material. The critical state for stability is achieved when the iterative process does not converge as the SRF of the shear strength parameters is divided to reduce them. The SSR-FEM technique offers a great advantage as it uses the reduced strength parameters as input into models, enabling the technique to be used with any existing FE analysis software (Hammah et al 2004). Again, (Koca and Koca 2020) agree that LEM could yield lower estimates of failure volumes than the SSR-FEM method in numerical modeling.

2.9 Elastic-plastic Constitutive Models for Peat

According to Briaud (2013), a mathematical representation of soil under load is defined as a soil model. Most often, the soil model gives a representation of the applied stresses to the strains experienced by the soil. Two types of models are used for modeling the behavior of peat: empirical models that correlate the geotechnical performance of peat materials with physical properties and constitutive models established on Terzaghi's principle of effective stress (Zhang and O'Kelly 2013). Changes in effective stress govern soil deformation properties. Terzaghi's soil deformation equation in response to changes in effective stress is calculated using the equation:

$$\sigma' = \sigma - u \qquad \text{Eqn (2.12)}$$

In which σ' is the effective stress, σ is total stress, *u* is the pore pressure. The constitutive model is used to study and describe the mechanical behavior of soils, but in most cases, the load history and stress path of soils. The simplest constitutive model employs a linear elastic relation between stresses and strains. Constitutive models established for peaty soils are currently in partial differential form, with separated deviatoric and isochoric responses (Zhang and O'Kelly 2013). Choosing an appropriate soil constitutive model is paramount for reasonable finite element

analysis (FEA). Den Haan (1997) emphasizes the need to introduce elastic anisotropy into the constitutive relation when using the FEM. This is an uncomplicated procedure to account for the strong anisotropy of peat soils.

2.9.1 Derivation of Constitutive Equations Models for Simulating Peat Behavior

A suitable constitutive law of behavior (stress-strain relation) is one that describes the actual mechanical behavior of materials (Profillidis 2014). The same author outlines that the deformation of ballast and subgrade as a result of passing loads of trains consists of two components: an elastic component that disappears after the passage of the train and a plastic component remaining after the train has passed.

2.9.1.1 Creep Movement and Failure Models for Peat

The deformation of soils is a function of time due to consolidation and creep processes. Settlement under embankments not associated with volume change is the result of a related form of lateral 'creep', spreading, or flow, all of which are the result of ongoing shearing (Hendry 2011). The Soft Soil Creep (SSC) model is appropriate for materials that display high degrees of compressibility as well as significant creep behavior. During numerical calculation, this model helps to simulate the consolidation settlement of the foundation and the secondary consolidation settlement of the total area (Zhao et al. 2015). In peat, primary compression is typically proceeded by some amount of secondary compression. Such performance is well handled by the SSC model predominantly in settlement problems of foundations and embankments, and for unloading (Makusa 2013). According to Gustafsson and Tian (2011), the SSC model is an extension of the Soft Soil model which takes into account the time dependency of soft soil strains. The Soft-Soil-Creep model is a three-dimensional creep model expanded by a one-dimensional creep model based on a standard 24h load test (Zhao et al. 2015).

The main features considered in this model include (Rocscience n.d.):

- stress-dependency of stiffness (logarithmic compression behavior);
- the distinction between primary loading and unloading-reloading.
- time-dependent compression.

- the memory of pre-consolidation stress; shear strength following the Mohr-Coulomb (MC) failure criterion.
- creep yield surface adapted from the Modified Cam-Clay model with an associated flow rule.

In this model, the key hypothesis is that the elastic strains are instantaneous and plastic strains are only viscous and develop over time when the creep behavior is taken into account.

$$\dot{\varepsilon}_{ij} = \dot{\varepsilon}^{e}{}_{ij} + \dot{\varepsilon}^{c}{}_{ij} \qquad \text{Eqn (2.13)}$$

In equation (2.13), the parameters given will determine the factors upon which the rate of development of the viscoplastic strains develops with time; where superscript e and c denote elastic and creep respectively (Rocscience n.d). Gustafsson and Tian (2011) explain that total strains are made up of two components; the elastic and the inelastic (visco-plastic or creep) strains. The inelastic part occurs under both constant effective stresses and is incorporated into the consolidation phase.

2.10 SSR-FEM Slope Stability Analysis in RS2

One of the most important engineering properties of soil is its ability to resist sliding along internal surfaces within a mass. This defines the shear strength provided by the soil along the probable surfaces of failure. The Shear Strength Reduction (SSR) method has quite a number of advantages as compared to the traditional LEM of analyzing the stability of slopes. For instance, the SSR serves as a complement that assists to reveal stiffness interactions and behavior that could be eluded when only limit equilibrium analysis is conducted (Hammah et al. 2006). Moreover, in SSR analysis assumptions are not made about the shape or location of the failure surface. The SSR method automatically determines the most critical failure mode with its corresponding FS. Another dominant and beneficial quality of SSR analysis often quoted is the method's capability to predict stresses and deformations of support elements, such as piles, anchors, and geotextiles, at failure (Hammah et al. 2006).

The SSR method in RS2 automatically conducts a finite element slope stability analysis and computes a critical strength reduction factor for the model. The critical strength reduction factor defines the "FS" of the slope. The SSR method works on the simple concept of reducing the

strength parameters of a slope by a certain factor and computing the finite element stress analysis. The process repeats for different values of strength reduction factor (SRF) until the model becomes unstable (the analysis results do not converge). Thus, the critical strength reduction factor (critical SRF) of the slope is deduced.

In RS2, the shear strength reduction method is compatible with materials models like Mohr-Coulomb, Hoek-Brown, Generalized Hoek-Brown, Drucker-Prager, and Discrete Strength Function.

Simulations are run for a series of increasing trial factors of safety, F, actual shear strength properties cohesion (c), and internal friction angle (φ) and reduced for each trial when performing slope stability analysis with the shear strength technique. The reductions are made simultaneously for all materials if multiple materials are present.

2.11 Rocscience's RS2 2019 – SSR-Finite Element Analysis Software

Rocscience's RS2 is a software program extensively used to simulate complex geotechnical problems. This research employs the application since it is capable of modeling and analyzing material (rock and soil) slope stability problems quickly and easily with FEM. In addition to its user-friendly interface, the software analyzes unlimited engineering projects such as excavation design, groundwater seepage, consolidation, and dynamic analysis.

One of the remarkable features of RS2 is finite element slope stability analysis using the shear strength reduction method. In RS2 consolidation can be modeled with coupled (Biot Theory) and dynamic analysis can be carried out by applying pseudo-static loads or defining an acceleration time history.

CHAPTER 3 KEY MODEL PARAMETERS

3.0 Introduction

To create a reasonable model that represents physical reality, it is important to identify key parameters that best describe the system which is essential for meaningful analysis of slope stability. Thus, this chapter of the thesis identifies the key model parameters which will be used in this research as well as a discussion on the controlling features that regulate the model's behavior. It provides highlights of the components of the strategy used for the entire work.

3.1 Key Model Parameters

Both slope and foundation failure can occur under railway embankments particularly in the light of increased loading due to extra tonnage hauled by modern railways. This may lead to stability problems and an increase in maintenance costs. The controlling factors that affect the stability of railway embankments built on peat are the traffic load due to passing trains, increase in pore water pressure, as well as stress. There are five (5) main components in the model: 1) the freight train, 2) the rail system, 3) the natural ground, 4) the condition of groundwater affected by the development of pore water pressure and stress, and 5) wooden piling. The key parameters discussed in detail include the dimension of railway embankments, slope inclination ratios, soil properties, loading due to trains and pile components, and properties (e.g., pile material, length, spacing, etc.).

3.1.1 Parameters for Railway Track Structure

Railway structures are intended to provide support to the track and facilitate operations. Railway structures, therefore, perform under heavier loads and are expected to have longer service lives. Thus, their design needs to be governed by the standard specification set by an acceptable authority such as Canadian National Railways (CN), The American Railway Engineering and Maintenance-of-Way Association (AREMA). The axle load and the traffic load (tonnage) running on the line are critical factors for track and subgrade fatigue.

3.2 The Superstructure

The parameters of the superstructure (rails, track gauge, sleeper, or cross ties) are summarized below. For the superstructure, the parameters selected for the rail gauge is 1435 mm as it is the

standard gauge in North America (Selig and Waters 1994). Based on Table 3.1, typical sleeper dimensions for a timber sleeper in North America are 229 mm in width, 2590 mm in length, and 495 mm in spacing (Selig and Waters 1994).

3.2.1 Rail and Wheel Contact

The train wheels are supported and guided by the rails. According to Profillidis (2014), the wheel and rail contact surface is around 1.3 cm^2 as shown in Figure 3.1(b). The standard-gauge railway is the most widely used railway track gauge across North America. A standard-gauge railway has a track gauge of 1,435 mm (4 ft 8 1⁄2 in). The spacing between the rails on a track is defined as the track gauge and is measured between the inner faces of the load-bearing rails. It is measured 14mm below the rolling surface and shown in Figure 3.1(a). A representative value of the track gauge in different countries is given in Table 3.2.

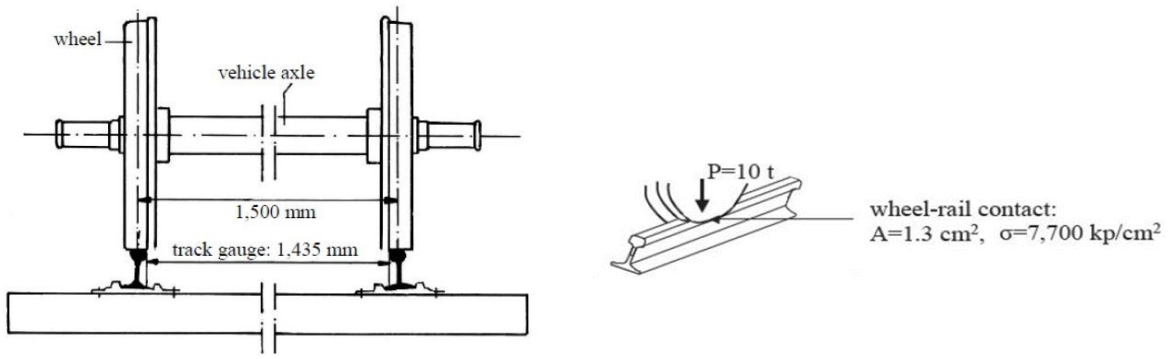

Figure 3.1. The base area (a) of wheel-rail contacts and (b) standard track gauge (Profillidis 2014)

Table 3.1. Typical sleeper dimensions (Selig and Waters 1994)

Location	Material	Width (mm)	Length (mm)	Spacing (mm)
Australia	Wood	210-260	2000-2743	610-760
	Concrete			600-685
China	Wood	190-220	2500	543-568
	Concrete	240-290	2500	568
Europe	Wood	250	2600	630-700
	Concrete	250-300	2300-2600	692
North America	Wood	229	2590	495
	Concrete	286	2629	610
South Africa	Wood	250	2100	700
	Concrete	203-254	2057	700
		230-300	2200	600

3.2.2 Sleepers (Cross Ties)

Wood (timber) and prestressed reinforced concrete are the two most commonly used materials for sleepers or ties (more specifically cross ties). Typical sleeper base dimensions and spacing for some countries are outlined in Table 3.2. Wood sleepers are generally easier to handle, distribute loads better and prove to be a more suitable material in terms of tensile and compressive strengths in comparison to concrete sleepers. Both geometric parameters and material properties are important factors that need to be considered for railroad sleepers. The mechanical characteristics of timber sleepers used in this study are taken from Table 3.3. Figure 3.2. shows typical geometric characteristics of timber sleepers for standard gauge tracks.

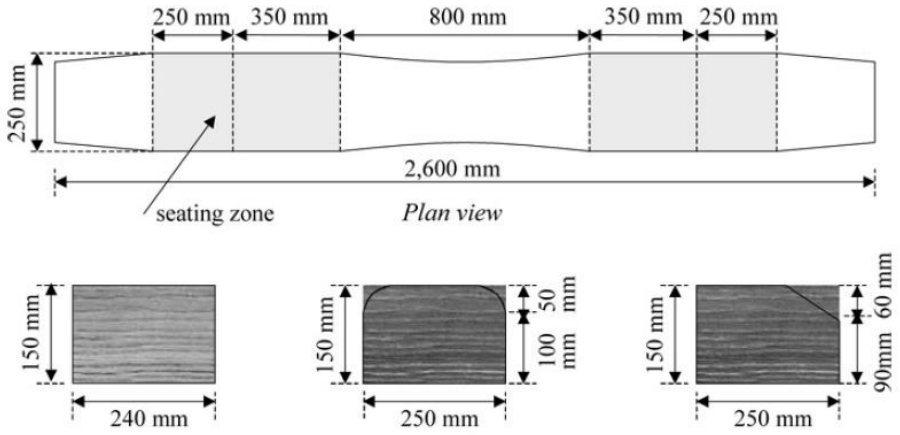

Figure 3.2. Typical geometric characteristics (dimensions in mm) of timber sleepers for standard gauge tracks (Profillidis 2014)

Table 3.2. Typical rail gauge values (Selig and Waters 1994)

Location	Gauge (mm)	Gauge (in.)
North America	1435	56.7
Europe	1435-1668	56.5-65.7
South Africa	1065	41.9
Australia	1524-1676	42-63
China	1435	56.5

Table 3.3. Values of the mechanical characteristics of superstructure materials (Profillidis 2014)

Material	Elasticity modulus (MPa)	Poisson's ratio	Tensile strength R_T (MPa)	Compressive strength R_C (MPa)
Reinforced-concrete sleeper	2.94×10^4	0.25	2.94	29.42
Prestressed-concrete sleeper	4.90×10^4	0.25	5.88	8.83
Tropical timber sleeper	2.45×10^4	0.25	9.81	98.07
Rail (steel)	2.06×10^5	0.25	686.47	588.40

3.3 Material Properties and Components of Substructure

The parameters of the substructure (such as the thickness of each layer, the slope geometry, and material properties and specifications of each layer) and dimensions, spacing, and material properties of the trackbed (ballast and subballast) are discussed and shown below.

CN Engineering Specifications for Industrial Tracks (2019) recommends the range of geometry parameters for the substructure. The railway ballast material shall be clean and free from clay and shale and an excess of dust or elongated pieces and composed of crushed rock for use primarily on mainline Class 1 railroad. It should be hard, strong, and contain durable particles. Granular ballast will be chosen for this research as they are suitable for all types of sleepers. The minimum ballast structure thickness of mainline track Class 1 is 12 inches (304 mm) recommended for standard gauge (1435 mm). While the ballast shoulder width must have a minimum of 6 inches (152.4 mm) for jointed rail or 12 inches (304 mm) for continuous welded rail to provide adequate lateral resistance and confinement.

Subballast shall be well-graded granular material; aggregates including crushed stone, natural or crushed gravels, natural or manufactured sands, crushed slag, or a homogeneous mixture of these materials. According to the suggestion of CN Engineering Specifications for Industrial Tracks (2019), the minimum depth of the subballast structure must be placed to a depth of 12 in. (305 mm). The subgrade usually comprises fine particles (soil types of clay and silt) with a thickness of over 2000 mm. Good quality subgrade will be used for modeling as the natural ground is a peaty formation. The grading of ballast aggregates shall conform to the requirements set in Table 3.4.

Table 3.4. Unit weight/volume relationships of ballast (Li et al. 2015)

Ballast Condition	FI	Unit Weight(lb/ft^3)	Void ratio	Void volume (%)
Loose	0	95	0.68	41
Compact	0	110	0.53	35
Moderately Fouled	20	125	0.35	26
Heavily Fouled	40	135	0.25	20

Table 3.5. Material properties of railway embankments (Li et al. 2016)

Name	Density (Mg/m^3)	Poisson's ratio	Modulus (MPa)	Thickness (m)	Resilient modulus (MPa)	Friction angle (°)
Ballast	1.76	0.3	276	0.3	140-550	40-55
Subballast	1.92	0.35	138	0.15	55-105	25-40
Subgrade	1.92	0.35	41	infinite	-	-

3.4 Soil Properties of Soil Mass

The foundation of the railway track affects the performance of the track system. The strength and deformation characteristic of the railway subgrade controls the operation of the track (Likitlersuang et al. 2018). For the input parameters used for geotechnical modeling analysis, general soil properties mainly used include unit weight, cohesion, internal friction angle, Young's modulus, and Poisson's ratio. The natural ground considered in this thesis is Peat soil. Kazemian et al. (2011) suggest a value range between 27-32° as its internal friction. Tables 3.6 and 3.7 present typical parameters for peat. Tables 3.8 and 3.9 outlines typical dry unit weight and Poisson's ratio parameter for various types of soils.

Table 3.6. Hydraulic conductivity and drainable porosity by von Post H value for peat of all origins (Verry et al. 2011)

Von Post H	K_{sat} (cm/d^{-1})	Drainable porosity (Decimal)	Peat passing fingers (% of volume)
1	18,317	0.60	0
2	7,690	0.34	0
3	4,170	0.29	0
4	2,160	0.23	0
4.5	1,296	0.20	1-2
5	788	0.18	3-10
5.5	409	0.16	11*25
6	215	0.13	26-35
6.5	86	0.12	36-45
7	35	0.12	46-55
7.5	26	0.11	56-65
8	17	0.10	66-75
9	11	0.09	76-95
10	8	0.08	96-100

Table 3.7. Typical soil parameter for Peat (Mochtar et al. 2015)

Peat Soil Parameter	Units	Value Ranges
Specific Gravity (G_s)		1.4-1.7
Water Content (W_c)	%	450-1500
Unit Weight (γ_t)	gr/cm^3	0.9-1.25
Void Ratio (e)		6.89-11.09
Acidity (pH)		3-7
Internal Friction Angle (φ)	°	30-50
Vane Shear	kPa	5-10

Table 3.8. Typical values of the dry unit weight for various soils (Kosthilaire 2015)

Soil Type	Dry Unit Weight (kN/m^3)
Sands and gravels	14.7- 22.6
Silts and clays	5.9 - 17.7
Glacial tills	16.7 - 22.6
Crushed rock	14.7 - 19.6
Peats	1.0 - 12.9
Organic Silts and clays	4.9 - 14.7

Table 3.9. Approximate values of Poisson's ratio of soils (Rowe 2012)

Material Type	Poisson's ratio
Saturated soil, undrained loading	0.5
Clay, drained loading	0.2 – 0.4
Dense sand, drained loading	0.3 – 0.4
Loose sand, drained loading	0.1 – 0.3
Peat, drained loading	0 – 0.4

Table 3.10. Typical values of Young's Modulus E and shear Modulus G (Budhu 2008)

Material Type		E[a](MPa)	G*(MPa)
Clay	Soft	1-15	0.5 – 5
	Medium	15 – 30	5 – 15
	Stiff	30 – 100	15 – 40
Sand	Loose	10 – 20	5 – 10
	Medium	20 – 40	10 – 15
	Dense	40 - 80	15 - 35
Peat		0.1 – 0.8	

3.5 Analysis of Traffic Load Due to Passing Trains

For a freight train, the parameters to use in estimating the load are the train dimensions, the quantity, and weight of axles, and allowable maximum operating speeds. A typical freight train with dimensions for a standard freight car used in North America is shown in Figure 3.4. The standard-wheel diameter ranges between 920 – 840 mm as the operational requirement (European

Commission 2013). A typical railway wheel has a diameter of 920 mm for a freight wheel (Thompson 2010).

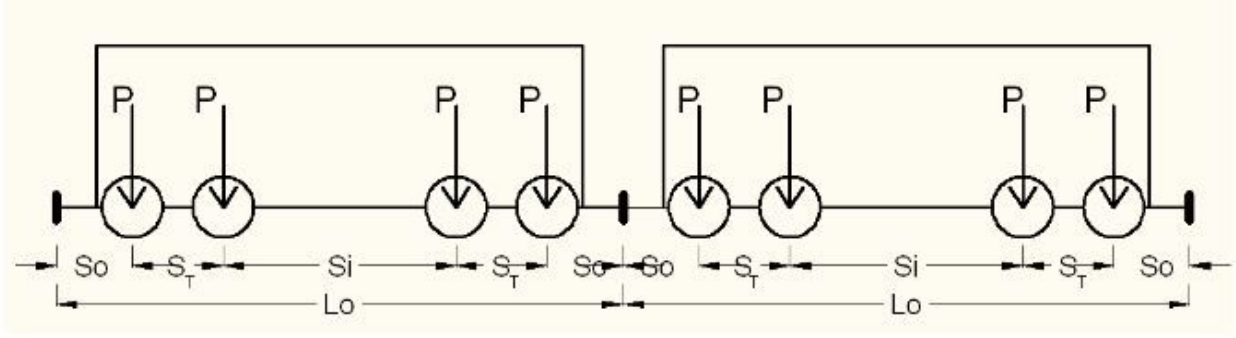

Figure 3.3. Typical railcar dimension for a standard freight car (Rakoczy and Nowak 2018).

P – Axle load (lbs/kN)

L_O – Overall length of railroad car measured over the pulling face of the coupler (meters/feet)

S_O – Outboard Axle Spacing (meters/feet)

S_T – Truck Axle Spacing (meters/feet)

S_I – Inboard Axle Spacing (meters/feet)

As seen in Table 3.11, the speed of a typical freight train varies from 30 km/h to 120 km/h. Since the maximum allowable train speed as a function of the settlement and consolidation process needs to be considered, the maximum train speed is limited to 120 km/h for freight trains on a mainline. Table 3.12 outlines both loaded and empty axle loads traversed on the rail and the number of axles for different typical train types.

Table 3.11. Maximum speeds for railways (Esveld 2001)

Type of railway lines	Passenger Train (km/h)	Freight Train (km/h)
Branch lines	-	30-40
Secondary line	80-120	60-80
Main lines	160-200	100-120
High-speed lines	250-300	-

Table 3.12. Vehicle and weight per axle of different types of rolling stock (Esveld 2001).

Description	Loaded (kN)	Empty Weight (kN)	Number of Axles
Trams	70	50	4
Light rail	100	80	4
Passenger coach	120	100	4
Passenger motor coach	170	150	4
Locomotive	-	215	4 or 6
Freight wagon	225	120	2
Heavy haul (USA, Australia)	250-350	120	2

3.5.1 Loading from Trains

Since the load transfer mechanism from moving trains to the subgrade is a complex process, several assumptions are established before processing the trainload transfer mechanism. Dynamic loads due to passing heavy-haul freight trains will be considered and calculated manually. The Average Ballast ressure is associated with axle load, modified by distribution, impact factors, and the bearing area of the tie. The calculation of Average Ballast Pressure (ABP) is given as:

$$ABP = [2 * PS(1 + 1F) * DF]/A \qquad \text{Eqn (3.1)}$$

where Ps is the static wheel loading (lb); IF is the impact factor in percentage; DF is the distribution factor in percentage; ABP is average ballast pressure at the base of the tie (psi); A is the area of contact face (in^2), equal to the width of sleeper times length (l) of sleeper.

To obtain this, the impact factor needs to be obtained through the use of the equation:

$$1F = \frac{33V}{100D} \qquad \text{Eqn (3.2)}$$

where V is the velocity (mph), and D is the diameter of the wheel (in).

Table 3.14 outlines the static-to-dynamic load factors for different train velocities. The tie and axle spacing and the percentage of the wheel-to-rail load carried by an individual tie are the parameters that affect the distribution of load. AREMA (2010) suggests determining the maximum rail seat load by the approximate percentage of wheel load distribution factor for an individual sleeper by crosstie spacing, as seen in Figure 3.4. The calculations for tie-ballast interfacial pressure

determination are guided by the AREMA (2010) formula for average ballast pressure at tie contact. Table 3.13 summarizes the typical axle load of freight cars around the world.

Table 3.13. Typical heavy axle loads of freight cars around the world (Li et al. 2016)

Country	Axle load (Tonnes)
United States and Canada	33
Australia	33-35
South Africa	26-30
Brazil	27.5-32.5
Sweden	30
China	25-27

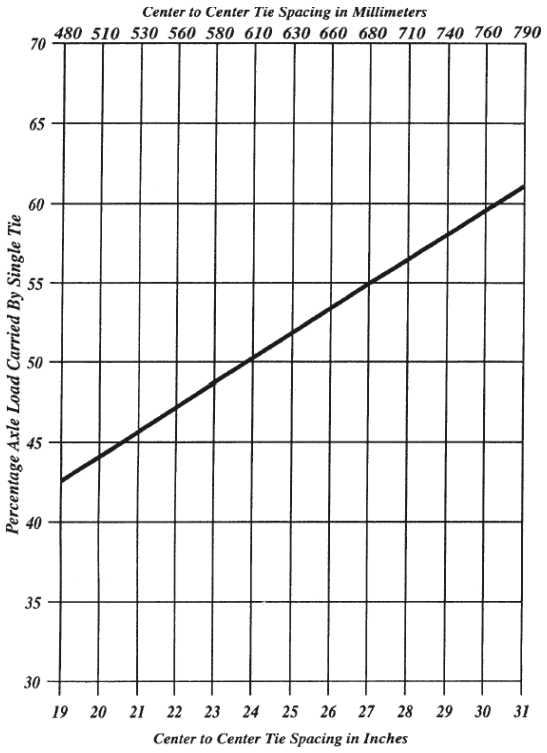

Figure 3.4. Estimated maximum distribution factor for a single sleeper (AREMA, 2010).

Table 3.14. Static-to-dynamic load factors for different train velocities (Forde et al. 2017)

Train Speed, km/h	0	50	100	150	190	250	300	400	500
Factor	1	1.31	1.62	1.94	2.18	2.55	2.86	3.47	4.12

3.5.2 Wheel Load Distribution into the Track Structure

The trainload is distributed to the track and subgrade through the contact points of the wheel and rail. The effectiveness of the load transmitted to the ballast through the sleeper depends on the elasticity of the sleeper, ballast geometry as well as the degree of compaction under the sleeper. The formula used to transform dynamic loading to static loading is given by the equation (AREMA 2010):

$$P_v = P(1 + \theta) \qquad \text{Eqn (3.3)}$$

where P_v is the vertical dynamic load, P is the static load, and θ is calculated from Eq 3.4 (AREMA 2010):

$$\theta = \frac{d_{33}v}{100d_w} \qquad \text{Eqn (3.4)}$$

Where d_w is the wheel diameter in inches, d_{33} is the wheel diameter of 33 inches, v is the train speed in mph.

3.6 Mechanical Properties of Subgrade Materials

The track equipment determines the allowable values of axle load and more specifically on the rail, sleeper, and ballast characteristics (Profillidis 2014). An increase in the thickness of the ballast layer will result in lower stresses in the subgrade and increased elasticity of the track (Profillidis 2014). In Table 3.15, different types of materials for subgrade use are listed together with their characteristic mechanical properties.

Table 3.15. Typical values of the mechanical characteristics of subgrade materials (Profillidis 2014)

Material	Elasticity modulus (MPa)	Poisson's ratio	Cohesion (kPa)	Friction angle (°)
Poor quality subgrade	12.26	0.4	14.71	10
Medium quality subgrade	24.52	0.3	9.81	20
Good quality subgrade	78.45	0.3	0.00	35
Rock subgrade	2942.00	0.2	1471.00	20
Ballast	127.49	0.2	0.00	45
Gravel sub ballast	196.13	0.3	0.00	35
Sand	98.07	0.3	0.00	30

3.6.1 Pore Pressure Response of Peat under Train Load

Excess pore pressure depends on various factors including the trainload and speed, the depth of the soil, and its hydromechanical properties. Observations by Hendry (2011) demonstrated that excess pore pressure of peat under train load is generated under the application of higher frequency loading. This phenomenon increases with an increase in the number of cycles of applied loading. Studies conducted by Wong et al. (2006) on peat foundations under train loading revealed dissipation of pore pressure response during the passage of trains. Table 3.16 summarizes typical hydraulic conductivity values of saturated soils.

Table 3.16. Typical hydraulic conductivity values of saturated soils (Budhu 2008)

Soil Type	K (cm/s)
Clean gravel	>1.0
Clean sands, clean sand, and gravel mixtures	1.0 to 10^{-3}
Fine sands, silts, mixtures comprising sands, silts, and clays	10^{-3} to 10^{-7}
Homogeneous clays	$<10^{-7}$

3.7 The Dimension of Railway Embankments

Since it is necessary to set a suitable dimension to represent the real conditions of the problem, a typical dimension value of the embankment model is needed to be set in advance for accurate numerical modeling. The thickness of the embankment and the pressure distribution on the subgrade follow closely together as the former influences the latter. Table 3.17 gives material properties for railway embankments. The height of the embankment measured from the subgrade level will be 1 m which complies with the minimum value suggested by AREMA (2010). The material properties of the embankment layer used in the model are tabulated in the preceding chapter. Embankments must have a side slope of not less than 2H: 1V (CN Engineering Specifications for Industrial Tracks 2019)

Table 3.17. Parameters of railway embankments (Xue and Zhang 2014)

Name	Unit Weight (kN / m^3)	Compression modulus (MPa)	Poisson's ratio	Cohesion (kPa)	Internal friction angle (°)	Damp. Ratio
Upper Layer of Formation	19.5	190	0.3	32	75	0.08
Lower Layer of Formation	19.0	100	0.3	26	25	0.07
Embankment Below formation	18.5	85	0.28	25	22.3	0.1

3.7.1 Slopes of Formation

CN Engineering Specifications for Industrial Tracks (2019) suggests that the side slope of embankments for a railway embankment track must not be less than 2H:1V (horizontal: vertical). The shearing strength of the soil and its angle of repose controls the stability of embankment slopes. Generally, a slope of 2:1 is recommended for sand or clay embankments. Table 3.18. suggests values of slope inclination for ballast, subgrade, and subballast. However, the slope ratio of ballast could be different from that of subballast and subgrade.

Table 3.18. Values of slope inclination (Baffinland Iron Mines LP 2019; Egeli and Usun 2012; Profillidis 2014)

Section Name	Slope inclination ratio (Horizontal: Vertical)
Ballast slope	1:1.5 2:1 2:1
Subballast and subgrade slope	1:2 3:1 2:1

3.8 Material Parameters for the Design of Piles

To meet the design objectives, load requirements must be proportionally related to the resistance requirements on the field when constructing a successful piled foundation. Static and dynamic stresses must be considered during the selection of material properties for piles. As seen in Table 3.20, wooden or timber piles are suitable material considering their advantage in comparison with other pile materials and soil properties of peat. Moreover, it's fit for use as friction piles in cohesive soils and piling beneath embankments (Abebe and Smith 2010). Table 3.20 outlines accepted

allowable stresses for timber pile groups with wet exposures at a normal temperature range (i.e., <100°F), as published by the American Wood Council (2017). The choice of wooden piles chosen for this study is the Pacific Coast Douglas Fir species as defined in ASTM D 1760. Thus, its physical and mechanical properties and manufacturing requirements are summarized in Tables 3.21 and 3.22. The preference owes to its high strength, renewability, and relatively low cost (Morrell et al. 1984). Commercial structures where Douglas Fir is used provide long service, even in a harsh environment when properly designed, constructed, and maintained (Morrell et al. 1984). Typical pile lengths used for these categories may range from 20 to 60 ft (6 to 20 m) for diameters of 6 to 16 in. (150 to 400mm) (Prakash and Sharma 1990). Dimensions of pile models used are in accordance with the Canadian Standards Association (CAN/CSA-056) as shown in Table 3.20. A pile must be able to withstand the dynamic stresses induced during the driving process, in addition to the static stresses that the pile is subjected to during service. Table 3.21 and Table 3.22 provides officially approved allowable stresses for wooden piles and compression strength parallel-to-the-grain as a function of the specified pile tip circumference respectively.

Table 3.19. Summary of characteristics of pile types and general use. (Timber Piling Council 2016)

Pile Type	Timber	Steel H-Pipe	Steel Round Pipe	Pre-Cast Pre-Stressed Concrete	Cast-in Place Concrete Mandrel Driven Shell	Cast-in-Place Concrete Shells Driven Without Mandrel
Typical Length (ft.)	20-75 (D-fir to 125)	20-100	30-120	30-45 (Precast) 45-120 (Pre-stressed)	10-120	15-80
Typical Axial Design Loads (kips)	35-80	100-500	200-600	100-300	100-300	100-300
Advantages	• Low Cost • Renewable Resource • Easy to handle • Easy to drive • Pile length variations easily accounted for • Tapered section provides higher resistance in granular soils than uniformpiles • Use as friction or end bearing pile	• Easy to splice • High capacity • Small displacement • Easy to drive • Good forpotential obstacles	• Open ended good against obstructions • High load capacity • Closed ended pipes	• High load capacity • Corrosion resistance obtainable • High breakage rate	• Initial economy • Tapered sections provide higher resistance in granular soils than uniform piles • Can be inspected after driving	• Can be redrive • Shell not easily damaged
Disadvantages	• Difficult to splice • Low axial capacity • Low uplift capacity	• Vulnerable tocorrosion • Not recommended for friction pile	• Displacement for closed end pipe • Open end not recommended as friction pile	• Vulnerable tohandling damage • High initial cost	• Difficult to splice after concreting • Thin shell vulnerable during driving • Considerable displacement	• Difficult to splice after concreting

Table 3.20. Sizes of Timber Pile per Canadian Standards Association (CAN/CSA-056). (Timber Piling Council 2016)

Diameter at ExtremeButt or Large End inches [centimeters]	14 [36]	13 [33]	12 [30]	11 [27]	10 [24]
Length feet	Diameter at Tip inches [centimeters]				
Up to 20	10 [25]	10 [25]	9 [23]	8 [20]	7 [18]
20 to 34	10 [25]	9 [23]	8 [20]	7 [18]	6 [15]
35 to 44	9 [23]	8 [20]	7 [18]	6 [15]	-
45 to 59	8 [20]	7 [18]	7 [18]	-	-
60 to 69	8 [20]	7 [18]	6 [15]	-	-
70 to 89	7 [18]	6 [15]	-	-	-
90 to 105	6 [15]	5 [13]	-	-	-

Table 3.21. Allowable Stress Values for Treated Round Timber Piles Graded in Accordance with ASTM D25 (Timber Piling Council 2016)

Species	Axial Compression (F_c) (psi)	Bending (F_b) (psi)	Shear Perpendicular to the Grain (F_v) (psi)	Compression Perpendicular to the Grain ($F_{c\perp}$) (psi)	Modulus of Elasticity (E)(psi)
Southern Pine[1]	1250	1950	160	440	1,500,000
Douglas Fir[2]	1300	2050	160	490	1,500,000
Lodgepole Pine	1150	1700	80	270	1,000,000
Red Oak[3]	1100	2450	135	350	1,250,000
Red Pine[4]	850	1350	125	270	1,300,000

1. Southern Pine design values apply to Loblolly, Longleaf, Shortleaf, and Slash Pines.
2. Pacific Coast Douglas Fir design values apply to this species as defined in ASTM D 1760.
3. Red Oak design values apply to Northern and Southern Red Oak.
4. Red Pine design values apply to Red Pine grown in the United States.
5. Data in Table above was taken from 2012 National Design Specifications.

Table 3.22. Allowable Pile Capacity in Compression (kips) (Timber Piling Council 2016)

Timber Species	Allowable Pile Capacity in Compression (kips)					
	Pile Tip Diameter					
	7	8	9	10	11	12
Southern Pine	48	63	80	98	119	141
Douglas Fir	50	65	83	102	124	147

CHAPTER 4 CREATION OF NUMERICAL MODELS USING FEM FOR SLOPE STABILITY ANALYSIS OF RAILWAY EMBANKMENTS CONSTRUCTED OVER PEAT

4.0 Introduction

The generation of numerical models using SSR-FEM will be accomplished in this chapter by incorporating key parameters identified in the preceding chapters. It is worth mentioning that, train loads on the tie-ballast interaction surface of all models were calculated manually and then applied to the model. The objective of this model excludes studies of the behavior of rails and ties since their behavior is not of interest in this study thus it is not considered in this research. The model geometry, which includes parts such as external train loads, superstructure of the track, substructure of the track, slope inclinations of the embankment, and groundwater conditions are addressed in Section 4.1. A study is conducted on mesh convergence to establish error-free and satisfactory results of the FEM models. In Section 4.2, a description is given for the verification of the use of RS2 to successfully conduct slope stability analysis of embankments constructed on soft soils.

4.1. Simulation of the Model

This part of the thesis provides a step-by-step process of generating a typical model as an example to demonstrate how the models are built. Prior to determining the model geometry, creating a simulation model starts with the selection of appropriate parameters and determining all the dimensions of the track superstructure. Considering the application of accurate trainload to the analysis, calculation results of external train loads on the tie-ballast contact surface are computed. Right after, the dimension of the embankment slope, the applied loads, and the water condition are established the model is completed. The model is assigned material properties, setting boundary conditions, and generating satisfactory mesh elements.

4.1.1 Track Geometry and Load Condition

Train load transfer from moving trains to the subgrade is a complex process. Thus, several assumptions are established to achieve the corresponding external train loads during the transfer mechanism. Within this frame of reference, the following specifying loading condition was made:

1. To satisfy plane strain assumptions, a straight section of a railway track will be considered in the simulation.
2. Temperature and other environmental conditions are neglected. Thus, neither lateral forces nor longitudinal forces caused by them on the rail track will be considered.
3. For the trainload calculation, vertical loads exerted from the operation of a train, are in a stationary condition or with a steady running speed.
4. The friction between the rail and wheel will be ignored. Consequently, the track, the rails, and the wheels are level, even, and smooth.

To simulate a practical case of heavy haul freight trains (AREMA 2010), the most often used locomotive and freight car used in Canada are chosen. The load per axle is assigned 36,000 lbs (160kN) with a typical freight car wheel diameter of 0.914 m (36 inches). Table 4.1 (Selig and Waters 1994) provides the dimensions of the track superstructure, such as rail gauge, tie width, length, height, and spacing, which are then determined as listed.

Table 4.1. Parameters of the freight train and track superstructure

Train Parameter	Value	Unit
Number of axles per car	4	-
Per axle load (loaded)	36,000	lbs
	160	kN
Wheel diameter	36	inch
	0.914	m
Rail gauge	1.435	m
Tie width	0.229	m
Tie length	2.590	m
Tie height	0.150	m
Tie spacing	0.495	m

The unknown parameters (such as wheel load, impact factor, distribution factor, and average ballast pressure at tie face) could be calculated through the aforementioned method from Section 3.5.1. The force to be applied between the sleepers and the ballast surface is calculated using the contact pressure method given by AREMA (2010) in the preceding chapter. The flow of load

transmission is from axle load to wheel load, then to rail seat to contact pressure at the sleepers. Imperial units employed during the calculation would be converted to metric units to integrate with those in the simulation software. The thickness of the model is set as one meter since it is a 2D simulation. Thus, the actual tie bottom area is the area of tie width and model thickness. Since the tie directly under the wheel carries the maximum rail seat load, it is given DF as 0.4 for calculation convenience and acquiring reasonable finite element simulation results. Calculated average sleeper/ballast contact pressures with assumed different train speeds with corresponding impact factors are thus presented in Table 4.2.

Table 4.2. Average Ballast Pressure (ABP) between sleepers and the ballast surface with corresponding impact factors for different train speeds

Parameter	Units	Value					
Train speed	mph	0	15	30	45	60	75
	km/h	0	24	48	72	96	120
Impact factor		0	0.1375	0.2750	0.4125	0.5500	0.6875
Impact factor in percent	%	0	13.75	27.50	41.25	55.00	68.75
Average ballast pressure	(kPa)	236.24	268.73	301.21	333.70	366.18	398.66

4.1.2 Model Geometry

Following the establishment of the ballast pressure at the tie face, the development of an embankment model is presented in this section. As shown in Figure 4.1, the structure of the embankment consists of timber sleepers, ballast, sub-ballast, and subgrade, constructed on a natural ground of peat. As shown in the same figure (Figure 4.1), the dimensions of the models are clearly depicted. The ballast shoulder width and roadbed shoulder width are set as 0.6 m and 0.8 m respectively which is in conformity with AREMA's Manual for Railway Engineering (AREMA 2010). This is because as the main restraint to lateral movement and fasteners, the ballast shoulder and roadbed shoulder cannot be less than 0.304 m and 0.608 m respectively. In this thesis, the depths of each layer of the substructure (ballast, subballast, and subgrade) from top to bottom are

set as 0.3 m, 0.3 m, and 0.4 m. This represents the typical minimum value recommended by AREMA (2010) for such railway embankments. The side slope inclination for the railway embankment is 3H:1V (three horizontal to one vertical).

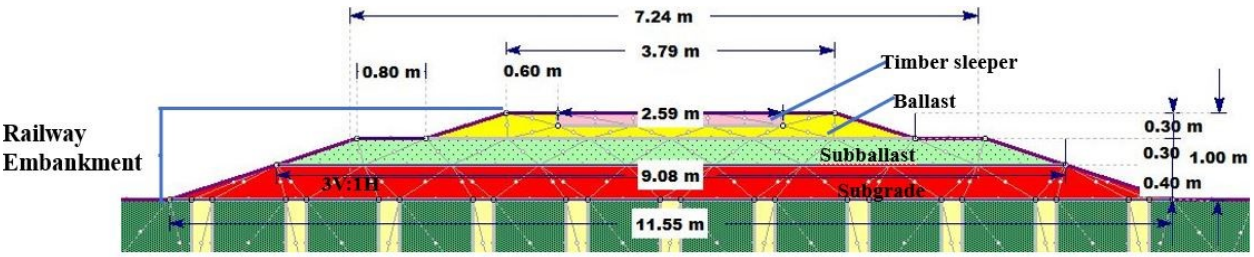

Figure 4.1. Cross-section of the railway embankment component with dimensions (for 3H:1V slope ratio).

As part of conducting a set of parametric studies, the height of the embankment, the wooden piles, and the slope inclination of the subballast and subgrade are considered variables that are investigated. The embankment height ranges from 1 m - 5 m by changing the subgrade height. Taking the subballast and subgrade slope as another variable to study, their slope inclinations are selected as 3H:1V or 2H:1V. The geometric parameters of the wooden pile (length, center-to-center spacing, and diameter) are also investigated in Section 5.23. Additionally, the speed of the train is considered as one variable as it applies equivalent uniform loading at the tie-ballast interface.

In order to complete the geometry of the model, the natural ground under the railway embankment needs to be taken into consideration. As seen in Figure 4.2, the dimensions of the natural ground foundation are set to ensure that the stress is not reflected by the outer boundaries of the model. It has a relationship such that the external boundaries are set at least 3 times the characteristic total length of the railway embankment (Mestat et al. 2017). The dimensions of the natural ground foundation together with the embankment have the following relationships (Figure 4.2):

- Both the right side (d) and left side height (e) of the natural ground is set approximately 1.5 times the total height of both the railway embankment and the bottom of the railway embankment, which can be expressed in Equation (4.1).

$$d = e \approx 1.5\,(g + b) \qquad \text{Eqn (4.1)}$$

- Both the left side and the right side of the exposed natural ground length ((a) and (c)) respectively, is at least equal to 2 times the embankment's bottom (b) which is expressed in Equation (4.2).

$$a = c \geq 2b \qquad \text{Eqn (4.2)}$$

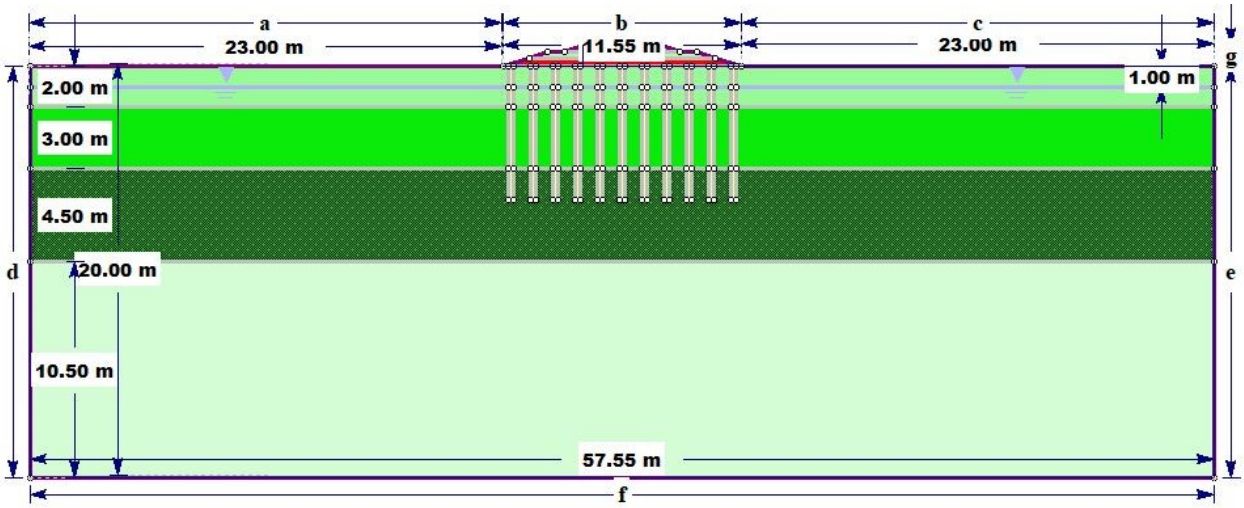

Figure 4.2. Cross-section of the pile-supported embankment for the model with dimensions (for 3H:1Vslope ratio).

The total height of the railway embankment from the top of the natural ground is 1.0m with a corresponding wooden pile length, diameter, and center-to-center spacing of 6.5m, 0.24 m, and 1.08 m respectively as illustrated in Figure 4.4.

In setting the groundwater table in the foundational soil, references were made to the reports of Uthayakumar and Oliver (2018) and Labadz et al. (2010). Uthayakumar and Oliver (2018) reported that the groundwater level of peat was 0.9 m to 1.8 m below the ground surface in Delta and Surrey, British Columbia. Since peatland is controlled by hydrological processes, Labadz et al. (2010) suggest that the groundwater table located at 0.4 -1.0 m below the ground surface is not unusual in North America and Europe. As shown in Figure 4.2, the groundwater table was therefore set to be located at 1.0 m below the bottom of the railway embankment.

4.1.3 Material Properties of Track Component, Natural Ground, and Wooden Pile

Table 4.3. summarizes the properties of the substructure component adopted for the numerical model. Table 4.4. and Table 4.5. provides details on the parameters of natural ground properties and the pile material adopted for the numerical analyses respectively. These parameters are taken from the previous chapter.

Table 4.3. Mechanical properties of the substructure component adopted for the numerical model

Name	Material	γ	Porosity	c	φ	v	E	Permeability
		kN/m^3	-	(kPa)	(°)	(-)	(kPa)	μ (cm/s)
Ballast	Crushed stone	22.0	0.4	0	40	0.25	220×10^3	1.0×10^{-1}
Subballast	Gravel	23.0	0.4	0	35	0.28	250×10^3	1.0×10^{-2}
Subgrade	Gravel and Sand	20.5	0.5	0	38	0.27	110×10^3	1.0×10^{-2}

Note: γ is unit weight; c is cohesion; φ is friction angle; v is Poisson's ratio; E is Young's modulus.

The main body of soft organic soil used in this study as the foundation ground is peat. The values of the material properties of the foundation soil are taken from the ones presented in Chapter 3 (Table 3.7 – Table 3.10). It is modeled as elastic-plastic materials with the failure criterion selected as Mohr-Coulomb. The natural ground of the model is depicted in Figure 4.3.

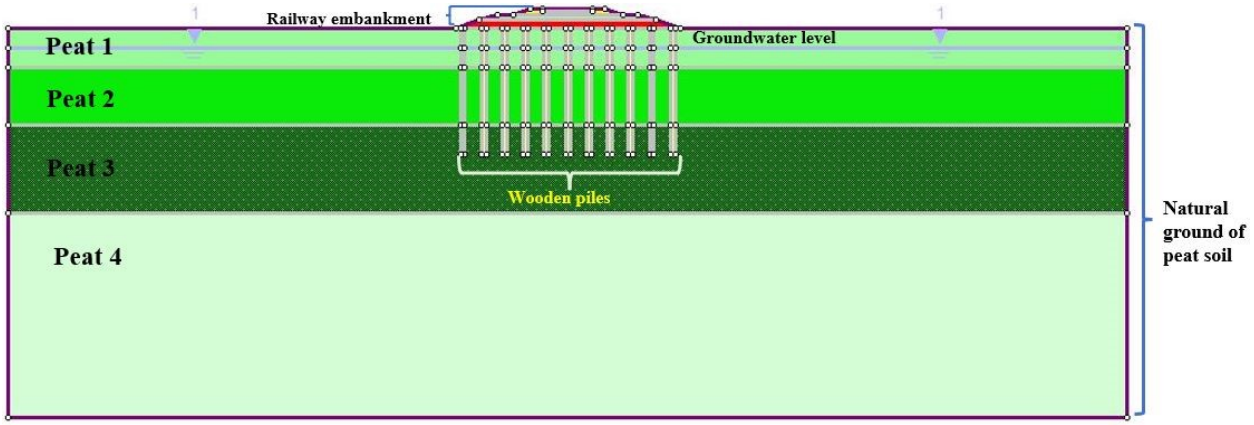

Figure 4.3. The natural ground of the model

Table 4.4. Parameters of natural ground material adopted for the numerical analyses

Material	Unit weight(γ)	Porosity	Cohesion c	Friction angle φ	Poisson's ratio v	Young's modulus E	Permeability μ
	(kN/m^3)	(%)	(kPa)	(°)	v (-)	(kPa)	μ (cm/s)
Peat 1	10.4	59	10	20	0.26	650	$1.0*10^{-1}$
Peat 2	11.5	60	9	22	0.28	687	$1.0*10^{-1}$
Peat 3	11.0	60	10	24	0.30	735	$1.0*10^{-1}$
Peat 4	12.5	59	10	28	0.30	750	$1.0*10^{-1}$

The properties used for the wooden pile element are provided in Table 4.5. The parameters are taken from the previous Chapter. The dimensions for the piles are in accordance with CAN/CSA 056 -M79 (CAN/CSA-056 1980) and are presented in Chapter 5 and the Appendix. The timber piles were modeled as "pile elements with joints" and the slip criterion was set as Mohr-Coulomb. The pile-soil parameters are given in Table 4.6. The dimensions of the piles under the embankment are depicted in Figure 4.9.

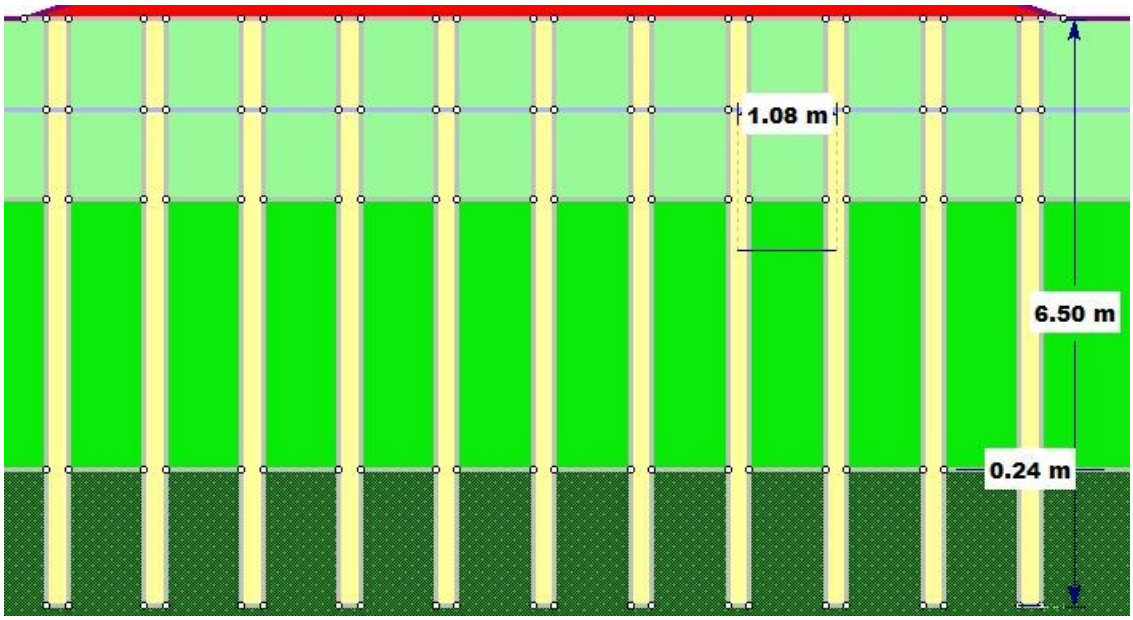

Figure 4.4. Dimensions for the wooden piles under the railway embankment.

Table 4.5. Material properties of the pile used in the numerical analysis

Material	Unit weight γ	Poisson's ratio ν	Young's modulus E
	(kN/m^3)	(-)	(kPa)
Wooden Pile	20.00	0.30	$2.95*10^6$

Table 4.6. Soil-Pile Parameters for the numerical analysis

Model parameter	Soil-Pile	Units
Normal stiffness	2.6	(MPa/m)
Shear Stiffness (MPa/m)	1.4	(MPa/m)
Interface Coefficient	0.11	
Residual Friction Angle (degrees)	23	(°)

4.1.4 Mesh Convergence Study

To develop accurate FE simulated models, the generation of a mesh is an important step. This involves the discretization of the boundaries followed by the selection of an element type made up of nodes. In this thesis, a six noded triangular element (quadratically interpolated triangular element order with midside nodes) was chosen for the FE model element type. This element type was chosen because it is adequate in providing accurate results. A uniform mesh type was chosen for the models.

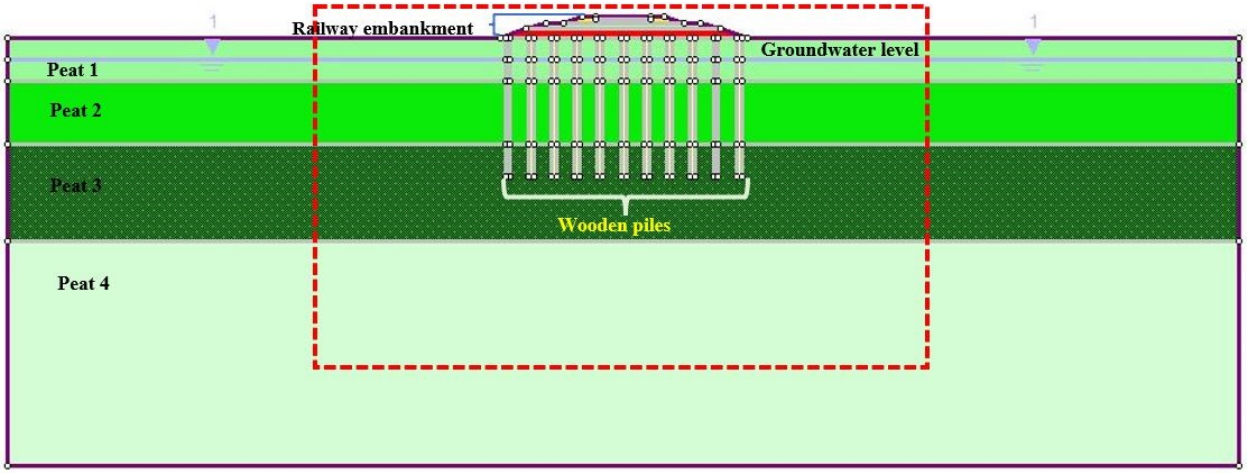

Figure 4.5. The numerical model showing a section with higher boundary discretization and element densities.

However, the embankment structure and potential deformation zone (the region within the rectangular dashed box) had the boundary discretization and element densities manually increased as illustrated in Figure 4.5. This is done so the software could obtain a more reliable and accurate result.

A mesh convergence study is carried out by the analyst to determine the accuracy of the simulation results by increasing the number of mesh elements in the same model. The solution converges to a value that no further augmentation can be achieved usually at a cost of time. To establish a suitable density of the mesh, the advanced mesh region is used in tailoring an average length of the elements on the model boundaries in the zone of interest. It is to be noted that, to discretize the numerical model in Figure 4.5, an approximate number of 600 elements was used for the start. The

number was increased to approximately 16,000 with an increasing number of gradation factors. Thus, in investigating the appropriate mesh element density for this study, the gradation factor was chosen as: 0.15, 0.02, 0.25, 0.3, 0.35, 0.40, 0.45, 0.50, 0.55, 0.6, 0.65, 0.7.

Table 4.7 summarizes the number of nodes and mesh elements for the model with the corresponding FS value in this study. Table 4.7 and Figure 4.6 shows that a critical FS value obtained for the model with high mesh density was 1.67. Thus, it was set as the criterion to calculate the differences in the FS. The FS discrepancy (%) of the numerical model was evaluated through the generation of different mesh settings and discretization densities and by comparing the effect on the FS value. The FS error is calculated by Equation (4.3).

$$Factor\ of\ Safety\ Error\ (\%) = \frac{Factor\ of\ Safety - 1.67}{1.67} \qquad \text{Eqn (4.3)}$$

Table 4.7. The FS and computation time correspond to a different number of mesh elements of the numerical model.

Number of Nodes	Number of Elements	FS	Computation time (min)	FS Error (%)
1361	384	1.92	1.22	14.97
1458	697	1.88	2.87	12.57
1784	855	1.83	3.27	9.58
2476	1191	1.72	10.58	2.99
5373	3644	1.69	13.71	1.19
10616	5957	1.67	20.52	0
14152	9005	1.67	39.49	0
18988	11875	1.67	45.05	0
23423	13456	1.67	57.57	0
27134	16162	1.67	68.74	0

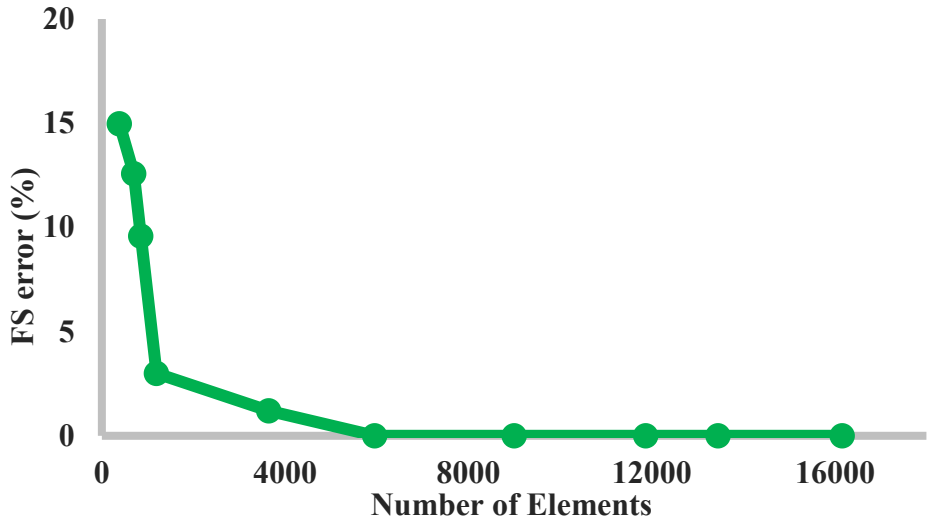

Figure 4.6. Mesh convergence - Critical mesh elements for the numerical model and the corresponding FS error and number of elements.

A 0 % FS discrepancy occurs at 5957 mesh elements as shown in Table 4.7 and Figure 4.6. It can be observed that the mesh converges at this number of elements as the curve reaches 0%. Thus, it could present more accurate and adequate simulation results. After examining the model for a suitable mesh element number to generate a quality solution, the 5957-mesh element number is adopted in this numerical model.

4.1.5 Boundary Conditions in the FEM Model

A suitable boundary must be placed on the model prior to analysis. To prevent lateral movement, the right, and the left side has a restraining boundary in the X direction. The top is without restraints to facilitate the free movement of the nodes in any direction. This helps to appreciate the deformation on the surface. At the bottom of the model, the boundary is restrained in both horizontal (X) and vertical (Y) directions, creating a pinned support. Throughout the entire simulation process, the boundary conditions remain unchanged. Figure 4.6 shows the complete model ready to be computed.

To model the stress and deformation analysis of the model, the time-dependent boundary conditions to analyze the pore pressure generated from the undrained material are defined. The

external boundary conditions for the model in this study are fixed and are described as a no-displacement type for stress analysis. The influence of the loading is considered within the model and disappears beyond the boundaries. In this study, the bottom of the numerical model is designated as a no-flow boundary. This physically allows the groundwater flow to be sub-horizontal mimicking the real behavior of groundwater for the model. Total head boundary conditions applied are solely due to water pressure. The boundary condition adopted for the numerical model influences the accuracy of the solution and are applied to ensure the quality and adequacy of the model.

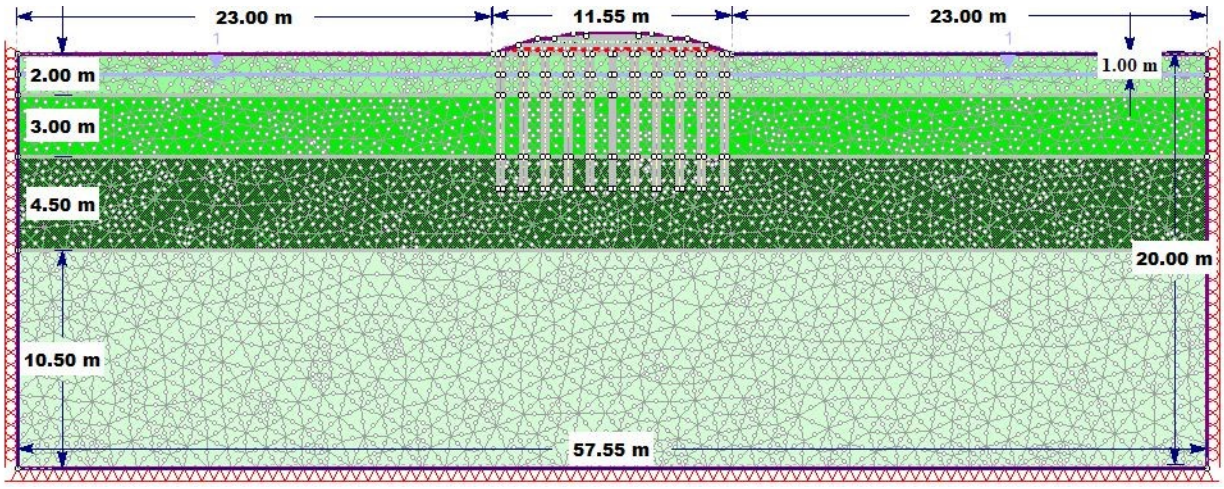

Figure 4.7. Cross section of a complete model.

4.2. Validation and Accuracy of Numerical Model

Embankment basal stability analysis using the shear strength reduction finite element method (Nakamura et al. 2008) is the selected reference study. The selected reference analyses the slope stability of an embankment constructed on soft soil. This reference is chosen because it employs the SSR-FEM with the provision of simulated results. This technique is the same method (also named SSR-FEM method) utilized for analyzing the numerical models in this thesis. The selected reference used both LEM and SSR-FEM to study slope stability. For the purposes of comparison, both simulation results obtained by RS2 as well as results found in the literature are attached.

4.2.1 Model Description

Five different model conditions were investigated for a homogeneous embankment constructed over two layered soil strata. The foundation ground is made up of an upper soft soil layer which is over a lower bearing stratum. The geometry of the model is presented in Figure 4.8. The width and height of the embankment were assumed as 20.0 m and 10.0 m respectively. The thickness of the lower bearing strata and the embankment dimensions are kept constant while that of the upper softer strata is varied. The material properties of the model are given in Table 4.8. Regardless of the soil, Young's modulus was assigned a value of $2x10^4$kPa and Poisson's ratio of 0.3.

According to Ti et al. (2009), the failure criterion for a Mohr-Coulomb model is defined by two parameters (friction angle and cohesion), in addition to a parameter used to describe the flow rule (dilatancy angle, which is caused by using the non-associated flow rule, when modeling an irreversible change in volume as a result of shearing). To make the flow rule non-associated or associated, the dilatancy angle should be less than or equal to the (residual) friction angle respectively.

Table 4.8. Material properties of earth dam and foundation

Layer	Friction angle	Cohesive strength
	φ (°)	c(kPa)
Embankment	35.0	0.0
Soft soil	0.0	35.0
Bearing stratum	0.0	100.0

For all soils the Dilation angle (ψ) = Friction angle (φ)

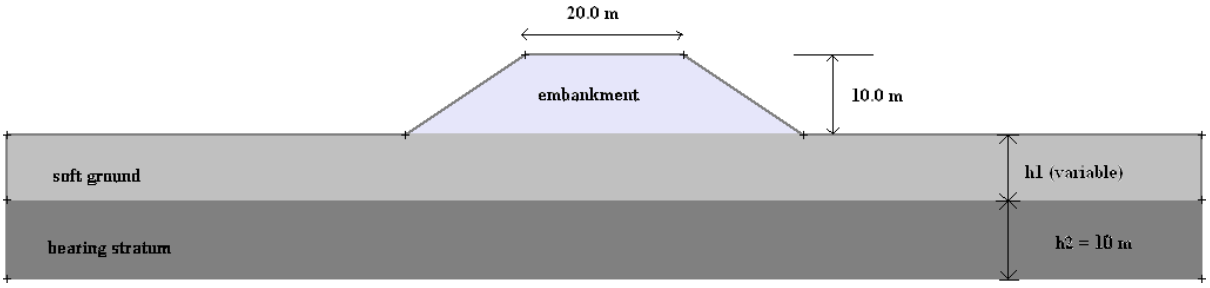

Figure 4.8. The geometry of the embankment for the verification model simulated by RS2.

4.2.2 Results and Discussion

The structure in Figure 4.9 has been investigated under five different conditions, i.e., changing the thickness of upper soft soil from 2.0m, 4.0m, 6.0m, 8.0m, to 10.0m. The results reported by (Nakamura et al. 2008) and RS2, both using SSR-FEM method, are shown as follows. The failure mechanism and critical SRF are mainly compared in Figures 4.9 – 4.13.

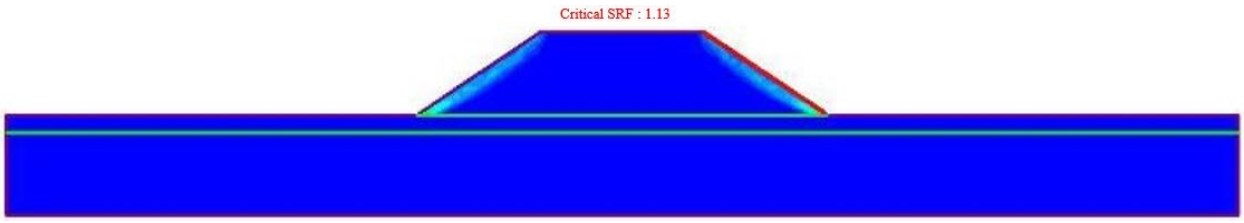

(a)

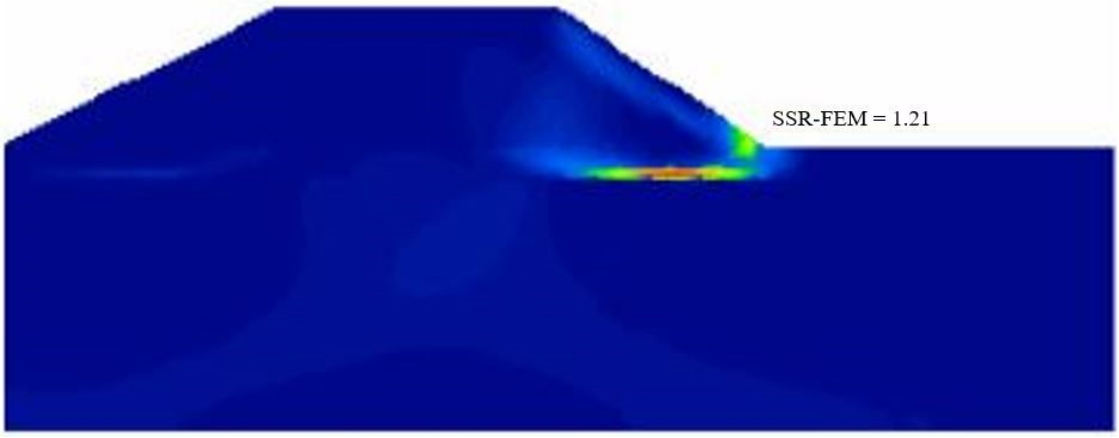

(b)

Figure 4. 9. Comparison of the critical SRF and failure mechanism for the embankment when the height of the soft soil is 2 m (h1=2 m): (a) results simulated by RS2 and (b) results captured in the work of Nakamura et al. (2008).

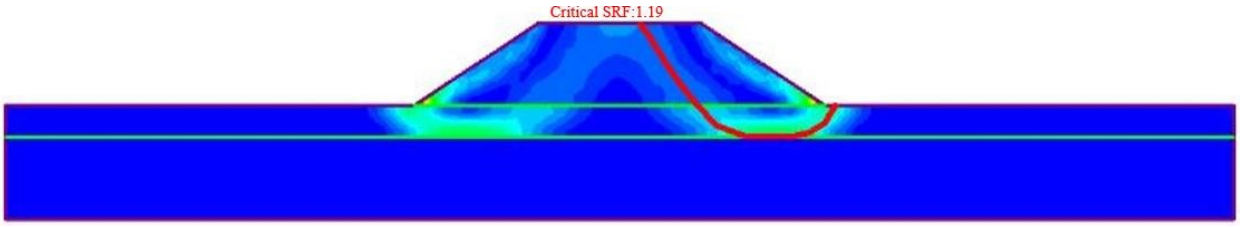

(a)

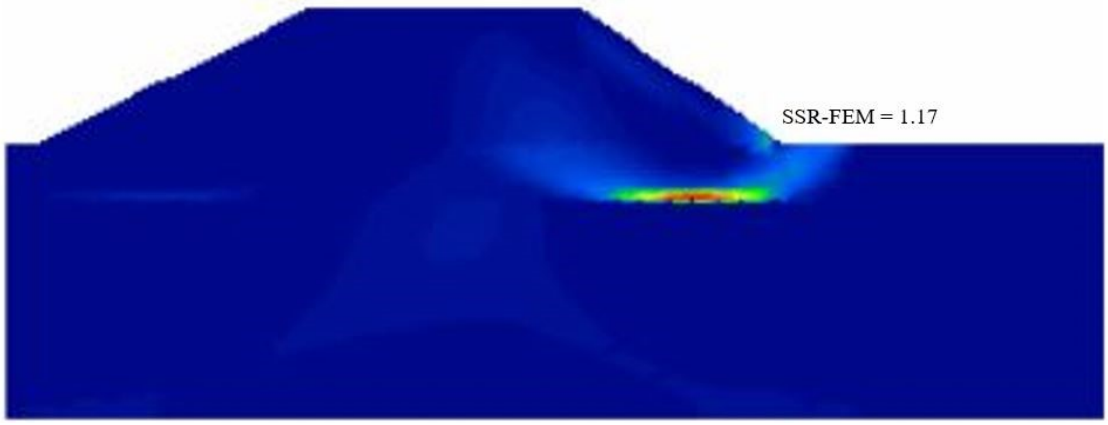

(b)

Figure 4. 10. Comparison of the critical SRF and failure mechanism for the embankment when the height of the soft soil is 4 m (h1 = 4 m): (a) results simulated by RS2 and (b) results captured in the work of Nakamura et al. (2008).

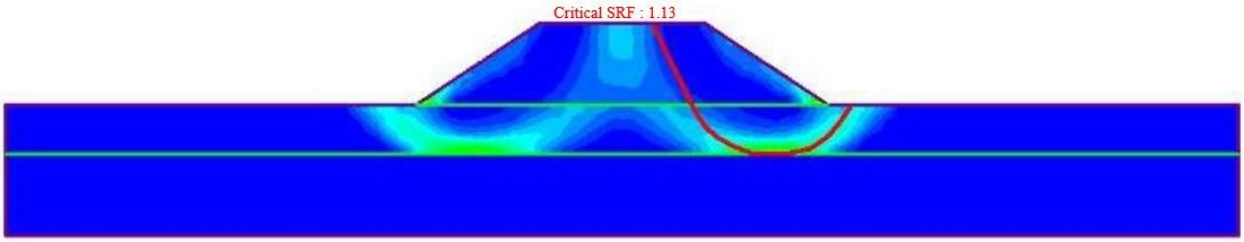

(a)

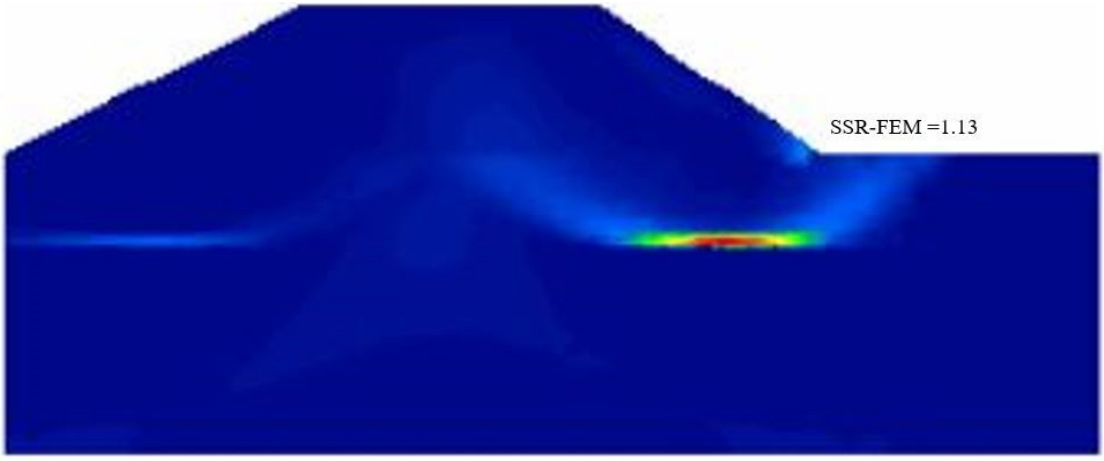

(b)

Figure 4.11. Comparison of the critical SRF and failure mechanism for the embankment when the height of the soft soil is 6 m (h1 = 6 m): (a) results simulated by RS2 and (b) results captured in the work of Nakamura et al. (2008).

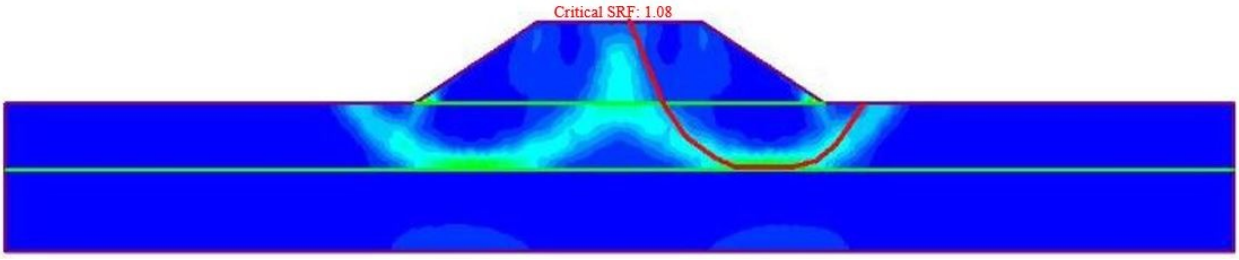

(a)

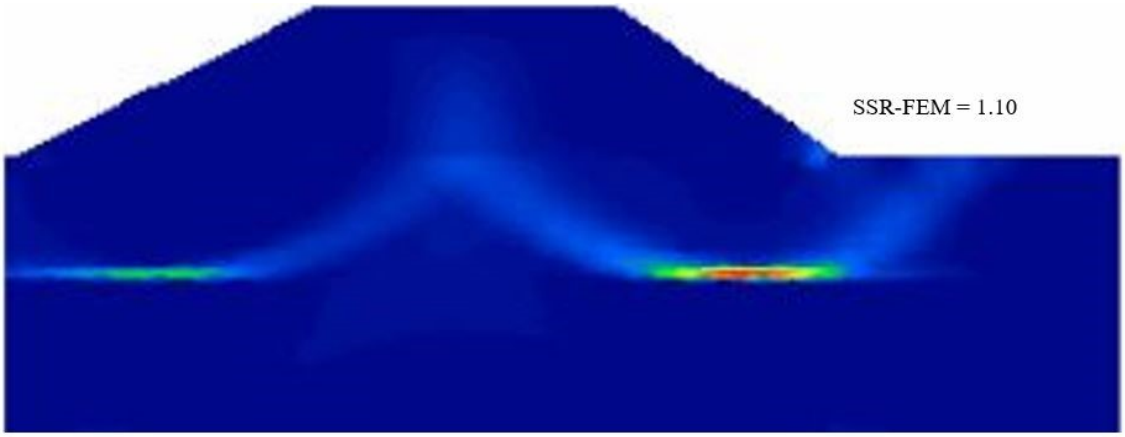

(b)

Figure 4.12. Comparison of the critical SRF and failure mechanism for the embankment when the height of the soft soil is 8 m (h1 = 8 m): (a) results simulated by RS2 and (b) results captured in the work of Nakamura et al. (2008).

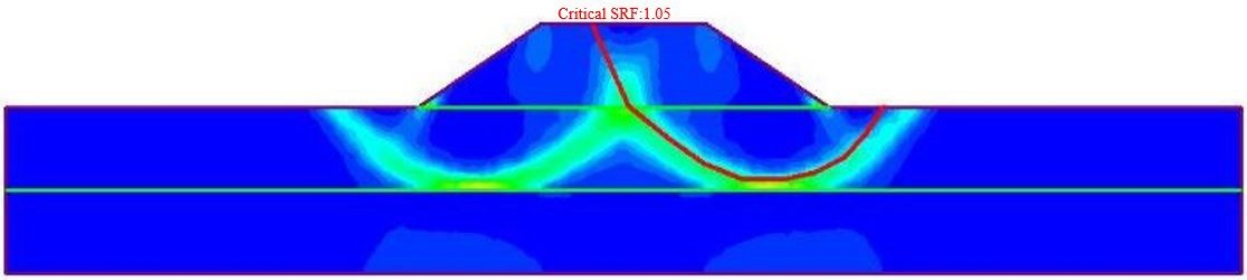

(a)

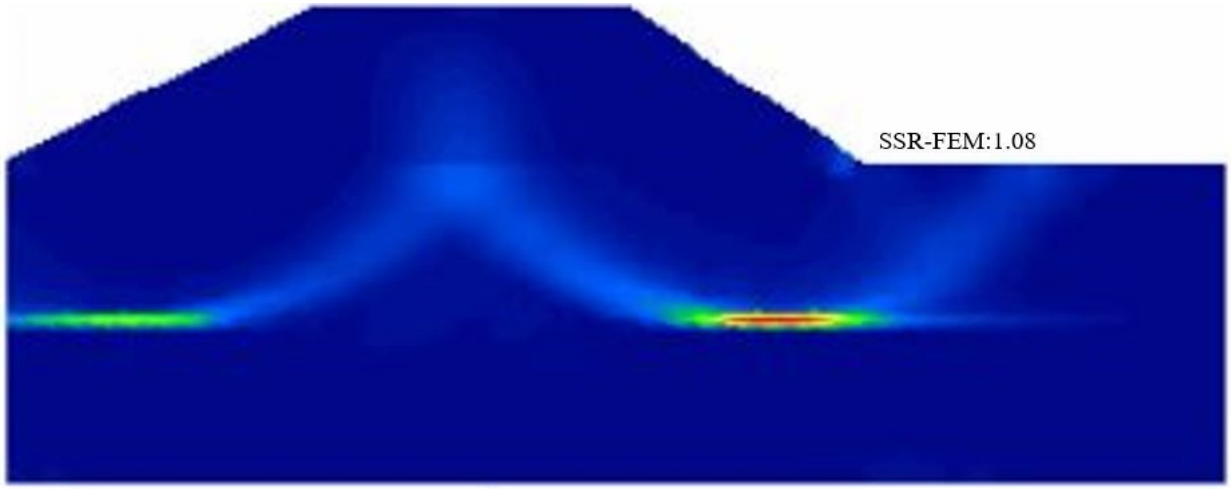

(b)

Figure 4.13. Comparison of the critical SRF and failure mechanism for the embankment when the height of the soft soil is 10 m (h1 = 10 m): (a) results simulated by RS2 and (b) results captured in the work of Nakamura et al. (2008).

Observations from Figures 4.9 - 4.13 and Table 4.9 point out that the critical SRF values computed by RS2 are relatively close to those reported by Nakamura et al. (2008). The critical SRF values obtained from RS2 as well as that reported by Nakamura et al. (2008) both by SSR-FEM and those obtained by LEM in the same reference. Again, it can be seen that three sets of failure mechanisms for the models in Figure 4.11 – 4.13 is consistent as obtained by SSR-FEM for both Nakamura et al. (2008) as well as RS2. Hence, RS2 can be used for analyzing the models in this thesis as the simulation results by RS2 using SSR-FEM proved to be reliable.

Table 4.9. Comparison of FS results obtained by different methods.

Layer thickness of soft soil (m)	FS		
	RS2	Reference	
	SSR-FEM	LEM	SSR-FEM
2	1.13	1.24	1.21
4	1.19	1.22	1.17
6	1.13	1.13	1.13
8	1.08	1.10	1.10
10	1.05	1.08	1.08

CHAPTER 5 DISCUSSION AND ANALYSIS OF SIMULATED FEM MODELS

5.0 Introduction

In this chapter, the simulated results obtained from using RS2 in studying the FEM models will be discussed and analyzed. Considering two different slope ratios (2:1 and 3:1 slope ratios), three models consisting of embankment heights ranging from 1 m to 5 m are discussed in this chapter. Again, three different scenarios are discussed in relation to the models. The first set of models analyzes an embankment on peat without piles (Scenario I). Two separate cases of wooden pile supported embankment are also investigated. One set involves a wooden pile supported embankment without a train load (Scenario II). The other set studied represents a wooden pile supported embankment with recommended various train loads (Scenario III). As part of directly capturing the development of excess pore pressures and stress, a consolidation simulation phase of the embankment was divided into stages of construction. This involved the in-situ condition, pile installation, embankment construction, and traffic load application.

As recommended by the UIC719-R code (International Union of Railways 1994), the minimum allowable FS to ensure adequate performance for railway embankment is 1.3 with an emphasis on geotechnical issues and operational loads. Thus, in this study, the minimum FS adopted is 1.3 in ensuring the satisfactory performance of slopes to meet the deformation tolerances considering the peat soil. A series of sensitivity analyses are conducted to examine the geometric parameters of the piles. This is to identify certain key factors that influence the stabilization of the embankment in reference to pile length, diameter, and spacing. Since the critical SRF and the vertical displacement along the ballast surface directly affects the safety of train operations, it is adopted as a measure of influence for determining the key parameters.

5.1 Staged Construction

For the purposes of appraising the excess pore pressure and settlement for stability analyses of the embankment over the peat soil, it is important to simulate the numerical models to reflect geotechnical scenarios. This is achieved through numerical analysis of staged construction to

consolidation development. The embankment construction was divided into several phases to forecast the time-dependent deformation of the model.

The first phase is recognized as an undrained stage that proceeds with the construction of the embankment. The second and third steps were identified as the installation of the wooden piles and construction of the embankment on the peat soils respectively prior to the train operation. The fourth phase simulates a 24-month consolidation period during the post-construction period. The fifth, sixth, and seven steps simulated train loading under both short-term and long-term conditions. The displacements of embankment layers, settlement of the ground surface, and excess pore water pressure were observed during the process of the numerical analyses. It is necessary to note that the vertical displacement and pore water pressure results used in this study were derived from the data points along the center-line which is representative of the cross-section of the model.

For better consolidation analyzes of the simulated models, a coupled model using Biot's consolidation was incorporated to describe the deformation of the saturated peat soil. The groundwater level is set to be 1 m below the bottom of the railway embankment, as peat soils have groundwater tables located at or within a few meters of the ground surface due to their excessive water content. The selected total head value chosen remained unchanged for all the analyses.

One of the factors that induce settlement in peat soils is groundwater. The groundwater table defines the phreatic surface and zero pore pressure head boundary. It is that location where the phreatic surface separates a saturated zone from an unsaturated zone. At this location, the pore water pressure is under atmospheric conditions, and below it the pore water pressure persists, reducing the shear strength and influencing the stability of the soil. It is assumed that the pores of the soil beneath the phreatic surface are completely filled with water. The significance of the groundwater table is to predict the pore water pressure to perform effective stress analysis. This aids in determining the stress-deformation behavior of the model.

5.2 Scenario I: Embankment on Peat without Wooden Piles

To understand the effectiveness of driven wooden piles under railway embankments constructed on peat soils, an embankment without wooden pile supported models is considered. This model represents an embankment with no piles and no train loads. It serves as the benchmark as it depicts the problematic nature of the peat foundation soil. Thus, the performance of the embankment

constructed on peat without pile support was studied involving two parameters in this case: slope ratio and railway embankment height. This is represented in Figure 5.1 in the schematic dendrograph which outlines a series of parametric studies conducted. A total of 10 cases are studied from 2 groups of models as listed in Table 5.1 which showcases the analyzed cases derived from the above two parameters.

In the preceding chapter, the geometry of the simulation model has been defined and remained unchanged through the analysis. The cases in Scenario I represent an increase in the height of the embankment from 1.0 m to 5.0 m as it is one of the parameters studied.

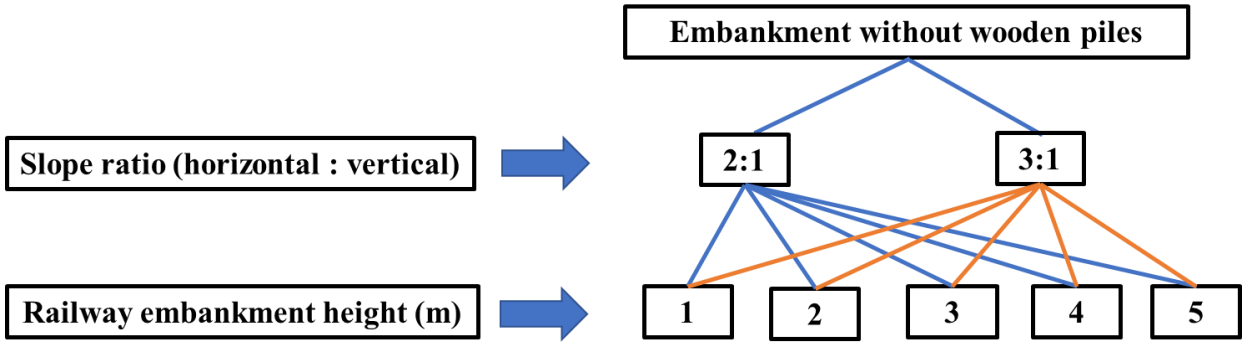

Figure 5.1. Simplified dendrogram of various cases in Scenario I – embankment without piles.

Table 5.1. Cases in Scenario I - embankment without wooden piles.

Groups	Slope ratio	Railway embankment height (m)
Group 1	2:1	1
		2
		3
		4
		5
Group 2	3:1	1
		2
		3
		4
		5

As mentioned earlier, two sets of conditions were analyzed for the slope ratio: 3H:1V and 2H:1V (horizontal: vertical). For descriptive purposes, the model results are displayed below. Figure 5.2 shows the 2H:1V slope ratio for the 1-meter railway embankment height. This gives the maximum shear strain contours and the critical SRF value as well as the total displacement contours for the embankment without wooden piles. The vertical displacement contours and the critical SRF value for this model are shown in Figures 5.3. Figure 5.2 (b) depicts the failure mechanism of the embankment without support. The deformed boundaries graphically depict the inward movement of the embankment boundaries. The deformation of the foundation is clearly visible. This visualization suggest that the predicted failure mechanism comprises a bearing capacity failure. It turns out to be a foundation failure with the ground surface beyond the toe of the embankment slope heaving up. This deformation response of peat foundations is recognized as punching shear failure as the embankment load induces stress on the foundation soil. This is attributed to the embankment resting on an unstable peat soil foundation which is characterized by low shear strength, high water content, and high compressibility. The shear strength of the peat is reduced as a result of the excess pore pressure which decreases the effective confining stress. The dissipation of the pore pressure adversely causes compressibility and permanent settlement. With an increasing settlement, shear bands emanate within the railway embankment as shear stress builds up. This is shown in Figure 5.2 (a).

As the load is continuously exerted by the railway embankment on the weak foundation soil, a gradual failure mechanism begins that triggers a shear punching phenomenon. This type of failure is accompanied by progressive collapse as the capacity of the peat is insufficient to support the weight under repeated loads.

In Figure 5.4, the yielded element distribution of the model displays the fact that tension and stress are built up in the granular embankment. The observation is related to the stiff embankment resting on the soft peat layer.

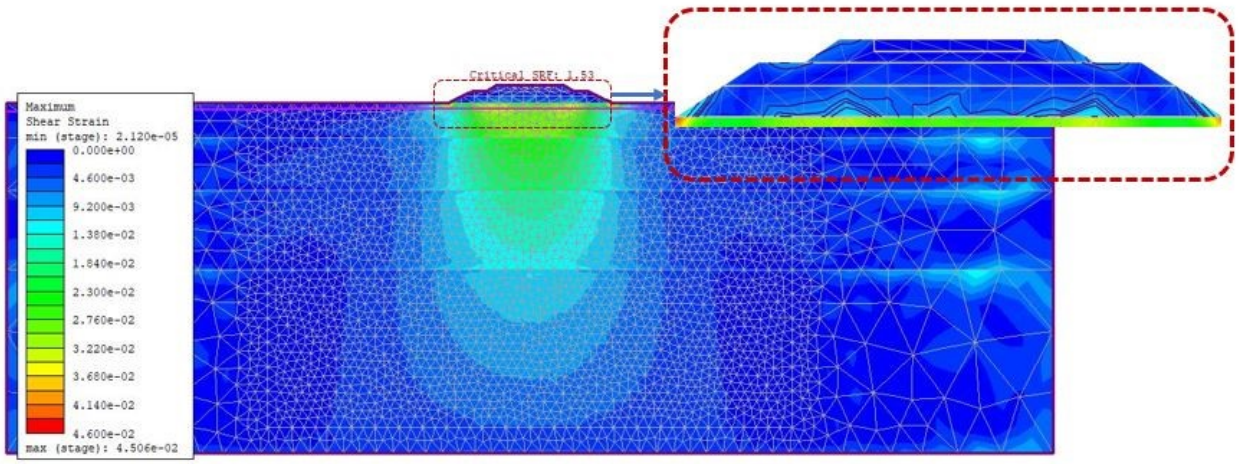

(a)

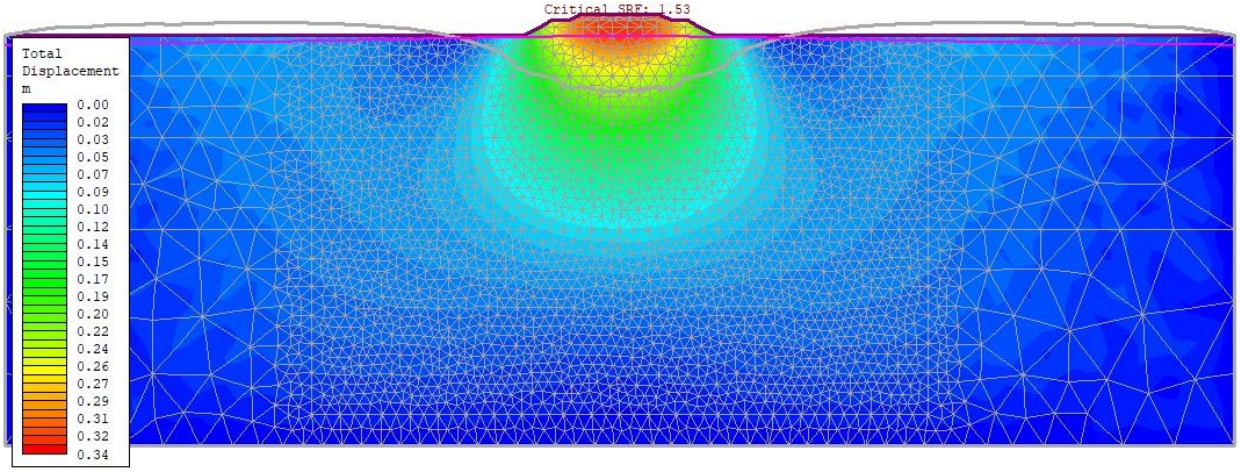

(b)

Figure 5.2. (a) Maximum shear strain contours and the critical SRF value for the embankment without wooden piles model; (b) Total displacement contours of embankment without wooden piles and deformation boundary when failure occurs: slope ratio = 2H:1V, embankment height = 1m.

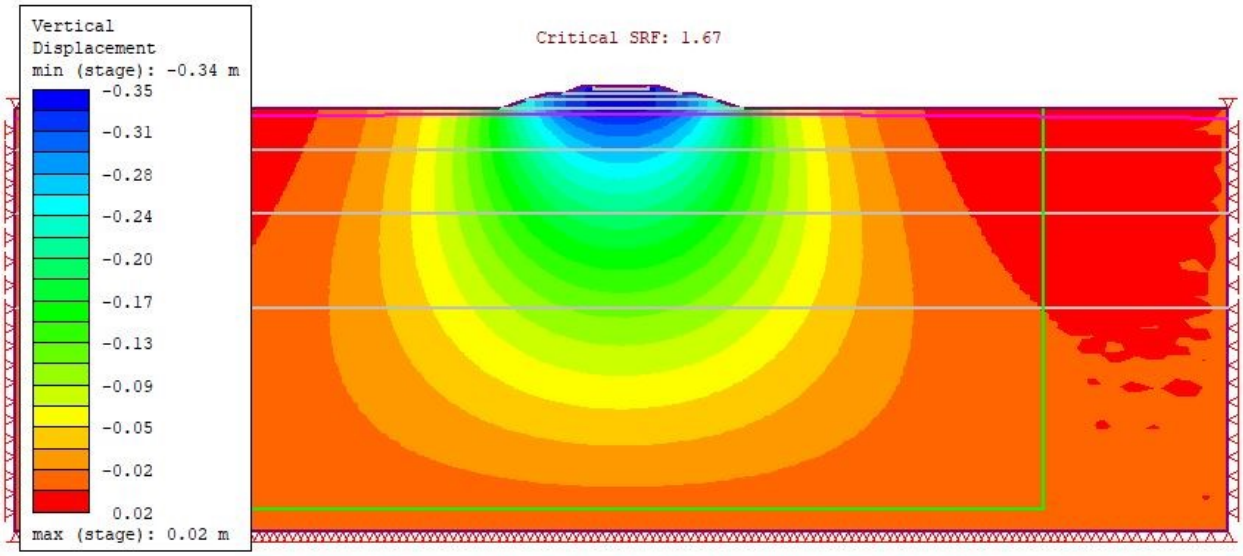

Figure 5.3. Vertical displacement contours and the critical SRF value for the embankment without wooden piles model: slope ratio = 3H:1V, embankment height = 1m.

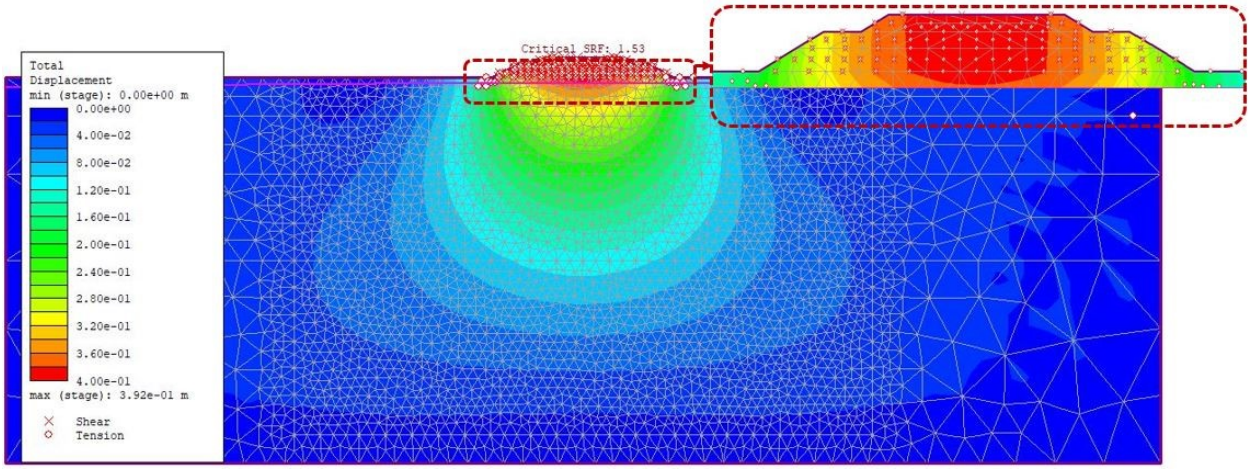

Figure 5.4. Total displacement contours and the critical SRF value for the embankment without wooden piles model: slope ratio = 2H:1V, embankment height = 1m.

Table 5.2. Simulation results of finite element analysis for Scenario I

Groups	Slope ratio	Railway embankment height (m)	FS for embankments without wooden piles	Maximum vertical displacement at center-line (m)
Group 1	2:1	1	1.53	0.39
		2	1.47	0.45
		3	1.30	0.52
		4	1.25	0.60
		5	1.20	0.67
Group 2	3:1	1	1.67	0.35
		2	1.55	0.41
		3	1.40	0.49
		4	1.35	0.58
		5	1.30	0.63

Remarks: * the minimum allowable FS is 1.3 as recommended by the UIC719-R code

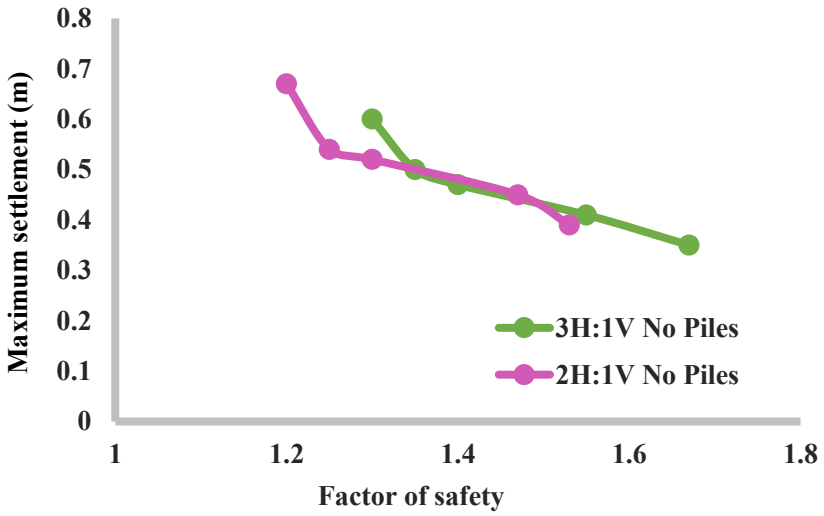

Figure 5. 5. Relationship between maximum vertical displacement and shear strength reduction factor (FS) for embankment without wooden piles models.

Figure 5.5 shows the relationship between FS and the maximum vertical displacement for the five-embankment height considered. The maximum vertical displacement at the end of 24 months is used in explaining the state of the models as it reflects the highest settlement condition for the

consolidation phase. Consolidation settlement of the embankment observed along the centerline of embankments at the ballast and ground surfaces is plotted and presented in Figure 5.6. At 60, 120, and 240 months, very little to no change was observed in the reading of the vertical displacement. As can be seen in Figure 5.6, it can be observed that most of the consolidation settlement will occur in the first 24 months.

Again, the maximum vertical displacement values reported in this study are along the centerline and noted to be on the track at the ballast and ground surface. The maximum vertical displacements recorded for Scenario I was 0.67m corresponding to the 5m embankment height with a 2H:1V slope ratio. The maximum differences decrease when the embankment increases from 1 m to 5 m for 2V:1H are reported in Table 5.3.

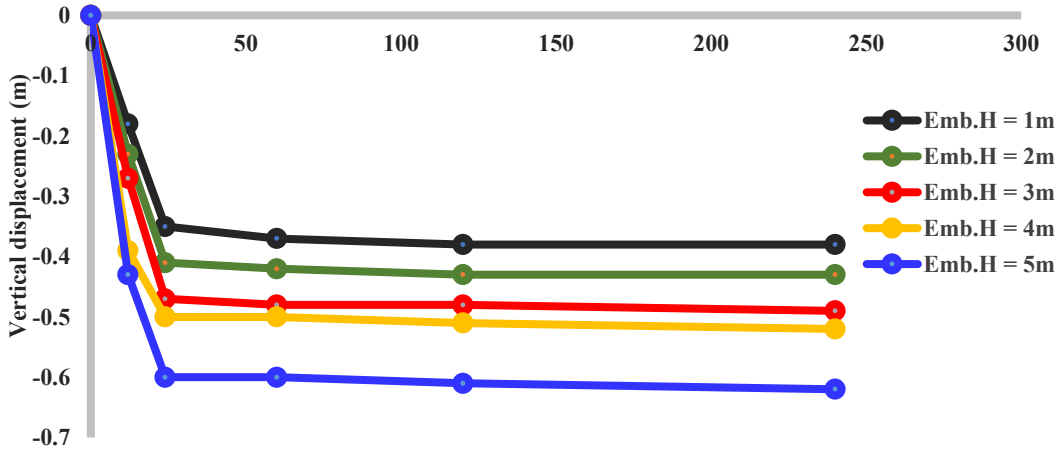

Figure 5. 6. Relationship between vertical displacement and versus time of ballast surface at the centerline of the embankment without wooden piles models.

The maximum values of vertical deformation occur at x = -1.5 m and x = 1.5 m in Figure 5.7(a), which are the positions of the sleeper under the rails referring to the positions in Figure 5.7(b). The results appear to follow a negative linear trend relation where higher FS produces lower vertical displacement.

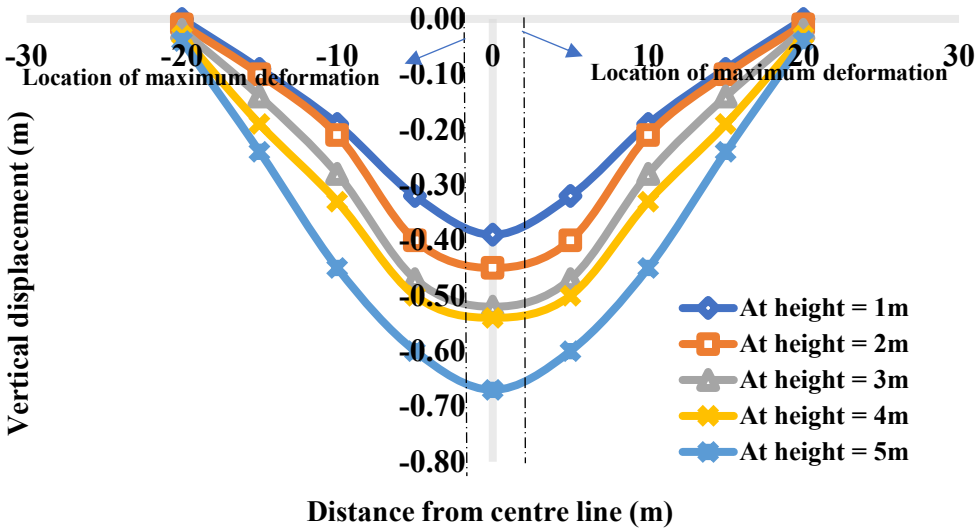

(a)

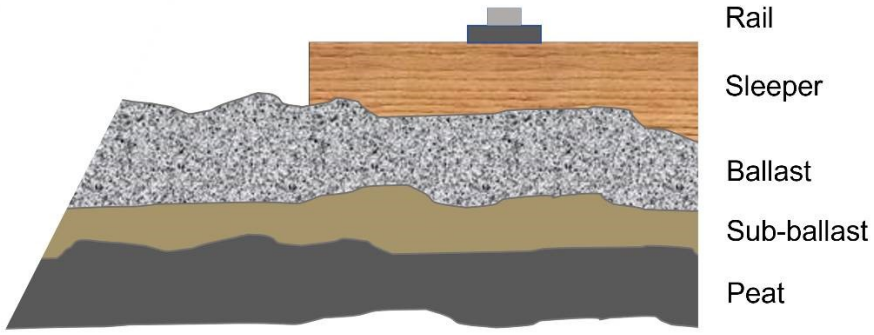

(b)

Figure 5. 7. (a) Vertical displacement of ballast surface at centerline of the embankment without wooden piles models km/h; (b)Simplified cross-section of railway embankments.

Table 5.3. Maximum settlement difference (%) for 2H:1V slope ratio

Embankment Height	Settlement of embankment		Settlement of Peat	
(m)	(m)	(%)	(m)	(%)
1	0.35	41.7	0.40	41.8
2	0.41	31.7	0.49	26.9
3	0.47	21.7	0.55	17.9
4	0.50	16.7	0.62	7.4
5	0.60	0.0	0.67	0.0

Results in Table 5.2 shows that increasing embankment height reduces the critical SRF value. Simultaneously, a lower critical SRF value results in higher vertical displacement. Again, FS results in Table 5.2 evidently establish the fact that flatter slopes yield higher critical SRF.

5.3 Scenario II: Wooden pile supported railway embankments

This scenario analyzes the influence of wooden piles as a support system on the performance of the embankment constructed on peat. Three factors (slope ratio, railway embankment height, and wooden piles) are discussed in this case. The wooden pile parameters considered are the center-to-center pile spacing, pile diameter, and pile length.

The designated pile size for the module creation is given in Table 1 of the Appendix. This selection was based on CAN/CSA 056 -M79 (CAN/CSA-056 1980) which outlines the recommended guide to the selection of pile sizes. Again, the pile spacing which was selected as the center-to-center spacing = 4.5D is also presented in the Appendix. The selection is based on the recommended pile-to-pile spacing for driven timber piles (Timber Pile Design and Construction Manual 2016; Hannigan et al. 1997). The equation used in estimating the pile length is also given in the Appendix. Five different pile sizes were considered in the analysis.

A FS of 2 is mostly recommended when static load analysis is often used for piles in estimating the ultimate capacity (Timber Pile Design and Construction Manual 2016). FS results obtained for the cases modeled are given and discussed. Figure 5.8 summarizes all combinations of the parameters studied in these models under wooden pile-supported embankment conditions. A total of 10 different cases are investigated in Scenario II which are broadly categorized into 2 main

groups as tabulated in Table 5.4. The groupings are based on two sets of conditions as analyzed in the previous scenario for the slope ratio: 3H:1V and 2H:1V (horizontal: vertical). As before, the height of the embankment ranges from 1.0 m to 5.0 m as it is one of the parameters studied.

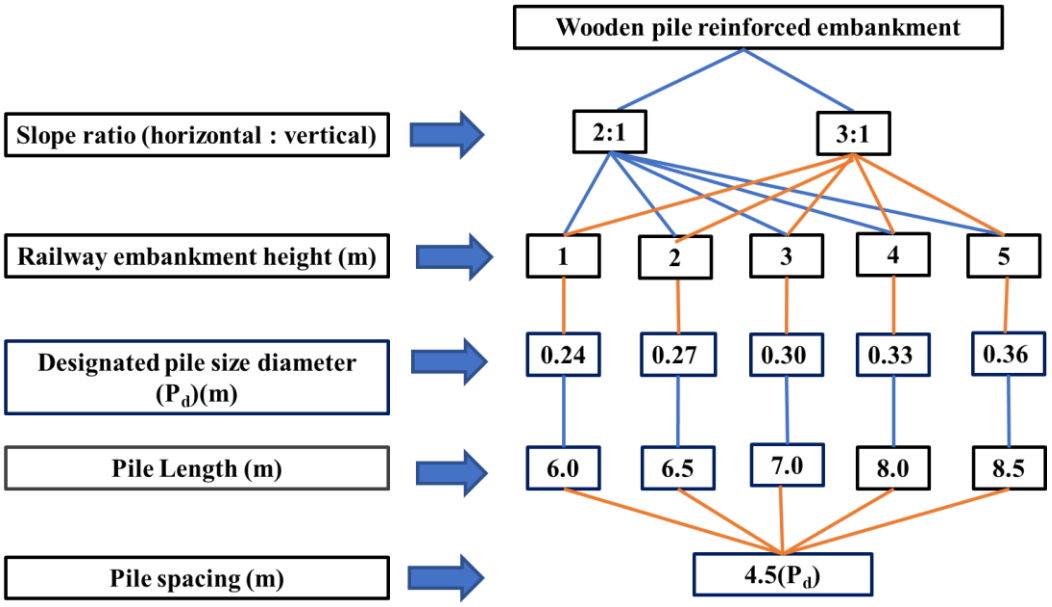

Figure 5.8. Simplified dendrogram of various cases in Scenario II – Wooden pile-supported embankments.

Table 5.4. Cases in Scenario II - Wooden pile-supported embankments.

Groups	Slope ratio	Railway embankment height (m)	Designated pile size (m)	Calculated Pile length (m)	Estimated Pile Spacing (m)
Group 1	2:1	1	0.24	6.0	1.08
		2	0.27	6.5	1.20
		3	0.30	7.0	1.35
		4	0.33	8.0	1.49
		5	0.36	8.5	1.62
Group 2	3:1	1	0.24	6.0	1.08
		2	0.27	6.5	1.20
		3	0.30	7.0	1.35
		4	0.33	8.0	1.49
		5	0.36	8.5	1.62

To compare to the embankment without support (Scenario I), the example for the 1m presented for the results in this scenario has the same model structure and dimension as in the previous one. Figure 5.9. shows the maximum shear strain contours and the critical SRF value for the wooden pile-supported embankment model. The pile diameters of this model were considered as 0.24 m, 0.27 m, 0.30 m, 0.33 m, and 0.36 m, taking into account increasing embankment height. Correspondingly, the resulting critical SRFs and vertical displacement contours obtained through the simulation have been presented in Figure 5.10. Table 5.5. lists the simulation results of finite element analysis for Scenario II.

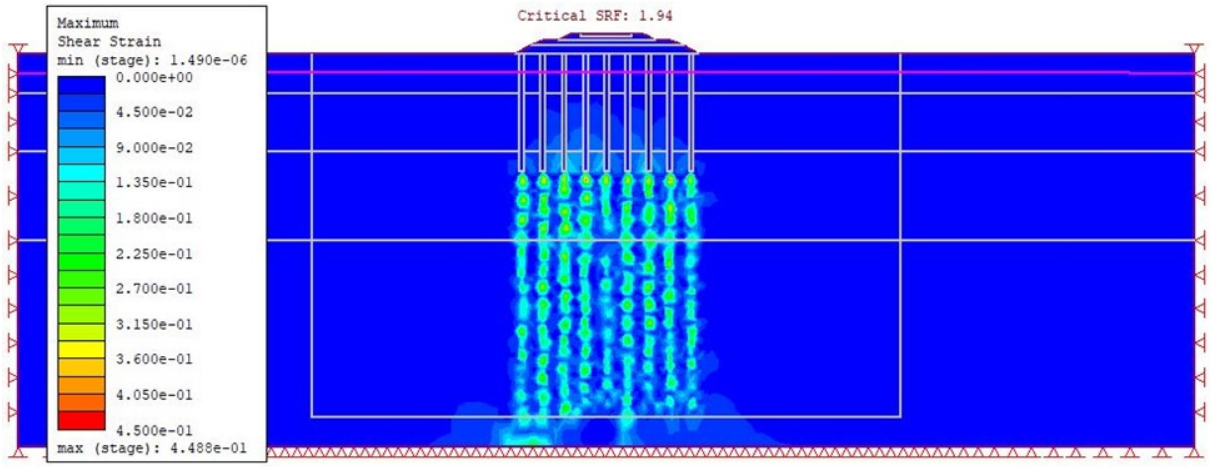

Figure 5.9. Maximum shear strain contours and the critical SRF value for the wooden pile reinforced embankment model: slope ratio = 2H:1V, embankment height = 1m.

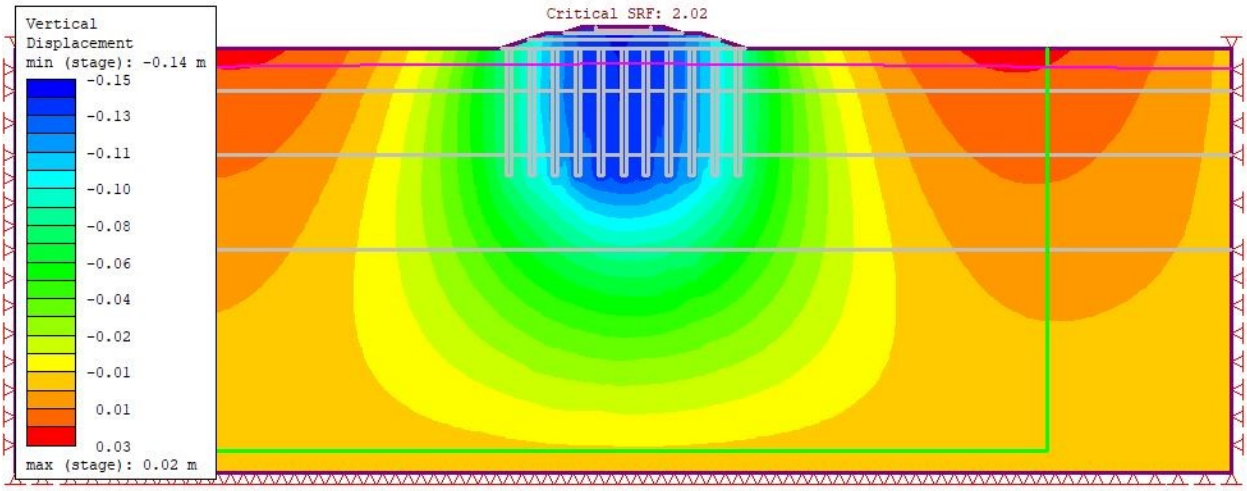

Figure 5.10. Vertical displacement contours and the critical SRF value for the embankment with wooden piles model: slope ratio = 3H:1V, embankment height = 1m.

Table 5.5. Simulation results of finite element analysis for Scenario II

Groups	Slope ratio	Railway embankment height (m)	Designated pile size (m)	Calculated Pile length (m)	Estimated Pile Spacing (m)	FS_{wp}	V_{md}
Group 1	2:1	1	0.24	6.0	1.08	1.94	0.19
		2	0.27	6.5	1.20	1.83	0.24
		3	0.30	7.0	1.35	1.73	0.29
		4	0.33	8.0	1.49	1.65	0.38
		5	0.36	8.5	1.62	1.57	0.44
Group 2	3:1	1	0.24	6.0	1.08	2.02	0.17
		2	0.27	6.5	1.20	1.92	0.21
		3	0.30	7.0	1.35	1.83	0.27
		4	0.33	8.0	1.49	1.72	0.33
		5	0.36	8.5	1.62	1.61	0.41

Remarks: * the minimum allowable FS is 1.3 as recommended by the UIC719-R code. FS_{wp} is the Factor of safety for the embankment with piles; V_{md} is the maximum vertical displacement at center-line

Owing to the installation of the wooden piles under the railway embankment within the peat soil, Scenario II models resulted in generating higher FS with corresponding minimal vertical displacement (settlement) as compared with the Scenario I model. This is a result of the section of the embankment being supported on the wooden piles. For example, for the 2H:1V slope ratio, the critical SRF for the 1 m embankment increases to 1.92 with the wooden piles beneath it. Meanwhile, the value of the Scenario I model was 1.53 (c.f. Table 5.5 and 5.2 respectively). This implies an assured standard level of performance suitable for controlling settlement and stability. The highest FS recorded is 2.02 for the 3H:1V slope ratio and the highest settlement is 0.44 m for the 2H:1V slope ratio. Again, flatter slopes are more effective in increasing FS value.

Figure 5.11 depicts the corresponding critical FS by SSR-FEM versus the maximum vertical displacements under different wooden pile parameters (pile spacing, pile length, and pile diameter).

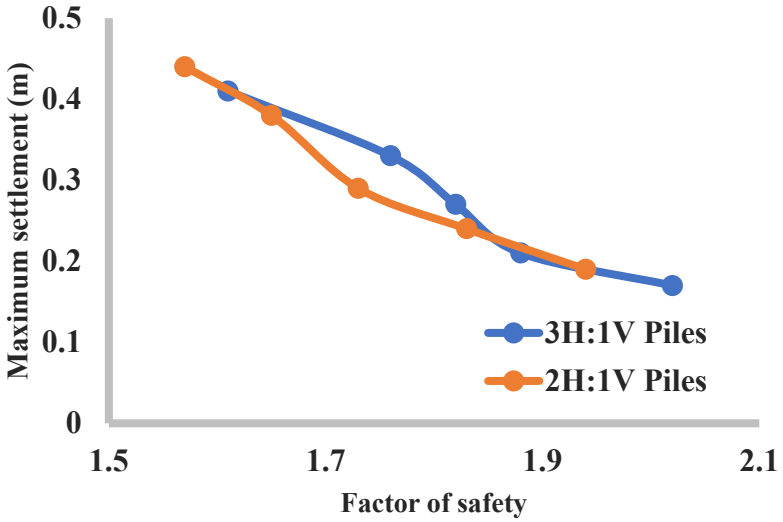

Figure 5. 11. Relationship between maximum vertical displacement and shear strength reduction factor (FS) for 2H:1V and 3H:1V models.

Similar to the previous scenario, the curves of the graphs showed a downward trend. This is interpreted as an increase in FS value generating a reduced vertical displacement. In addition, it can be seen from Figure 5.11 that as the railway embankment height increases, slope stability is more affected by an increase in vertical displacement. The trends are consistent with the case of an embankment without wooden piles.

Comparing simulated results in Tables 5.2 and 5.4, it can be inferred that the wooden piles have a more significant impact on the models for both slope ratios of 2H:1V and 3H:1V. The FS differences are evaluated by Equation (4.1), as follows:

$$D_F = \frac{FS_P a - FS_N a}{FS_P a} \qquad \text{Eqn (5.1)}$$

where D_F is the difference in FS value, p is the embankment with wooden piles and N is the embankment without wooden piles, and a is the embankment height (a = 1, 2, 3, 4, 5). For example, for the 2H:1V slope ratio if FS results for embankments without wooden piles are compared to the wooden piled supported embankment when the embankment height is 1 m, the calculation of D_F is

$\frac{FS_2 1 - FS_2 1}{FS_2 1} = \frac{1.94 - 1.53}{1.94} = 21.1\%$. This means that the 1 m embankment FS value increased by 21.1

% after the embankment was supported with wooden piles. The percentage differences for both 2H:1V and 3H:1V FS values are given in Tables 5.11 and 5.12 respectively.

Higher FS results are generated for wooden piles supported embankment. Additionally, a reduction was observed in the vertical displacement when the embankment was stabilized with the wooden piles.

5.4 Scenario III: Wooden Pile Supported Embankment and Train Loads Conditions

Models in Scenario III are derived by the addition of a freight train moving with different speeds to Scenario II and observing the effect of these train speeds through the simulation of railway operation. Thus, the influence of different train speeds on the ballast surface will be investigated. To design against both foundation failure and excessive settlement, there is a need to evaluate the suitability of the foundation in the short and long terms. For short term analysis, the end of the consolidation period is set as a threshold where settlement observations show vertical displacement that is leveled off with no further increment. With regards to long term analysis, the end of the consolidation period in the short-term analysis is used as the starting threshold to observe the settlement behavior of the embankment over time. This study considers a 0, 12, 24, 60, 120, and 240 months period phase for the consolidation analysis. Both short-term and long-term vertical displacement was observed to know the different settlement magnitudes, rates, and patterns.

Figure 5.12 summarizes the six key parameters studied in the model for train loads in the dendrogram. The maximum safe train speed is searched in a range of 0 mph (0 km/h) to 75 mph (120 km/h). To determine the maximum allowable train speed for safe performance, the set of train speeds mentioned is considered. Table 5.6 lists all combined cases, with 2 groups in total, consisting of 36 cases. The controlled settlements of ballasted track settlement within acceptable limits of the design criteria adopted for this thesis is a settlement rate of 3 cm/year as recommended by the Chinese Railways (Wang et al. 2014).

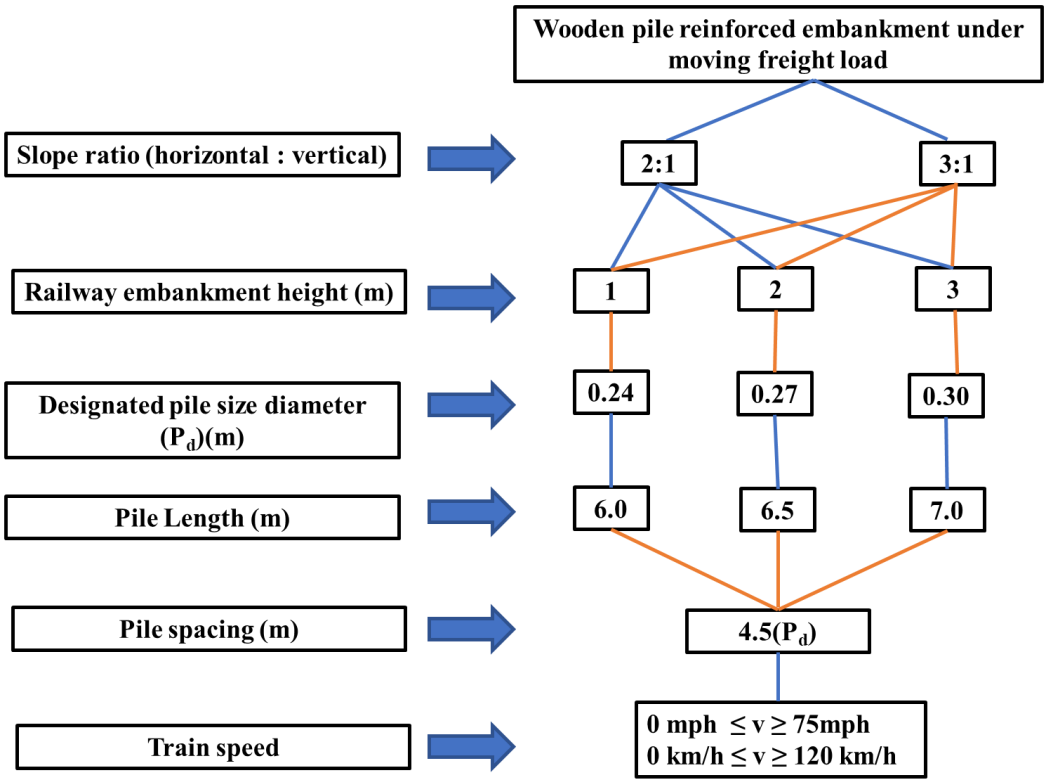

Figure 5.12. Simplified dendrogram of various cases in Scenario III – Wooden pile-supported embankments and freight train loads conditions.

The train speeds listed in this process were calculated in the previous chapter and are in accordance with the train load applied to the sleepers. The starting train speed is set as 0 mph (0 km/h) to search for a possible slope failure state with a maximum speed set to 75 mph (120 km/h).

Table 5.6. Cases in Scenario III- Wooden pile-supported embankments with train load conditions

Groups	Slope ratio	Railway embankment height (m)	Designated pile size (m)	Calculated Pile length (m)	Estimated Pile Spacing (m)	Number of corresponding train speeds (mph or km/h)
Group 1	2:1	1	0.24	6.0	1.08	6
		2	0.27	6.5	1.20	6
		3	0.30	7.0	1.35	6
Group 2	3:1	1	0.24	6.0	1.08	6
		2	0.27	6.5	1.20	6
		3	0.30	7.0	1.35	6

With an initial starting speed of 0 km/h (0 mph), the train speed is sequentially increased by an additional 24 km/h (15 mph) until it reaches 120 km/h (75 mph) in search of slope failure. Slope failure has earlier been defined as the value of FS less than 1.3.

The critical SRF results of the models for Scenario III which considers the train load on the railway embankment are summated in Tables 5.7 to 5.10 for both short-term and long-term analysis. In the same Tables, the speed of the train converted to Average Ballast Pressure (ABP) (kPa) for each case is listed. The short-term and long-term vertical displacement distributions caused by the six train speeds considered (0, 24, 48, 72, 96, 120 km/h) are depicted in Figures 5.15 and 5.16. This is to further explain the relationship between the FS and the vertical displacement when the moving freight train loads are considered. The graphs clearly evince that both the railway embankment as well as the ground moves downward with an increasing trainload; the peat foundation soil is compressed by the applied trainloads.

For some cases in Tables 5.7 to 5.9, the resulting FS values are less than 1.3 which is the required FS for slopes to perform satisfactorily in this thesis. For this reason, the freight trains cannot stop or pass the track, and there is no acceptable safe train speed for models that yielded unsatisfactory results.

Table 5.7. FS simulation results for short term analysis of FEM for wooden pile supported embankment with train load conditions for 2 H :1V slope ratio

Average Ballast Pressure (ABP) (kPa)	236.24	268.73	301.21	333.70	366.18	398.66
Embankment Height (m)	SRF results					
1	1.72	1.68	1.62	1.60	1.57	1.51
2	1.55	1.53	1.49	1.45	1.41	1.40
3	1.40	1.37	1.27	1.25	1.22	1.21

Table 5.7. FS simulation results for short term analysis of FEM for wooden pile supported embankment with train load conditions for 3H :1V slope ratio

Average Ballast Pressure (ABP) (kPa)	236.24	268.73	301.21	333.70	366.18	398.66
Embankment Height (m)	SRF results					
1	1.77	1.70	1.64	1.61	1.59	1.57
2	1.57	1.54	1.49	1.45	1.40	1.37
3	1.51	1.49	1.46	1.38	1.31	1.30

Table 5.8. FS simulation results for long term analysis of FEM for wooden pile supported embankment with train load conditions under 2H :1V slope ratio

Average Ballast Pressure (ABP) (kPa)	236.24	268.73	301.21	333.70	366.18	398.66
Embankment Height (m)	SRF results					
1	1.74	1.70	1.67	1.63	1.60	1.58
2	1.59	1.57	1.55	1.53	1.47	1.43
3	1.42	1.37	1.29	1.26	1.23	1.21

Table 5.9. FS simulation results for long term analysis of FEM for wooden pile supported embankment with train load conditions for 3 H :1V slope ratio

Average Ballast Pressure (ABP) (kPa)	236.24	268.73	301.21	333.70	366.18	398.66
Embankment Height (m)	SRF results					
1	1.81	1.75	1.70	1.66	1.59	1.57
2	1.64	1.59	1.52	1.47	1.43	1.37
3	1.57	1.49	1.46	1.38	1.37	1.30

By way of precisely demonstrating the influence of train loads on the models' FS value, Figures 5.13 to 5.16 is used as an example to show the results for both short-term and long-term analysis. Again, the maximum shear strain profile and the vertical displacement of the selected models are depicted in the same figures with a freight load.

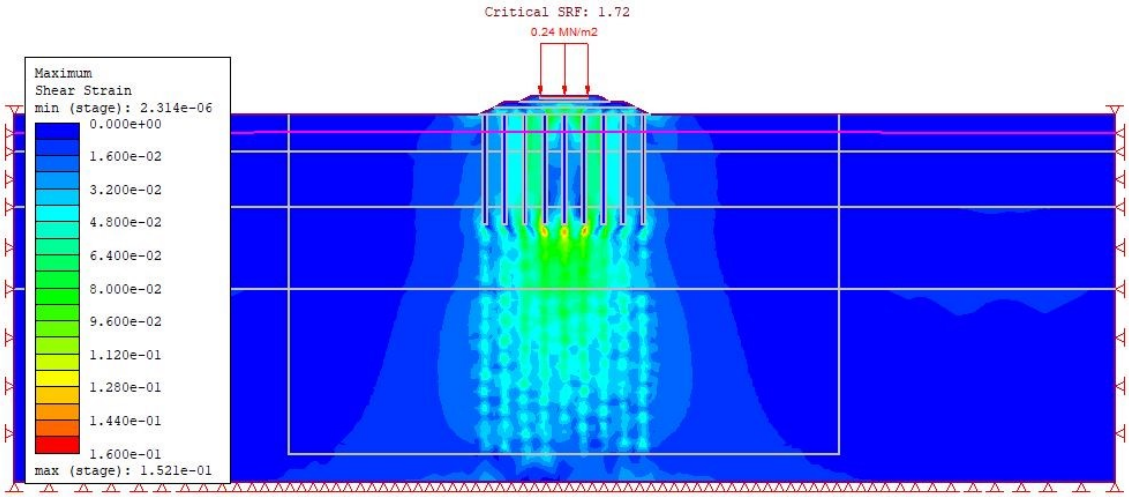

Figure 5.13. Short-term analysis results for maximum shear strain contour for the model with slope ratio = 2H:1V, embankment height = 1 m and an AVP = 236.24 kPa.

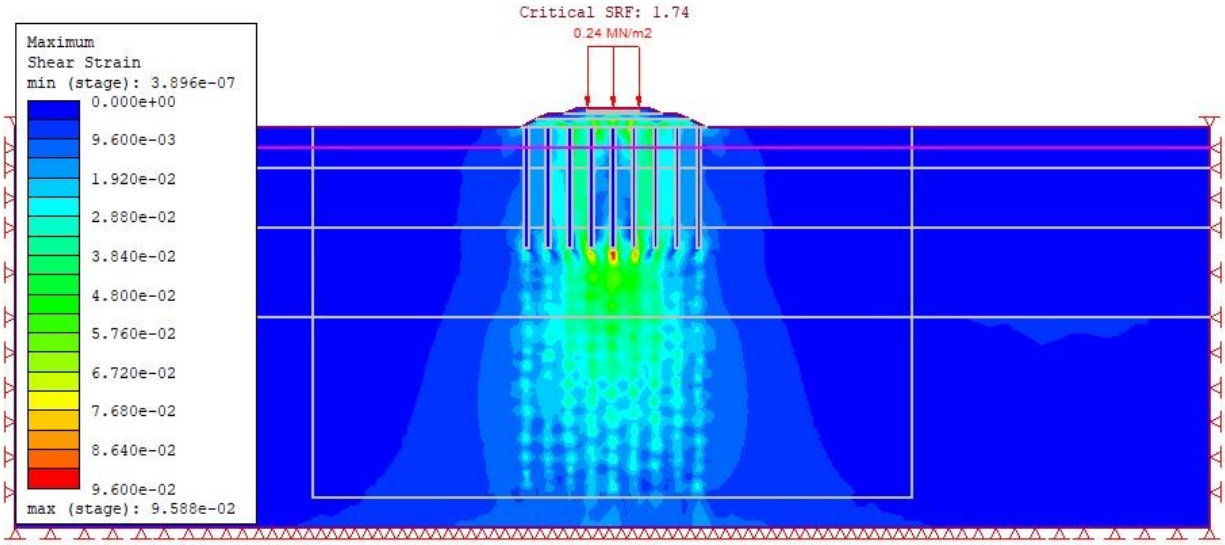

Figure 5.14. Long-term analysis results for maximum shear strain contour for the model with slope ratio = 2H:1V, embankment height = 1 m and an AVP = 236.24 kPa.

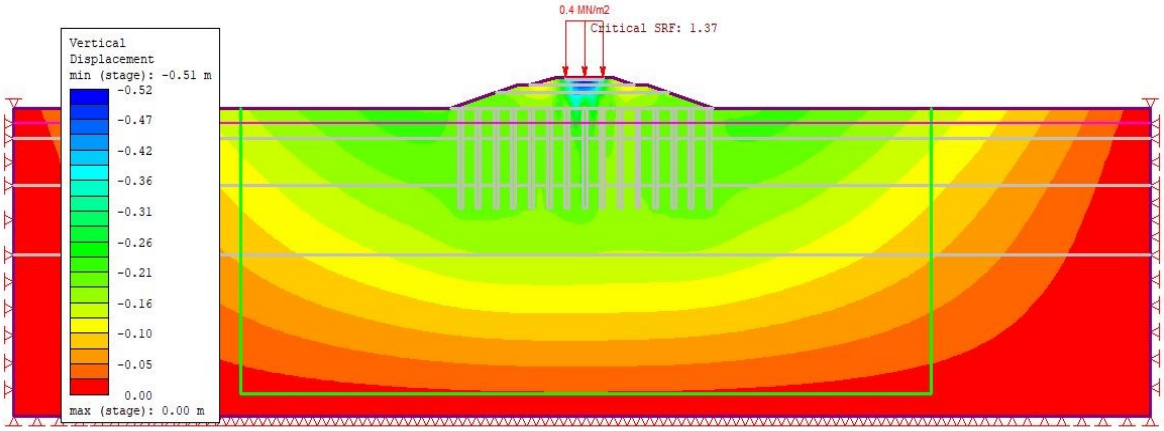

Figure 5.15. Short-term analysis results vertical displacement contour for the model with slope ratio = 2H:1V, embankment height = 2 m and an AVP = 398.66 kPa.

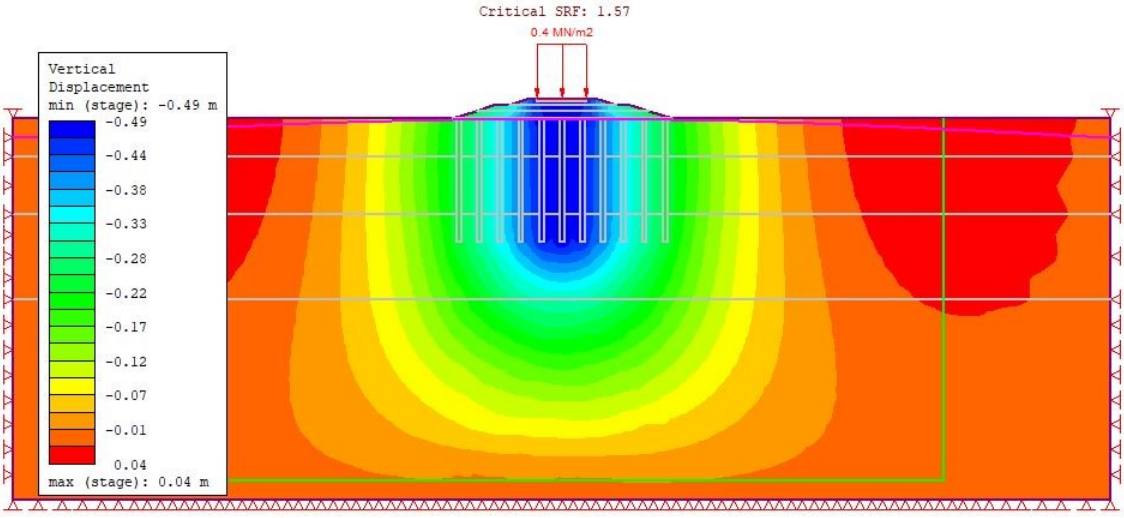

Figure 5.16. Long-term analysis results for vertical displacement contour for the model with slope ratio = 3H:1V, embankment height = 2 m and an AVP = 398.66 kPa.

The results of FS tabulated in Tables 5.6 to 5.9 for the models in Scenario III with a stationary train on the railway embankment which yields values less than 1.3 are interpreted as having unstable slopes. That implies that, for those models, it is safer for the freight train to avoid passing or parking on the track. When the moving freight train loads are considered, Figures 5.17 and 5.18 directly reflect that the application of external train loads on models can reduce slope stability. In addition, based on the plot pattern of models in Figures 5.17 and 5.18, increasing train speed increases the value of vertical displacement.

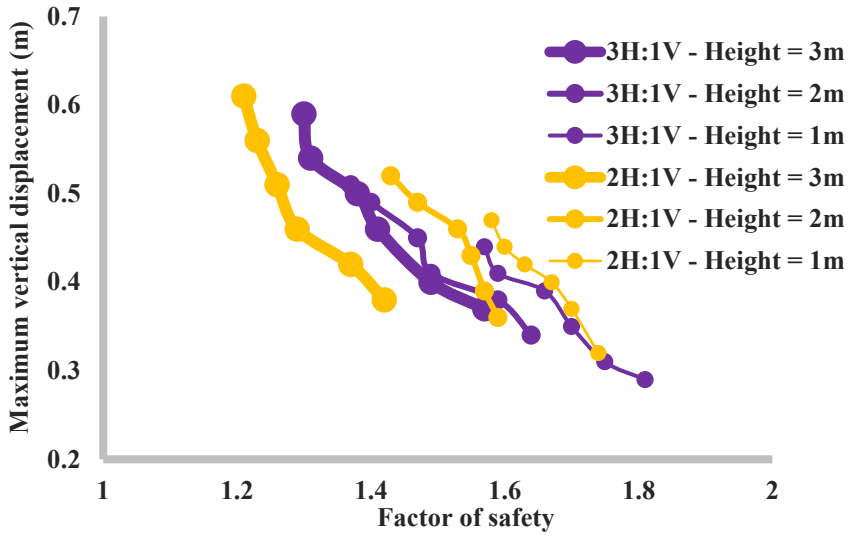

Figure 5.17. Short-term Relationship between maximum vertical displacement and shear strength reduction factor (FS) caused by the six different train speed for 2H:1Vand 3H:1V models.

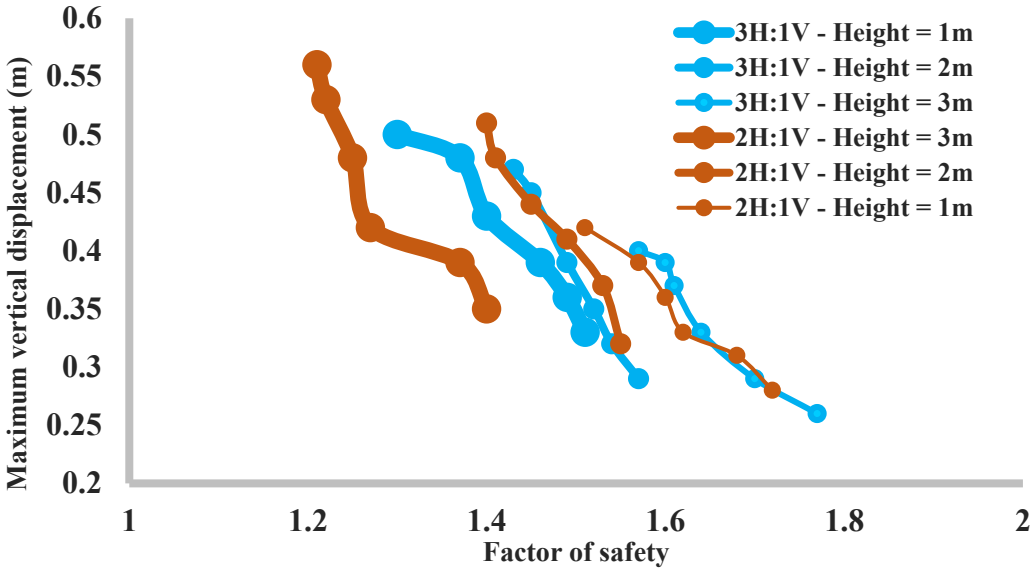

Figure 5.18. Long-term Relationship between maximum vertical displacement and shear strength reduction factor (FS) caused by the six different train speed for both 2H:1V and 3H:1V models.

5.5 Distribution of pore water pressure of models in three Scenarios

The previous discussions for the three Scenarios simulated relating to the FS values, maximum shear strain, and maximum vertical displacements are shown. In this section, the distribution of pore water pressure of models in the three different simulated Scenarios is discussed. In-depth

comprehensive knowledge of the mechanism of development of excess pore water pressure plays an integral contribution to the interpretation of results produced. This is crucial to the understanding of the development of settlements and the stresses in the embankment structure and peat soil foundation.

5.5.1 Influence of pore water pressure of models in Scenario I and II

The pore water pressure distribution of models in Scenario I and II are evaluated. Both positive and negative pore pressure occur under undrained conditions for the saturated soil. Considering the above-mentioned circumstances, the models in Figure 5.19 and Figure 5.20 are used to demonstrate the conditions stated.

A fully saturated soil (below the groundwater table) gives rise to a positive pore water pressure. The effect of capillarity causes some portions of the embankment to be saturated with water. Due to this effect, some parts of soil above the water level get saturated to generate negative pore water pressure. It is worth mentioning that, increasing depth leads to a decrease in the value of negative pore pressure whereas, the positive pore pressure value increases with increasing depth.

Figure 5.21 shows that the Scenario I model is without a pile reinforcing the embankment. As a result of the introduction of the wooden piles, the model is observed to evidently have a considerable reduction in excess pore pressures built up in the embankment layer. This is demonstrated in Figure 5.22 which shows that the pore pressure value at the sleeper/ballast interface in Scenario II models is low.

The pore pressure profiles along the center line for both sets are shown in the graphs of Figures 5.19 and 5.20. In particular, the pore pressure observed between the ballasts and sub ballast within the embankment without piles is 17 kPa. This value significantly reduces to -10 kPa after the wooden piles were introduced as a mechanism to transfer the embankment load. This profile is for the 2 m embankment height of the 2H:1V slope ratio for both Scenarios. In the 24 months phase, the results displayed by the embankment in Figures 5.20 and 5.22 show a decrease in pore water pressures due to the installation of the wooden piles. The negative pore pressure temporarily increases the soil shear strength by effectively increasing the normal stress on the ballast surface. The performance of the pile-supported embankment is significantly improved thereby signifying a corresponding decrease in stress applied to the peat.

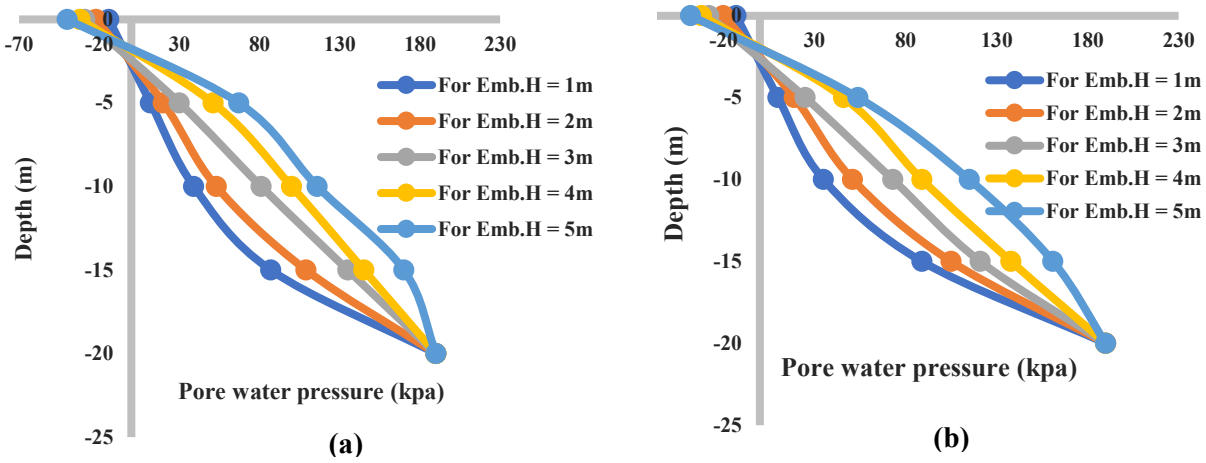

Figure 5.19. Pore water pressure distribution for embankment without wooden piles at the center-line of the embankment for slope ratio (a) 2H:1V and (b) 3H:1V model.

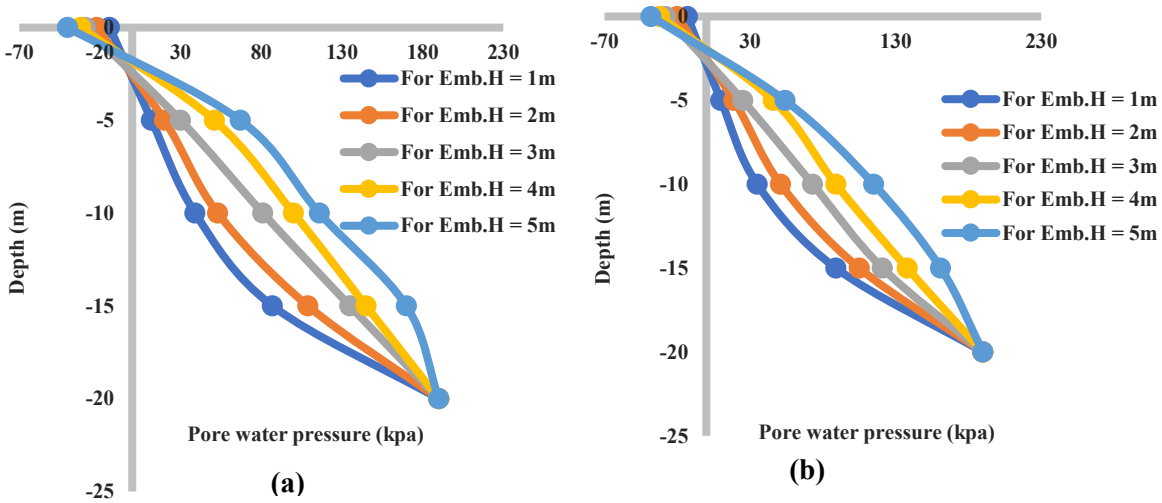

Figure 5.20. Pore water pressure distribution for embankment with wooden piles at the center-line of embankment for slope ratio (a) 2H:1V and (b) 3H:1V model.

The relationship from the graphs in Figures 5.19 and 5.20 suggest that increasing embankment height increases the pore water pressure with a reduction in the FS value.

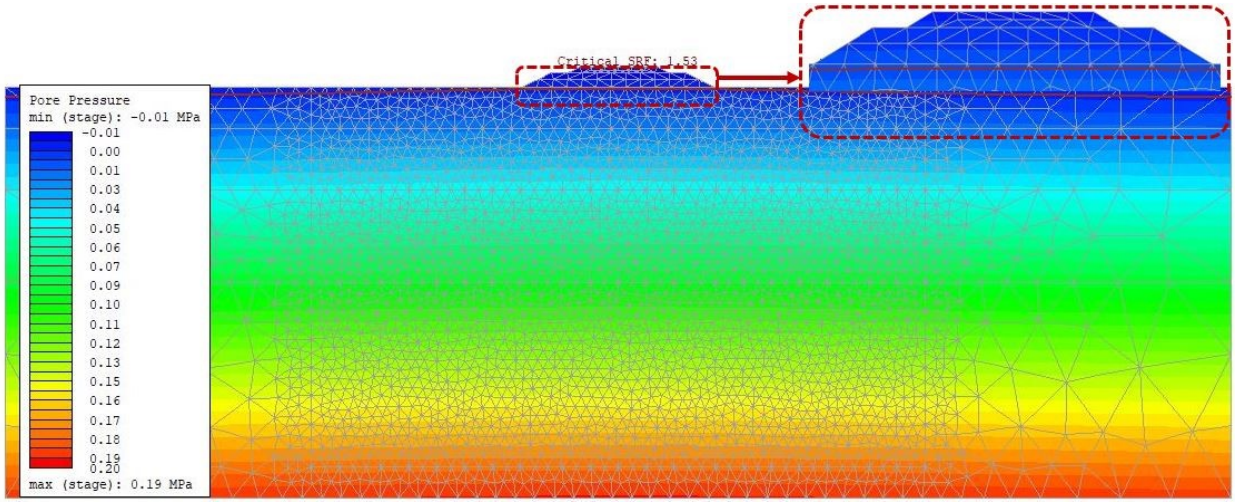

Figure 5.21. The distribution of pore water pressure of Scenario I models; embankment without wooden piles with slope ratio = 2H:1V, embankment height = 1 m.

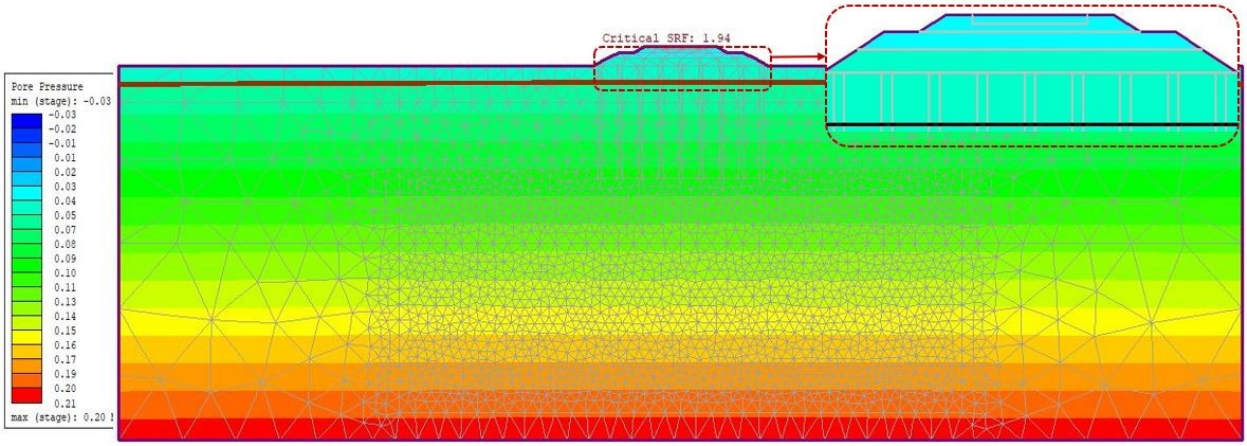

Figure 5.22. The distribution of pore water pressure of Scenario II models; embankment with wooden piles with slope ratio = 2H:1V, embankment height = 1 m.

5.5.2 Influence of train speed for Scenario III models under a freight train with different speeds considering pore water pressure

For this section, the effect of an increase in a freight train with increasing speed on the pore pressure of the foundation soil (peat) as well as the sleeper/ballast interface is reviewed. A general trend observed from the results revealed that an increase in train speed creates an increase in pore water pressure. Although this increase in excess pore pressure was relatively small as the train speed increased from 0 km/h in an increment of 24 km/h. However, expected noticeably high

values are recorded as the speed increased up to 120 km/h. The pore water pressure value at the sleeper/ballast interface of the railway embankments in the Scenario III models is plotted in Figures 5.23 and 5.24. The pore pressures in short-term and long-term periods at this interface of the embankment are illustrated. This is because the maximum pore water pressure presented at this interface provides a significant influence on stresses yielded in the embankment under train loading. The results show increases in pore water pressures are due to the increasing train speeds.

All plots in Figures 5.23 and 5.24 have an upward trend as the train speed increases. As shown in the graphs of Figures 5.23 -5.24 ((a) and (b)), a negative effect is produced. This means that the more the train speed increases, the more significant increase in pore water pressure of the models.

It can be seen from Figures 5.23 and 5.24 that all the lines have an upward trend as the natural slope height increases, which means that the more the embankment slope height increases, the more significant the decrease in the FS value of models. In addition, it can be seen that as the railway embankment height increases, pore water pressure increases.

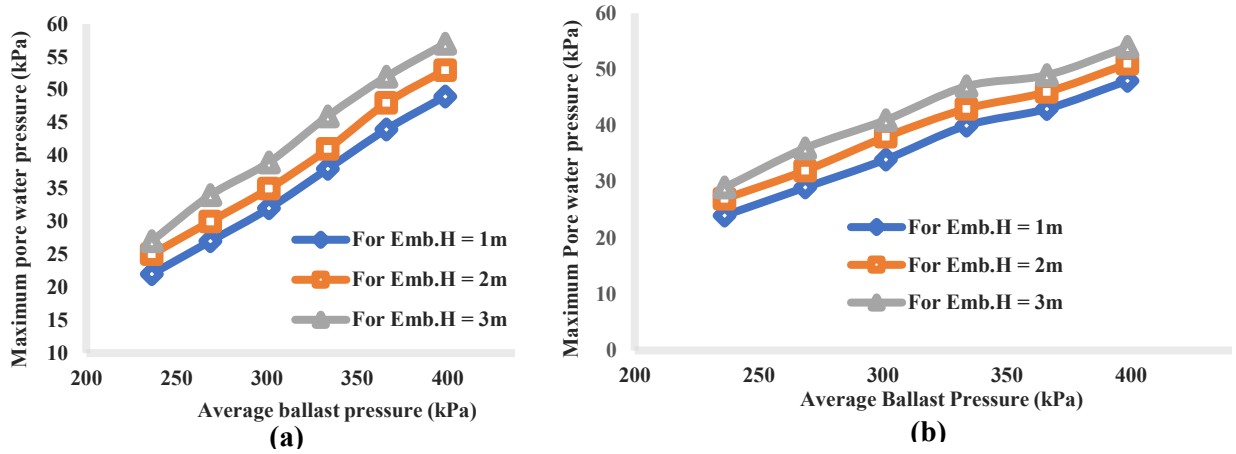

Figure 5.23. Pore water pressure distribution at sleeper/ballast interface for short term period analysis of embankment for slope ratio (a) 2H:1V and (b) 3H:1V model.

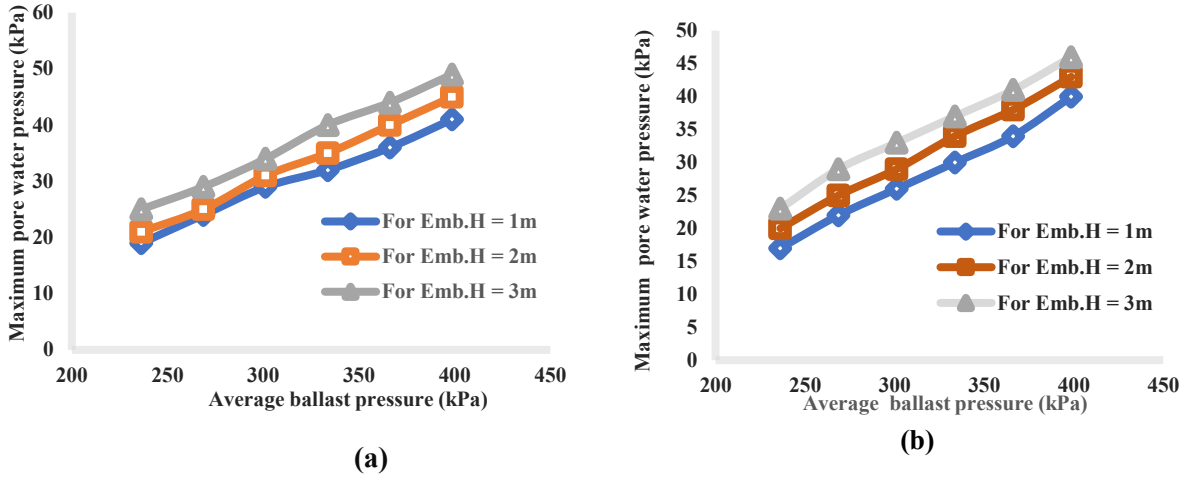

Figure 5.24. Pore water pressure distribution at sleeper/ballast interface for long term period analysis of embankment for slope ratio (a) 2H:1V and (b) 3H:1V model.

5.6 Discussion of Parametric Influence on Results for models in Scenario I and II

Both Scenarios I and II simulation results are further discussed under this subsection. For Scenario I, railway embankment height, and slope ratio are the key parameters scrutinized. Under scenario II, in addition to those listed in Scenario I, the parameters of wooden piles (length, diameter, and spacing) were analyzed. A set of graphs are presented to better communicate the developmental trends of FS so as to reveal how FS mutually relates with each geometric parameter.

5.6.1 Comparison of Simulation Results for Models in Scenario I

As introduced in Section 5.1, the geometric parameters studied in this model are the railway embankment height and slope ratio. The impact of these parameters on slope stability and the maximum vertical displacement along the ballast surface is analyzed step by step. Two graphs in Figure 5.26 plot FS results and maximum vertical displacement as a function of the five railway embankment heights considered in Groups 1 and 2 correspondingly. Both plots appear to follow a linear trend.

Figure 5.25 illustrates the vertical displacement contour for the five different embankment heights. In agreement with the results shown in Figure 5.26, the peat soil foundation is noticed to generate large deformations as the embankment is without a pile to provide reinforcing support.

Consequently, leading to a considerable increase in vertical displacement (settlement). All graph plots for the vertical displacement are along the center line. This plot is used to illustrate the settlement patterns of railway embankments. Based on that, it was found that the maximum vertical displacement for the model took place along the centerline of the embankment, right beneath the center of the track at the ballast and sleeper.

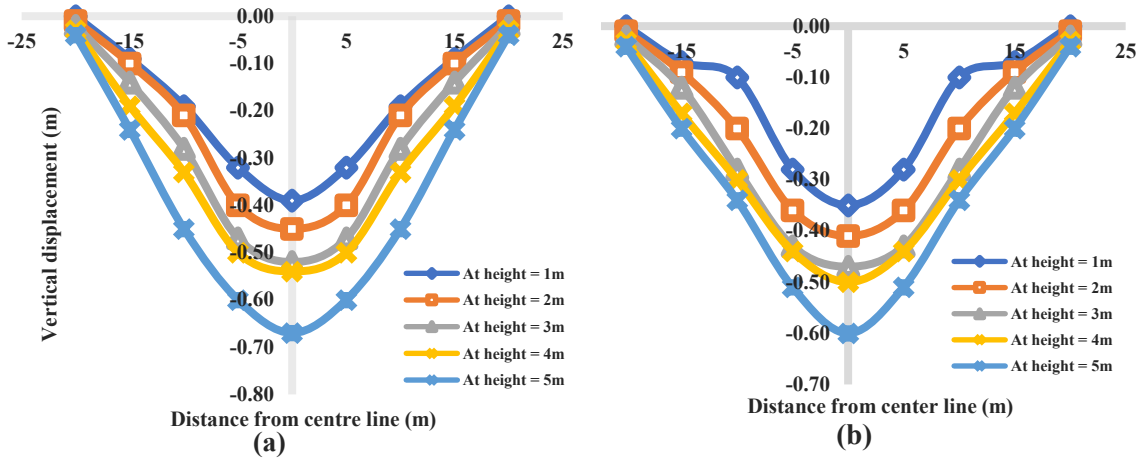

Figure 5.25. Vertical displacement along the ballast surface caused by increasing embankment height for embankment without wooden piles. Slope ratios are (a) 2H:1V and (b) 3H:1V.

Evidently, higher railway embankment heights reduce FS results as seen in Figure 5.26. Increasing FS yields lower vertical displacement. Again, higher embankment heights have a negative impact on the vertical displacement of the structure. The impact of increasing the railway embankment height on models increases vertical displacement. Finally, yet importantly, the embankment structure is more stable when the slopes are flatter. For both groups studied in Scenario I, the 5-meter embankment height produced the lowest FS and the highest maximum vertical displacement. It is worth mentioning that, a value of 1.20 as the FS and 0.67 m as vertical displacement is recorded for the 2H:1V slope ratio. These values are the lowest for the models in Scenario I.

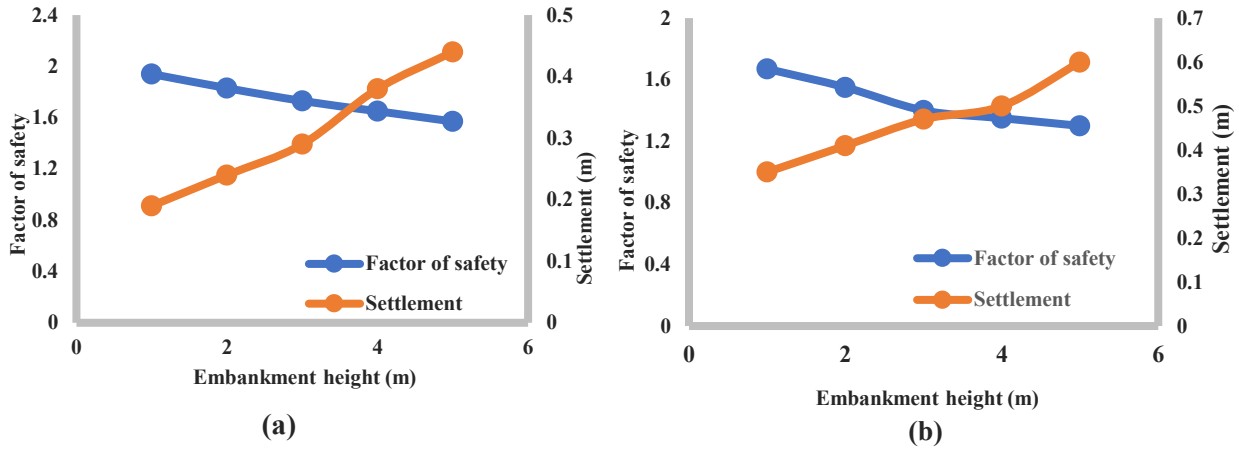

Figure 5.26. FS results and vertical displacement versus embankment heights in a range of 1 m to 5 m for embankment without wooden piles. Slope ratios are (a) 2H:1V and (b) 3H:1V.

5.6.2 Comparison of Simulation Results for Models in Scenario II

Investigations of the wooden pile parameters (the diameter, length, spacing, number of piles, and location in the embankment section) behavior on the railway embankment are addressed in this session. The purpose of the wooden piles is to increase the FS against slope and foundation failure thus, stabilizing the peat under railway embankments. Furthermore, it aided in minimizing the magnitude of vertical displacement as discussed later. Based on plots in Figure 5.27, the settlement patterns of railway embankments were observed to generate lower vertical displacement values compared with Scenario I. It can be concluded that the installation of the wooden piles can be used to effectively improve the stability of the railway track foundation thereby reducing the compressibility of the peat organic soil.

The initial two parameters analyzed (railway embankment height and slope ratio) and studied in Scenario I are further examined in Scenario II models prior to analyzing the influence of the wooden pile parameters on the FS value of the model. Much like the analysis of Scenario I models, the values of the FS results and maximum vertical displacement as a function of the five railway embankment heights are plotted as represented in Figure 5.28. Similar observable trends are noticed to those detected in Scenario I. However, minimum vertical displacement values with higher FS values are obtained for Scenario II.

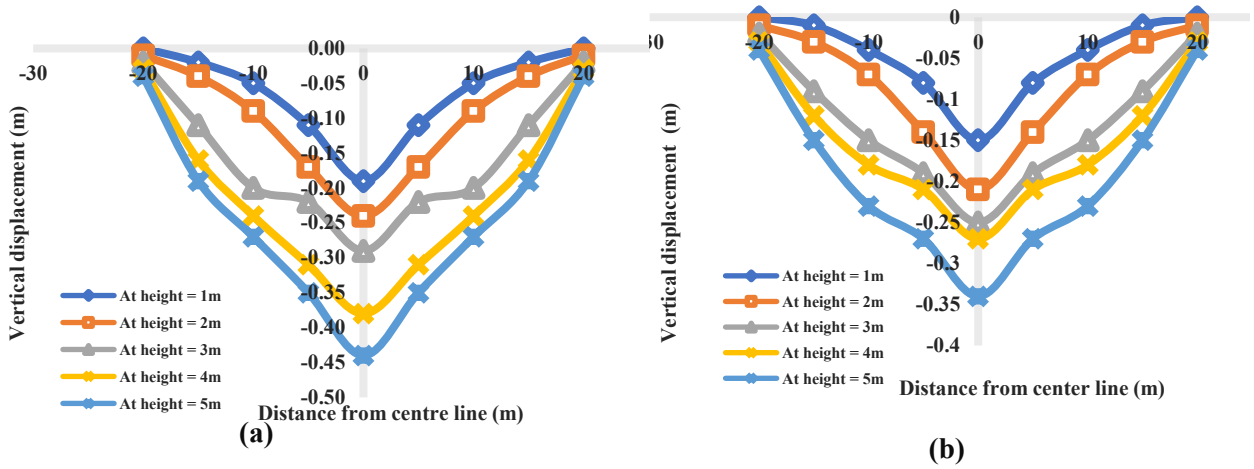

Figure 5.27. Vertical displacement along the ballast surface caused by increasing embankment height for embankment with wooden piles Slope ratios are (a) 2H:1V and (b) 3H:1V.

The 5-meter embankment height yielded a 1.57 FS value for 2H:1V being the lowest FS in Scenario II. Even though the 4-meter and 5-meter FS values are higher than the threshold 1.3, the models for Scenario III are further analyzed with three railway embankment heights (1-meter to 3-meter) for both 2H:1V and 3H:1V slope ratios. This is because they were considered more stable for detailed analysis as the train load is inputted in Scenario III.

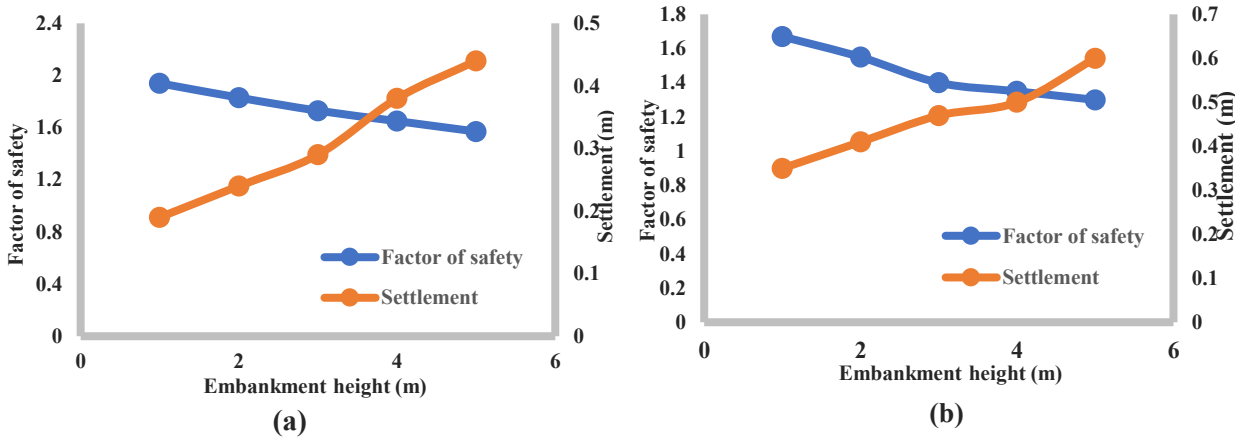

Figure 5.28. FS results and vertical displacement versus embankment heights in a range of 1 m to 5 m for embankment with wooden piles. Slope ratios are (a) 2H:1V and (b) 3H:1V.

5.6.3 Effectiveness of the wooden piles

For a straightforward comparison, the calculated percentage differences between the FS values produced for both Scenarios I and II from the shear stress reduction method are reported in Tables 5.11 and 5.12. The wooden piles noticeably increase the FS of the embankment by more than 23 % as the values of FS also increase. This is observed in the case of the 5 m embankment for the 2H:1V embankment.

Furthermore, a comparison of the vertical displacement for Scenario I and II was used in inferring the effectiveness of the timber piles in carrying the embankment load, and thus minimizing the loads carried by the peat. Both Figures 5.20 and 5.29 show that the pore water pressures and vertical displacements (settlement) respectively improved from having very large to relatively low values after using the wooden piles. Figure 5.29 shows the difference between the wooden pile supported embankment and an embankment without a pile.

The wooden piles proved to be an efficient strengthening mechanism employed on the peat soil foundation. The load distribution employed by the piles in transmitting structural loads reduces stresses built up in the structure. Thus, confirming that the wooden piles can be used as a method of stabilization of peat under railway embankments.

Table 5.11. Percentage difference between simulated results of finite element analysis of embankment for 2H:1V slope ratio.

Embankment height (m)	Embankments without wooden piles FS	Wooden piled supported embankment FS.	Differences in FS for Scenarios I and II (%)
1	1.53	1.94	21.13
2	1.47	1.83	19.67
3	1.30	1.73	24.85
4	1.25	1.65	24.24
5	1.20	1.57	23.56

Table 5.12. Percentage difference between simulated results of finite element analysis of embankment for 3H:1V slope ratio.

Embankment height (m)	Embankments without wooden piles	Wooden piled supported embankment FS.	Differences in FS for Scenarios I and II (%)
1	1.67	2.02	17.32
2	1.55	1.88	17.55
3	1.40	1.82	23.07
4	1.35	1.76	23.30
5	1.30	1.61	19.25

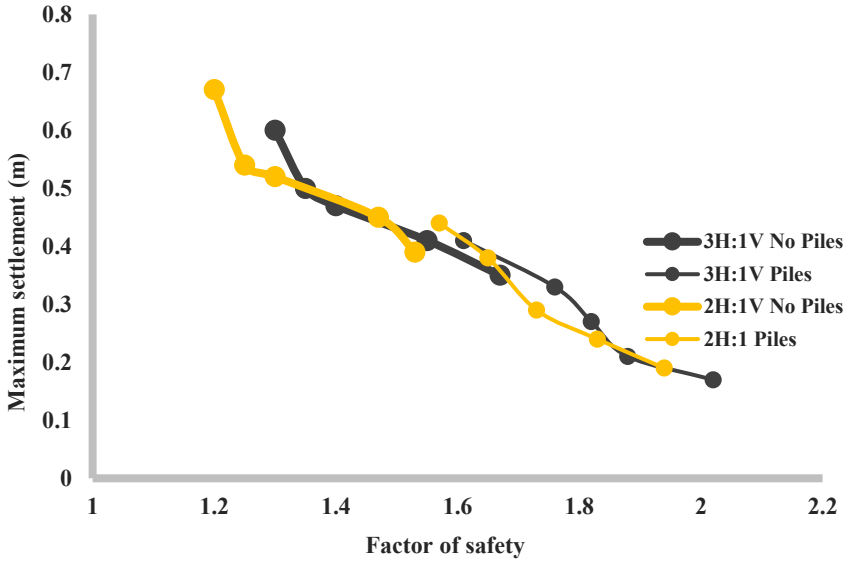

Figure 5.29. Relationship between the FS and maximum vertical displacement for embankment with slope ratio 2H:1V and 3H:1V.

5.6.4 Sensitivity Analysis on the Geometric Parameters of Piles

A number of geometrical, mechanical, and bi-product parameters are to be studied for the stabilization of railway embankments. The important geometric parameters of piles to be studied include the pile length, diameter, location in the embankment slope, number, and spacing. Under

the other conditions, the mechanical parameters of the soil properties (e.g., modulus of elasticity, Poisson's ratio, etc.) and the bi-product parameters include the interaction factors (e.g., pile-soil) that influence the performance of the structure. The effect of each parameter on the FS of the slopes is expressed through the relationship between the FS versus the maximum vertical displacement. A linear graph was derived after plotting the variations of the geometric pile parameters. The diagrams are illustrated for each subsection where the relation between the vertical displacement and their corresponding FS values are plotted.

For the purposes of employing two-dimensional (2D) FEM to simulate the railway embankment conditions, a sensitivity analysis was performed on the basis of the above-mentioned parameters. The sensitivity analysis is to help determine the influence of each pile parameter in achieving the minimum threshold FS value. As mentioned earlier, the parametric study on the design of the piles was to assure conformance with the requirements of the National Building Code of Canada (NBCC) (2005) as recommended in the Canadian Foundation Engineering Manual (2007). The pile is adjusted to suit the dimensional information for CSA Standard CAN3-056-M79 (Round Wood Piles) (1980) and CSA Standard CSA CAN3-O86-M84 (Engineering Design in Wood). A total of 27 different cases are investigated for the analysis. Table 5.12 to Table 5.20 list all these cases, with 9 subgroups in total and 3 groups. It is worth mentioning that the embankment with a height of 2 m for the 3H:1V (Horizontal: Vertical) was used to analyze and study the model parameters. The main criterion for selecting this embankment height is that it is practicable in visualizing the FS results to describe conditions under an organic soil state. Thus, making it easy to capture the behavior of the embankment in relation to pile geometry in controlling settlement and deformation when considering embankment height and load application.

5.6.4.1 Influence of Pile Diameter

In finding out the efficiency of this parameter, three different pile diameters were considered. They were selected as 0.24 m, 0.27 m, and 0.30 m based on CSA CAN3-O86-M84 (1980) recommendations. Tables 5.13 to 5.15 present the FS results associated with different pile diameters after simulation. The outcome of the analysis indicated that larger pile diameters have larger spacing and inversely lower FS values. This is evident as the 0.3 m pile within the 5D pile group has the lowest FS of 1.48. The FS decreased because of a reduction in the number of piles. Figure 5.30 presents the relationship between the vertical displacement and FS values. It can be

stated that the pile diameters can influence higher factors of safety values based on the number of piles. The results of sensitivity analysis as seen in the relationship between FS values and vertical displacement notably show that the 0.24 m yielded higher critical SRF values with minimum vertical displacements. This is attributed to it having a higher number of piles and minimal pile spacing thus, it adequately strengthens the embankment.

Table 5.13. The critical SRF results obtained for sensitivity analysis with a 0.30 m pile diameter

Pile diameter (m)	Pile length (m)	Pile spacing (m)	Critical SRF
0.24	6.0	1.20	1.74
		1.44	1.72
		1.68	1.66
	6.5	1.20	1.83
		1.44	1.80
		1.68	1.70
	7.0	1.20	2.03
		1.44	1.91
		1.68	1.76

Table 5.14. The critical SRF results obtained for sensitivity analysis with a 0.27 m pile diameter

Pile diameter (m)	Pile length (m)	Pile spacing (m)	Critical SRF
0.27	6.0	1.35	1.69
		1.62	1.65
		1.89	1.59
	6.5	1.35	1.77
		1.62	1.71
		1.89	1.63
	7.0	1.35	1.81
		1.62	1.78
		1.89	1.70

Table 5.15. The critical SRF results obtained for sensitivity analysis with 0.30 m pile diameter

Pile diameter (m)	Pile length (m)	Pile spacing (m)	Critical SRF
0.30	6.0	1.50	1.65
		1.80	1.60
		2.10	1.48
	6.5	1.50	1.70
		1.80	1.64
		2.10	1.51
	7.0	1.50	1.75
		1.80	1.72
		2.10	1.54

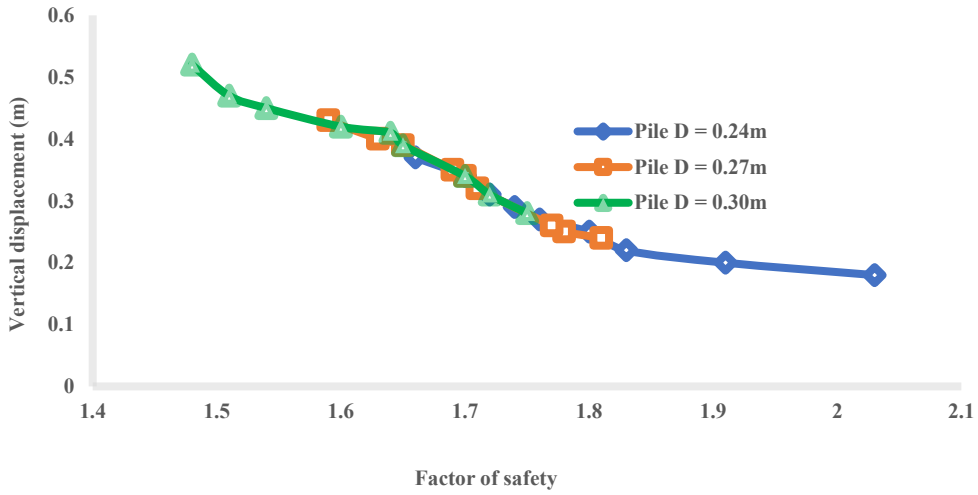

Figure 5.30. Relationship between the vertical displacement and FS values of pile diameter variation on the settlement of wooden pile embankment.

5.6.4.2 Influence of Pile Length

To understand the influence of this parameter on the stability of the embankment, three different pile lengths (6 m, 6.5 m, and 7 m) were considered in the analysis. The calculations used in deriving the pile length are given in the Appendix. It was investigated in the form of a FS associated with other pile parameters (pile spacing and pile diameter). The FS for each length calculated are given in Tables 5.16 – 5.18. Considering the results in Tables 5.16 – 5.18, the pile length of 7 m yielded higher FS values of 2.03 in comparison with the other pile length for the embankment. Although

the FS of the model with the 6 m pile length meets the threshold of the FS value of this study, the minimum vertical displacement is relatively large. As shown in Figure 5.31, the displacement is 45 % and 20 % respectively that of the minimum vertical displacement of the embankment when the pile length is 7 m and 6.5 m. This amount of vertical displacement has a great impact on the performance of the embankment. Hence, the suitable pile length should be chosen to regulate the vertical displacement of the embankment when supported with wooden piles.

Therefore, longer wooden piles generally have a positive influence on the vertical displacement of the pile foundation according to the curve trends in Figure 5.31. This confirms that a longer pile length can increase the stability of the embankment.

Table 5.16. The critical SRF results obtained for sensitivity analysis with 6.0 m pile length

Pile length (m)	Pile diameter (m)	Pile spacing (m)	Critical SRF
6.0	0.24	1.20	1.74
		1.44	1.72
		1.68	1.66
	0.27	1.35	1.69
		1.62	1.65
		1.89	1.59
	0.30	1.50	1.65
		1.80	1.60
		2.10	1.48

Table 5.17. The critical SRF results obtained for sensitivity analysis with 6.5 m pile length

Pile length (m)	Pile diameter (m)	Pile spacing (m)	Critical SRF
6.5	0.24	1.20	1.83
		1.44	1.80
		1.68	1.70
	0.27	1.35	1.77
		1.62	1.71
		1.89	1.63
	0.30	1.50	1.75
		1.80	1.64
		2.10	1.51

Table 5.18. The critical SRF results obtained for sensitivity analysis with 7.0 m pile length

Pile length (m)	Pile diameter (m)	Pile spacing (m)	Critical SRF
7.0	0.24	1.20	2.03
		1.44	1.91
		1.68	1.76
	0.27	1.35	1.81
		1.62	1.78
		1.89	1.70
	0.30	1.50	1.75
		1.80	1.72
		2.10	1.54

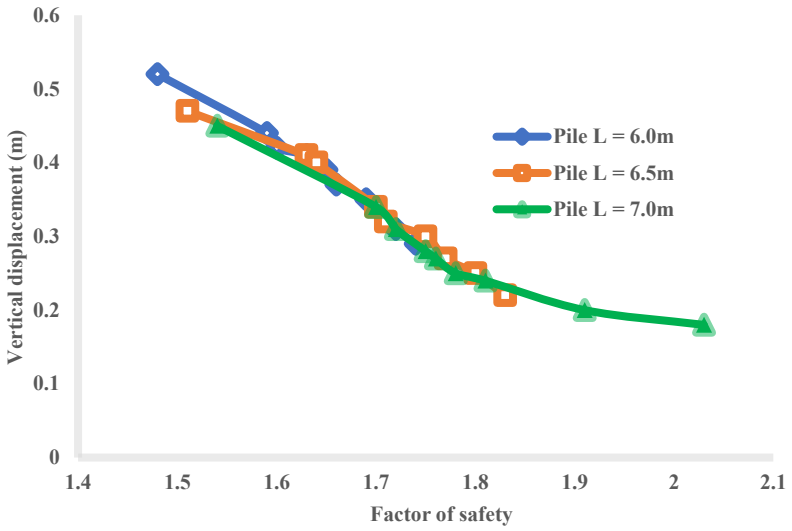

Figure 5.31. Relationship between the vertical displacement and FS values of pile length variation on the settlement of wooden pile embankment.

To capture the influence of pile length on the load settlement behavior of the simulated models, Figure 5.31 presents the relationship between the vertical displacement and FS values. It can be stated that the longer the pile length the higher the FS and minimal settlement. Thus, it played a major role in stabilizing the weak organic peat soil and transmitting the load.

5.6.4.3 Influence of Piles Spacing

In this section, varying the pile spacing was studied to observe its influence on the performance of the embankment. This parameter was selected as center-to-center spacing being 5D (the diameter of the pile), 6D, and 7D. The selection is based on the minimum recommended pile-to-pile spacing

for driven timber piles (Timber Pile Design and Construction Manual 2016; Hannigan et al. 1997). According to the values of FS presented in Table 5.19 to Table 5.21, results showed that wider pile spacing yielded lower FS values. The value of the FS increases considerably by decreasing pile spacing. Among all models studied in this group, the lowest FS of 1.48 was captured for the 7D model in Table 5.15 with a 6-meter pile length. Thus, the analysis was continued by using the allowable minimum center-to-center spacing to achieve the threshold FS. It has been seen that the efficiency at 5 D spacing is more than that of 6 D and 7 D spacing. The trend observable is that with smaller pile spacing, the vertical displacement of the piled supported embankment reduces more effectively. For example, from the graph in Figure 5.32 the influence of the wooden piles on the vertical displacement of the embankment increases by more than 30 % when the pile spacing is varied from 5D to 7D.

Again, if FS results for 5 D pile spacing are compared to those with 6 D pile spacing, a reduction of 5.91 % is detected. The influence of this amount of displacement on the embankment is significant thereby revealing that the piles can better improve the foundation when spacing is smaller. Thus, a positive linear trend observed is that a significant reduction in vertical displacement occurs with decreasing pile length.

Table 5.19. The critical SRF results obtained for sensitivity analysis with 5 D pile spacing

Pile spacing (m)	Pile length (m)	Pile diameter (m)	Critical SRF
1.2	6.0	0.24	1.74
	6.5		1.83
	7.0		2.03
1.35	6.0	0.27	1.69
	6.5		1.77
	7.0		1.81
1.50	6.0	0.30	1.65
	6.5		1.70
	7.0		1.75

Table 5.20. The critical SRF results obtained for sensitivity analysis with 6 D pile spacing

Pile spacing (m)	Pile length (m)	Pile diameter (m)	Critical SRF
1.44	6.0	0.24	1.72
	6.5		1.80
	7.0		1.91
1.62	6.0	0.27	1.65
	6.5		1.71
	7.0		1.78
1.80	6.0	0.30	1.60
	6.5		1.64
	7.0		1.72

Table 5.21. The critical SRF results obtained for sensitivity analysis with 7 D pile spacing

Pile spacing (m)	Pile length (m)	Pile diameter (m)	Critical SRF
1.68	6.0	0.24	1.66
	6.5		1.70
	7.0		1.76
1.89	6.0	0.27	1.59
	6.5		1.63
	7.0		1.70
2.10	6.0	0.30	1.48
	6.5		1.51
	7.0		1.54

The influence of pile spacing variation on the settlement of wooden pile embankments has been depicted in Figure 5.32. The plots affirm that for smaller pile spacing the settlement reduction rate is steeper and flatter for the larger pile spacing. It can be therefore concluded that the larger spacing of the piles reduces the effectiveness of pile efficiency.

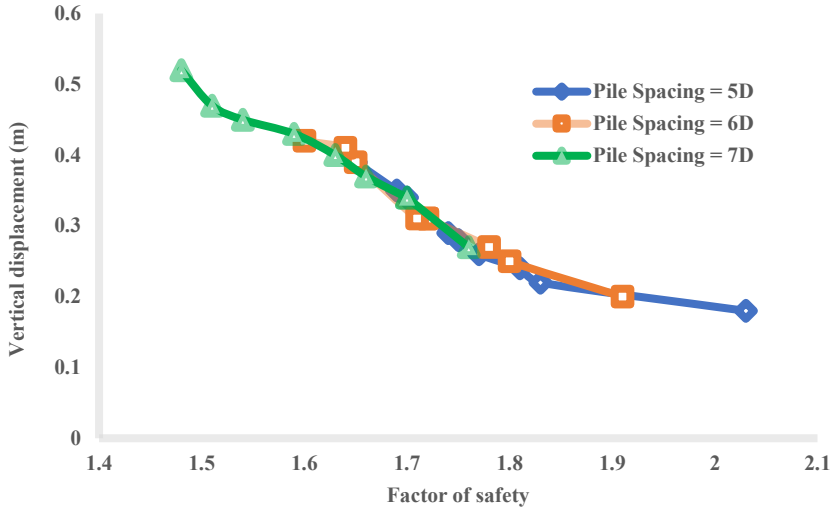

Figure 5.32. Relationship between the vertical displacement and FS values of pile spacing variation on the settlement of wooden pile embankment.

5.6.4.4 Influence of Number of Piles and Location in Embankment Section

These parameters were influenced by the pile spacing as well as the ability of the embankment to perform satisfactorily against collapse mechanisms. Thus, in order to overcome foundation failure, an increase in FS and a decrease in foundation settlements are achieved by installing piles under the embankment section to stabilize the peat under railway embankments. This increases stability and reduces deformation. This is to ensure that the load-carrying ability of the embankment does not exceed the load-carrying ability of the ground that supports the foundation. Hence, it should be taken into consideration that the arrangements should suitably support the embankment so as to achieve a FS that will not hinder the serviceability of the embankment.

Furthermore, results showed that a smaller pile diameter has an increased number of piles being installed beneath the embankment. This is illustrated in Figure 5.32 for the 5 D model with different pile diameter and their corresponding spacing for the 7 m pile length. Accordingly, to establish the ideal design strategy a balance between the pile spacing, pile diameter, and pile length should be ascertained.

5.6.4.5 Pile-soil interaction

Considering the fact that the pile-soil interaction contributes significantly to the behavior of the pile-soil system, the interface was modeled to avoid pile deflection. The complexity of this phenomenon depends on many factors such as loading type and soil profile. The interface between piles and soil was simulated considering the slip surface due to the friction on the pile-soil interface. Since timber piles are considered to be displacement-type piles, the slip criterion was selected as a Mohr-Coulomb. The strength and slip properties have been given in Section 4.9. No failure was recorded during the simulation of the model.

5.6.5 Comparison of simulation results for Scenario III.

As discussed in the previous section, the train loads added on the track are the main difference compared to the case in Scenario I and II. Much like the preceding analysis above, the influence of slope geometry and maximum vertical displacement on Scenario III models are analyzed and shown in Section 5.6.5.1. The maximum freight train speed that the models can withstand is studied in Section 5.7.

5.6.5.1 Influence of Slope Geometry and Maximum Vertical Displacement for Scenario III Models under Train Loads

As reported by the previous observation, the embankment structure disturbs the peat foundation soil and causes most of the vertical surface displacement changes along the ballast surface. The vertical surface displacement changes and the trend caused by train operation are discussed. In a limited range under various train speed conditions, the effect of increasing train speed to determine the influence on ground surface displacement generated by other parameters is analyzed. The corresponding vertical displacement along the ballast surface induced by train operation for both short-term and long-term analysis is presented in the Appendix. This data is used in depicting the relationship between an increase in train speed and settlement in the subsequent section. Thus, the influence of these parameters on Scenario III models is examined in more detail in this section in three aspects:

(a) influence of the slope ratio,
(b) influence of the railway embankment height,
(c) influence of the train speed,

(a) Influence of the Slope Ratio

The slope ratio (2H:1V and 3H:1V) affects the vertical surface displacement as well as the FS values. To verify its influence, the values of maximum vertical displacement with increasing train speed at the ballast surface are summarized and plotted in Figures 5.28 and 5.29. The graphs are a representation of the settlement pattern for the 1 m embankment height for both short-term and long-term periods. From the plots, observations due to slope ratio variations are evaluated. Corresponding to the results in all the graphs, the displacement distribution plot patterns after similar geometry of a Gaussian curve. A negative trend is noticed which is indicative that, increasing train speed causes an increase in vertical displacement. Again, for both short-term and long-term periods, the 2H:1V slope ratio produced higher vertical displacement as compared with the 3H:1V. For instance, for the 1 m embankment height, the values of maximum vertical displacement for the short-term analysis when an Average Ballast Pressure (ABP) of 268.73 kPa is applied to models with a slope ratio of 2H:1V is 0.31m whereas that of 3H:1V is 0.29 m. Correspondingly, the increments of maximum vertical displacement listed in Tables 3 - 14 of the Appendix show increasing train speed provides a clear depiction of the influence of the slope ratio. From Figures 5.33 and 5.34 as well as Tables 3 - 14, it can be established that a flatter slope generates less ground vertical displacement than a steeper slope. Consequently, it is conclusively suggested to design the slope with a ratio of 3H:1V to warrant satisfying results to stabilize the slope.

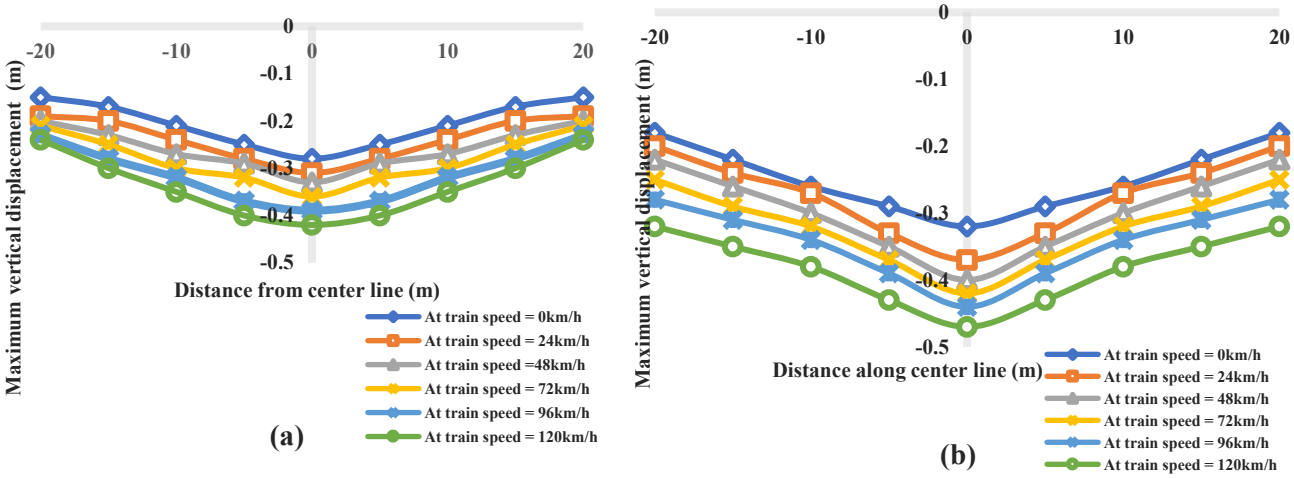

Figure 5.33. Vertical displacement along the ballast surface caused by increasing train speed for (a) short-term and (b) long-term analysis. The slope ratio is 2H:1V.

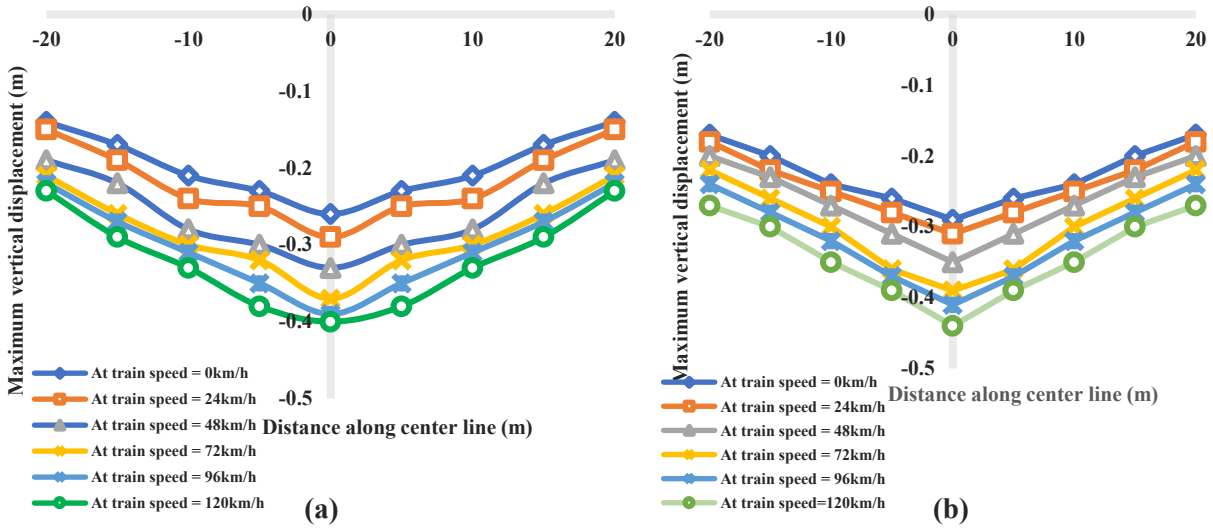

Figure 5.34. Vertical displacement along the ballast surface caused by increasing train speed for (a) short-term and (b) long-term analysis. Slope ratio is 3H:1V.

(b) Influence of the Railway Embankment Height

In this study, the railway embankment height varies from 1 m to 3 m under the influence of train speed. Again, results summarized in Tables 3 - 14 of the Appendix are selected to analyze the influence of the railway embankment height. Figures 5.35 and 5.38 visualizes the relationship between the embankment height versus the maximum vertical displacement along the ballast surface. According to the data from Tables 3 – 14 of the Appendix, increasing train speed results in a steady decrease in vertical displacement as embankment height increases for both long-term and short-term simulated models. The curves plotted in the graphs representing the comparison results of models with the railway embankment heights show a steady surge of settlement with an increase in train load. In addition, these results graphed in Figures 5.37 and 5.38 show that the strength of the embankment is much higher when the embankments have lower heights. It may prove that larger train loading generates appreciable downward movement as a result of the load-deformation response of the embankment subjected to heavy axle loads. Correspondingly, the data shown in Tables 5.6 - 5.9 indicates that FS values decline with a larger embankment height. Hence, it can be concluded that, under tolerable conditions, it is preferable to choose a lower height for a

more serviceable embankment. With augmenting maximum vertical displacement, FS value continuously reduces in a quasi-linear way as train speed increases as presented graphically.

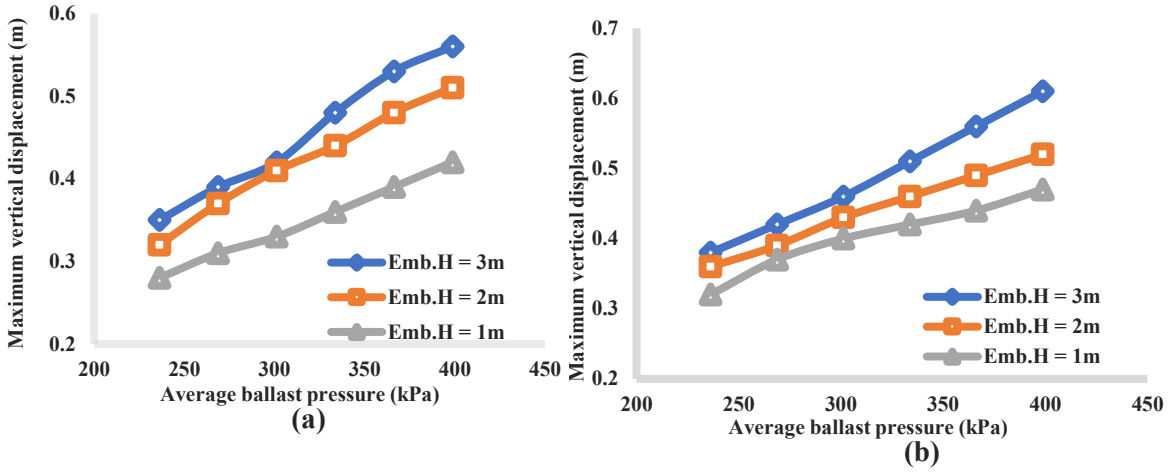

Figure 5.35. Relationship between the vertical displacement along the ballast surface and increasing train speed for (a) short-term and (b) long-term analysis. Slope ratio is 2H:1V.

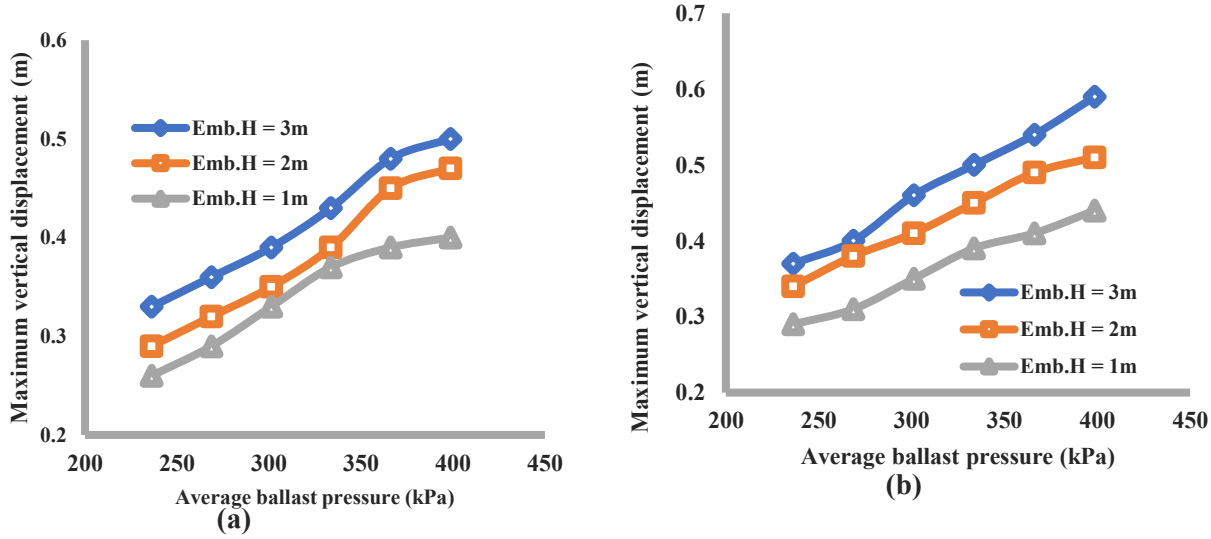

Figure 5.36. Relationship between the vertical displacement along the ballast surface and increasing train speed for (a) short-term and (b) long-term analysis. Slope ratio is 3H:1V.

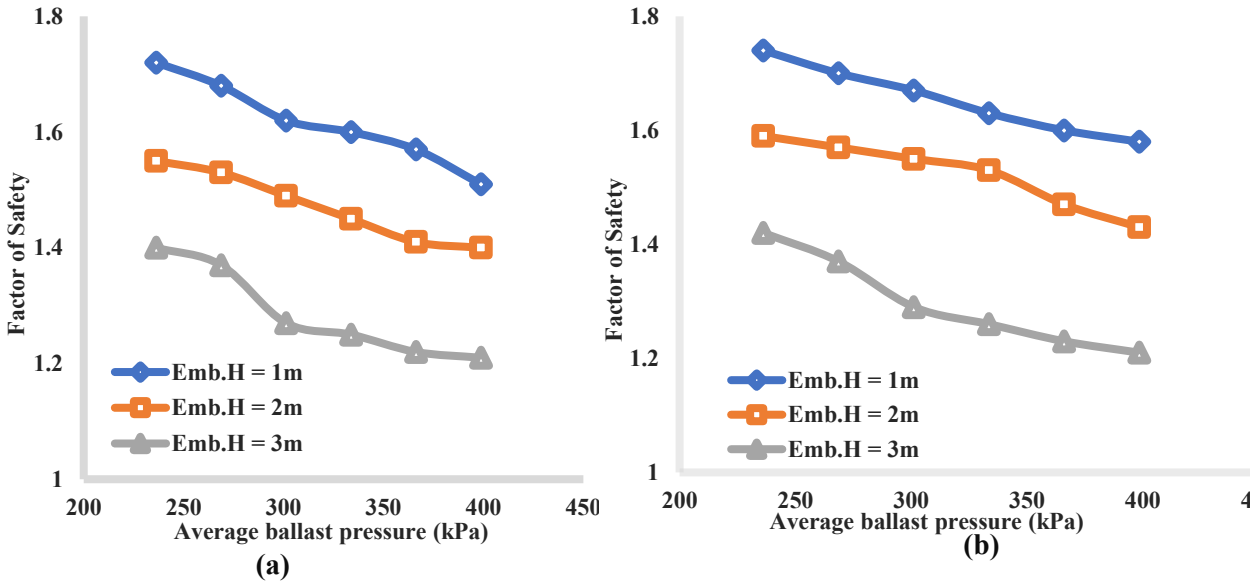

Figure 5.37. Relationship between the FS and increasing train speed for (a) short-term and (b) long-term analysis. Slope ratio is 2H:1V.

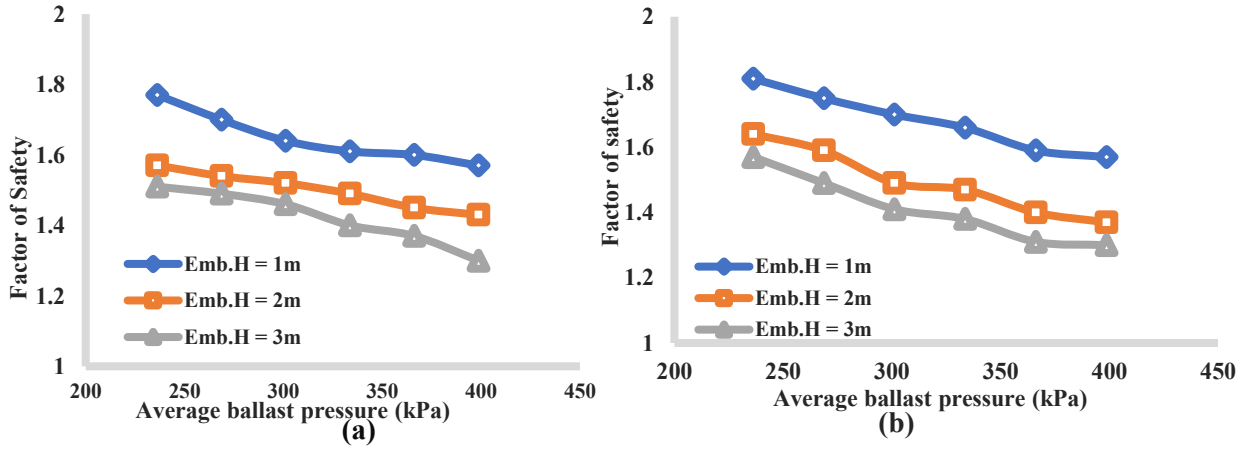

Figure 5.38. Relationship between the FS and increasing train speed for (a) short-term and (b) long-term analysis. Slope ratio is 3H:1V.

(c) Influence of Train Speed for Scenario III Models under a Freight Train with Different Speeds

With the consideration of a moving train on the track, the range of the moving train speed is from 0 mph to 75 mph with a step of 15 mph. A summary of the maximum displacement with corresponding FS results listed in Tables 3 - 14 of the Appendix and Tables 5.6 and 5.9 respectively have been plotted in Figures 5.39 and 5.40. This is to distinctly categorize FS values versus maximum vertical displacement and train speed. To easily capture the difference in the graphs, the color bar remains unchanged with a minimum of 1.20 and a maximum of 1.82. For each graph, it is distinguishable that FS results dwindle with high train speeds resulting in escalating vertical displacement.

The relationship between both short term and long-term analysis FS values and the embankment height and train speed is well established in all graphs in Figures 5.39 and 5.40. At a lower embankment height and a lower train speed, an appreciable FS result was achieved for each graph.

Moreover, compared to models with a slope ratio of 2H:1V, models with a slope ratio of 3H:1V have a greater FS value under the freight train with the same speed as observed from the graphs in Figures 5.39 and 5.40. Thus, flatter slopes are more stable in ensuring serviceable slopes.

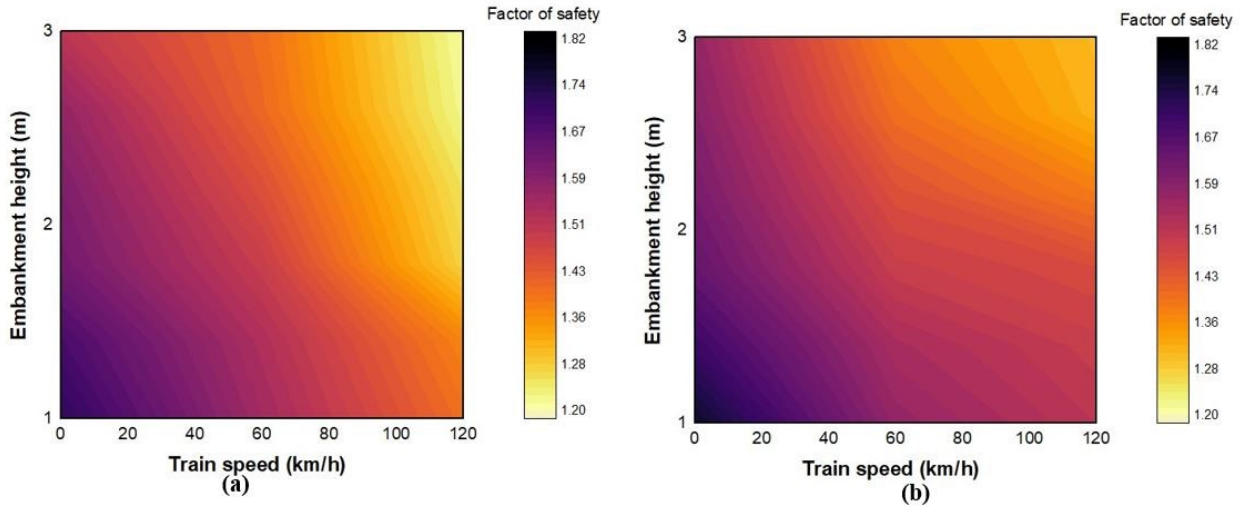

Figure 5.39. Pseudocolor graphs of FS results for short term analysis in Tables 5.6. and Tables 5.7 (a) slope ratio 2H:1V; (b) 3H:1V.

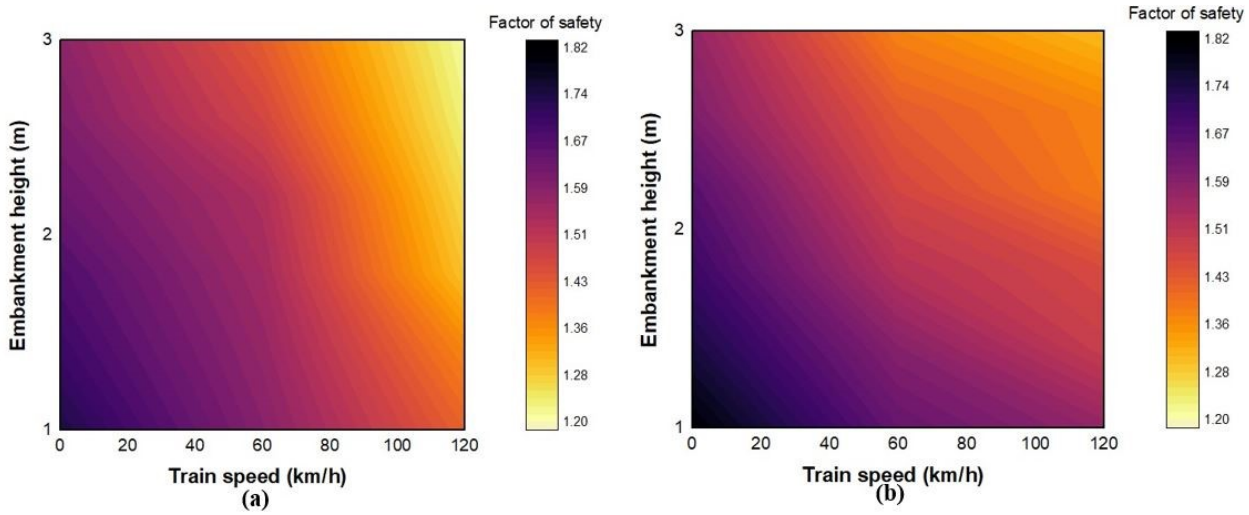

Figure 5.40. Pseudocolor graphs of FS results for long term analysis in Tables 5.8. and Tables 5.9 (a) slope ratio 2H:1V; (b) 3H:1V.

Using the short-term analysis of the 2H:1 slope ratio for the 2 m embankment height, a plot of the change in pore pressure and maximum vertical displacement at the ballast surface versus the train speed is shown in Figure 5.41. From this Figure, it is noticeable that there exists a strong linear correlation between the magnitude of the train speed, the stress in the ground and the resulting pore pressure response, and the maximum vertical displacement.

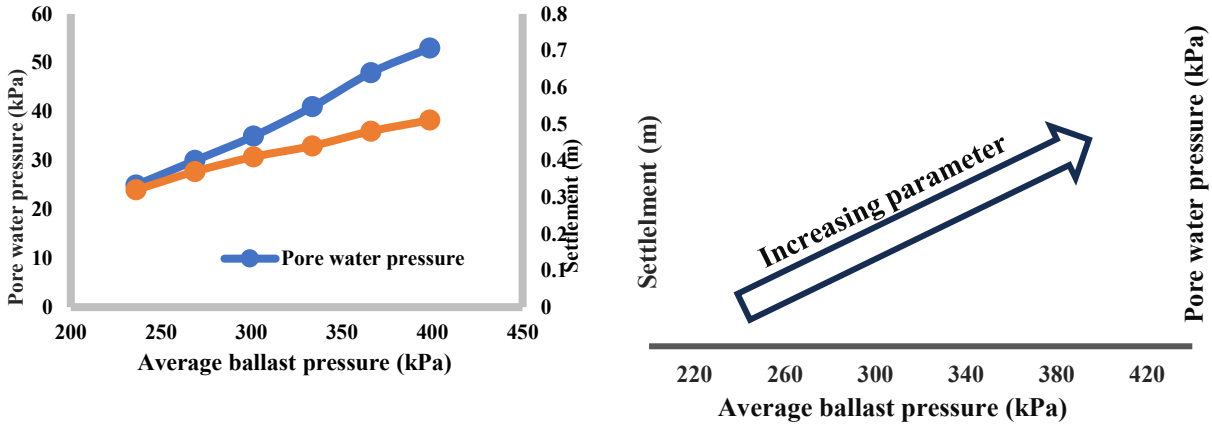

Figure 5.41. Effect of train loading on vertical displacement and pore water pressure

5.7 Recommendation of Allowable Maximum Displacement to Guarantee Safe Railway Performance

It was postulated that loading-induced pore pressures in the peat foundations were the main cause for the record of slightly higher FS values in the long-term analysis as compared with the short-term analysis. Over a short period, increasing pore pressure temporarily reduces the soil shear strength and the pile capacity; as the pore pressure dissipates, the pile capacity increases.

The installation of wooden piles as a method of stabilization of peat under railway embankments is recommended to stabilize the embankment, strengthen the soil and reduce vertical displacement. As listed in Table 5.22, Wang et al. (2014) define the allowable controlled settlement value in addition to railway embankment deformation for a ballasted track. However, when comparing the results for the vertical displacement in this study with the settlement rate of 3 cm/year recommended by the Chinese Railway in Table 5.22, the settlement should not exceed 15 cm in the first 5 years. Based on these results, it is highly recommended that the organic foundation soil layer be made competent using additional ground improvement techniques by employing geotextiles.

Both the short-term and long-term analysis of maximum safe train speed and settlement is represented in Figures 5.42 and 5.43 respectively. With regards to the FS standpoint for a larger maximum safe train speed, all slopes of 3H:1V is a good choice. Consequently, unlike the 2H:1V, it can support the freight train moving at a speed of 75 mph.

Table 5.22. Controlled settlements of ballasted track high-speed railway in China (Wang et al. 2014)

Description	Unit	Design speed (km/h)	
		250	300 to 350
Embankment zone	cm	10	5
Settlement rate	cm/year	3	2

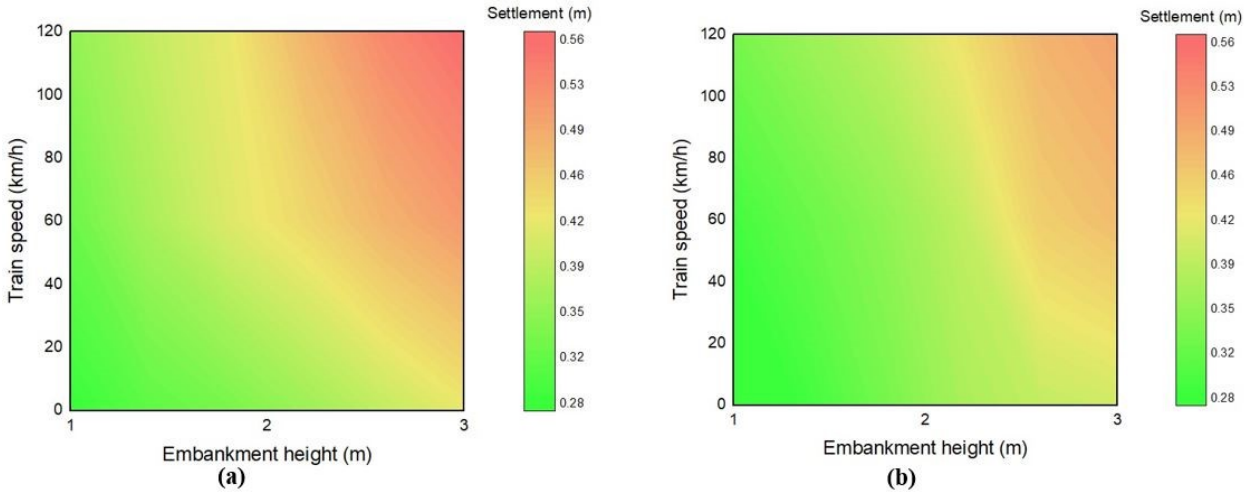

Figure 5.42. Pseudocolor graphs of maximum safe train speed and settlement for short term analysis of (a) 2H:1V and (b) 3H:1V.

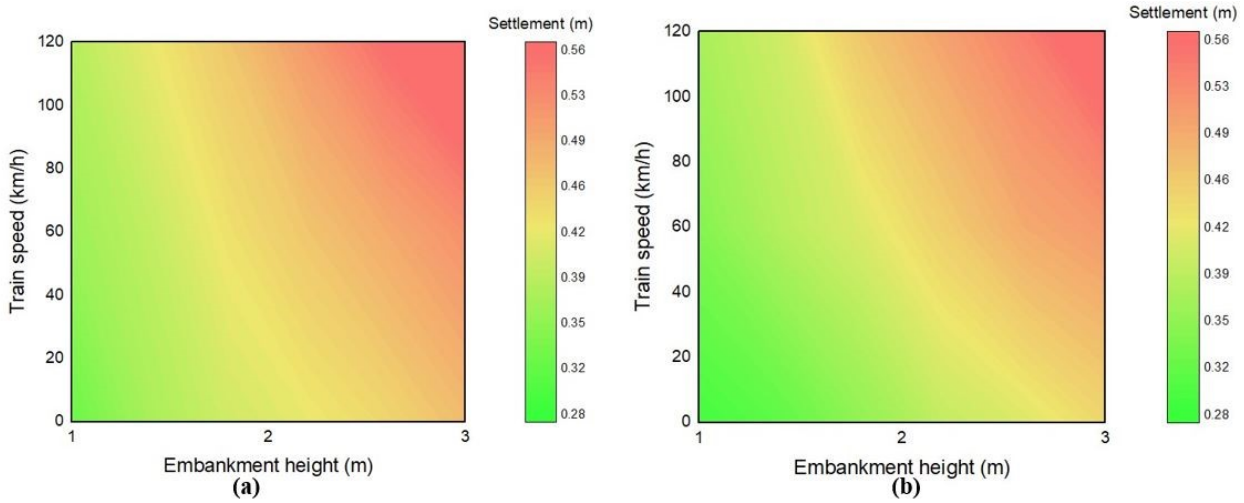

Figure 5.43. Pseudocolor graphs of maximum safe train speed and settlement for long term analysis of (a) 2H:1V and (b) 3H:1V.

5.8 Summary

RS2 software was used to create two-dimensional FEM models with the objective of researching the influence of train speeds, wooden pile geometry (diameters, spacing, and length), and embankment slope ratio (2:1 and 3:1) with the consideration of settlement, pore water pressure, and stress.

To derive the maximum allowable train speed as a function of settlement and consolidations, three sets of models are developed and studied. Namely; embankments without wooden piles, wooden pile-supported embankments but no train load, and wooden pile-supported embankments with a moving freight train. This is to help appreciate and evaluate the behavior and effectiveness of driven wooden piles under railway embankments constructed on organic peat foundation soil. Thus, making it easier to develop the models through each scenario with coherent inferences.

Scenario I revealed the need to support the embankment with driven wooden piles to adequately strengthen and transfer the loads without failure. Scenario II studied the models with wooden piles and confirmed the competence of the piles. In Scenario III, investigations are made into the effect of loading the track with varying train speeds. Based on the aforementioned scenario, a short-term analysis was conducted to evaluate the stability of embankments after construction. Furthermore, a long-term analysis was performed to identify expected consolidation settlements in the future. It is worth mentioning that the settlement as well as the pore-pressure behavior of the organic soil was studied during all three scenarios.

To conclude, the resulting data numerically proves that the installation of driven wooden piles within the peat is an effective technique for decreasing the load exerted on the peat. This assessment verifies the design assumptions – that the embankment loading is transferred to the piles and from the piles to deeper compressible soil layers. The FS results is satisfactory to prove this point.

Regardless of the above-mentioned deduction, it is highly proposed that other soil reinforcement should be added as well as geotextiles embedded during the construction of railway structures on peat. This is to adequately enhance the stability and strength of the organic peat foundation. Thus, minimizing significant settlement of the railway track during long-term post-construction consolidation phase.

CHAPTER 6 CONCLUSION AND RECOMMENDATIONS FOR FUTURE WORK

6.0 Introduction

In this chapter, a summary of the core outcome of the thesis with conclusions drawn from the findings is elaborated. It highlights the magnitude to which the research objectives and aim have been accomplished and potential future guidance in association with the project. Four subsections are devoted to detailing these observances. A summary of the research objective and methodology is outlined in Section 6.1. Section 6.2 addresses the conclusions deduced from the studies. The limitations associated with this study are discussed in Section 6.3. Finally, Section 6.4 closes by suggesting recommendations based on the results of the lessons from the findings for future work.

6.1 Thesis Summary

This thesis presented a 2D finite element analysis that was conducted for predicting the behavior of railway embankments constructed on soft peat soil under increased loading due to extra tonnage hauled by modern railways. The main aim of this research was to derive a guideline to identify the maximum allowable safe train speed. Important input parameters were used in creating the numerical model and the software RS2 was used for the analysis. A highlight of the methodological steps applied to this study can be summarized as follows:

a) Simulation of the numerical models to present existing situations and identify key trends and formulate guidelines.
b) Prior to building the models, a suitable mesh is identified by careful adjustment to get reliable results.
c) To validate the accuracy of FEM models built, model verifications were performed.
d) To identify the major causes of embankment failure, a set of parametric studies was carried out.

Topics reviewed in Chapter 2 from literature include:

a) Slope stability using LEM / FEM (Shear Strength Reduction).
b) Load transfer mechanism/loads due to passing trains.
c) Foundation instability under embankments (organic soils).

d) The use of wooden piles as foundation support.
e) Settlement (consolidation) of soils; organic soils with a focus on peat.

A presentation of credible ranges of model parameters based on literature is documented in Chapter 3. This is to offer reliable parameters and simulate results tantamount to those from the literature. The process of the built models is presented in Chapter 4. Again, in this chapter, the geometries of the boundary and mesh were methodically controlled. To establish the models, the convergence of the mesh elements is performed to obtain stabilized results. In Chapter 5, the results of the analyses are presented and discussed. Simulation results for the three models (Scenario I, II, and III) established are compared within this chapter. Thus, it was easier to clearly develop the models from Scenario I to III with logic.

6.2 Conclusions on Findings

The conclusions made in this study are pulled from the research findings and based on an analysis of the results. Observations in the preceding chapter revealed that considerations significant to stabilizing a given wooden pile supported slope geometries for maximum safe train speeds can be summarized as follows:

a) Based on the results of sensitivity analysis, longer pile length and smaller pile spacing provide adequate support to both slope and foundation when opted as a method of stabilization of railway embankments constructed on peat.
b) Overall, it appears that a gentler slope is more stable than a steeper one for both long-term and short-term embankment analysis.
c) Hypothetically, results demonstrated that lower slope height yielded a higher slope FS and allows a higher maximum safe train speed.
d) Vertical displacements (settlement) and excess pore water pressure in the railway track foundation increased with increasing train speeds.

6.3 Limitations of the Study

To have a more accurate simulation of the actual train loading conditions, additional critical parameters should be factored in during the modeling. This will help to propose practical standards and measures for the effective and efficient operation during the simulation of railway systems for

future work. As many key parameters were included during the study, contributory conditions could complement it, such as:

a) Centrifugal forces are considered such that the railway track should not have been assumed to be a straight line. Studies could be conducted on the centrifugal forces on the rail generated as a result of the curved tracks. The centrifugal forces acting on the train can significantly impact the lateral stability and dynamic behavior of the train.
b) The load due to trains is not considered static, so the train speed is changed when passing along the track. This is because RS2 cannot combine SSR and dynamic loading.
c) Incorporation of friction between the train wheels and the track such that the track is not assumed to be smooth. Friction plays a crucial role in providing traction and stability to the train, allowing it to accelerate, decelerate, and maneuver safely.
d) To properly define the process of soil failure in the embankment model, environmental factors, like temperature and rain, should be accounted for during the studies. In Canada, the performance of soil varies significantly between the hot summer and cold winter seasons.

6.4 Recommendations for Future Research

Regardless of the above-mentioned deduction, it is highly proposed that other soil reinforcement should be added as well as geotextiles embedded during the construction of railway structures on peat. This is to adequately enhance the stability and strength of the organic peat foundation. Thus, minimizing significant settlement of the railway track during long-term post-construction consolidation phase. Additionally, the following recommendations can be given to optimize future work:

a) To help simulate complex situations which are closer to the realistic field construction, a 3-dimensional model is strongly suggested considering various spatial and dynamic factors that may impact the performance and safety of trains and track systems.
b) The soil ground profile can comprise multiple layers of soil to mimic closer soil layers that exist in realistic situation.

References

1. Abebe, A., and Smith, G.N. I. (2010). *Pile Foundation Design: A Student Guide*, Napier University, Edinburgh, U.K.
2. Adams, J. I. (1965). "The engineering behavior of a Canadian muskeg, " *Proc., 6th International Conference on Soil Mechanics and Foundation Engineering*, University of Toronto Press, Montreal, QC, Canada, 3-7.
3. American Wood Council. (2017). *National Design Specification (NDS) Supplement: Design values for wood construction 2018 Edition*. Leesburg, Virginia, VA.
4. Amorim Cork Composites. (2018). Reinventing elasticity into the railway structure. https://amorimcorkcomposites.com/media/5215/rail_presentation_2018.pdf (accessed 12 June 2020)
5. Anbazhagan, P., Bharatha, T. P., and Amarajeevi, G. (2012). "Study of ballast fouling in railway track formations." *Indian Geotechnical Journal*, 42(2), 87–99.
6. Andrey, J., Kertland, P., Mortsch, L., Canada, E., and Garbo, A. (2014). "Water and transportation infrastructure." *Canada in a Changing Climate: Sector Perspectives on Impacts and Adaptation*, F. Warren and D. Lemmen, eds., Ottawa, ON, Canada, 233–252.
7. AREMA (American Railway Engineering and Maintenance-of-Way Association). (2010). *AREMA manual for railway engineering*, Landover, MD
8. Aryal, K. P. (2006). "Slope stability evaluations by limit equilibrium and finite element methods." Doctoral Thesis, Norwegian University of Science and Technology, Trondheim, Norway.
9. Baffinland Iron Mines LP. (2019). *Design criteria: Railway Design Criteria and Design Rational*. North Baffin, Nunavut, Canada.
10. Beckwith, C. W., Baird, A. J., and Heathwaite, A. L. (2003). "Anisotropy and depth-related heterogeneity of hydraulic conductivity in a bog peat . I : laboratory measurements." *Hydrological Processes*, John Wiley & Sons, Ltd., 89–101.
11. Bell, F.G. (2000). "*Engineering properties of soils and rocks*." 4th Edn., Blackwell Science, Oxford, London,UK.
12. Bogusz, W., and Godlewski, T. (2019). "Geotechnical design of railway embankments – requirements and challenges." *MATEC Web of Conferences*, 262(11002), 1–8.

13. Bourgeau-Chavez, L.L., Grelik, S.L., Billmire, M., Jenkins, L.K., Kasischke, E.S and Turetsky, M.R. (2020). Assessing boreal peat fire severity and vulnerability of peatlands to early season wildland fire, <https://www.frontiersin.org/articles/10.3389/ffgc.2020.00020/full> (accessed 27 June 2020).
14. Briaud J-L. (2013). "Soil constitutive models". Geotechnical Engineering: Unsaturated and Saturated Soils. John Wiley & Sons, Inc. Hoboken, New Jersey (NJ), USA pp 345 – 358.
15. Briggs, K. M., Loveridge, F. A., and Glending, S. (2017). "Failures in transport infrastructure embankments." *Engineering Geology*, 219, 107–117.
16. Budhu, M. (2008). *Soil mechanics and foundations*, 3rd Ed., John Wiley & Sons, Hoboken, New Jersey, NJ, USA.
17. Burrow, M. P. N., Ghataora, G. S., and Bowness, D. (2007). "A comparison of railway track foundation design methods." *Proceedings of the Institution of Mechanical Engineers Part F Journal of Rail and Rapid Transit*, 221(1), 1–12.
18. Cai, F., and Ugai, K. (2000). "Numerical analysis of the stability of a slope reinforced with piles." *Japanese Geotechnical Society*, 40(1), 73–84.
19. Canadian Commission on Building and Fire Codes., and National Research Council Canada. (2015). *National building code of Canada*, National Research Council Canada, Ottawa, Ontario, Canada.
20. Canadian Geotechnical Society. (2006). *Canadian foundation engineering manual*, 2nd Ed., Canadian Geotechnical Society, Canada.
21. Canadian Standards Association. (1980). *Round wood piles*, Canadian Standards Association. Toronto,ON, Ontario.
22. Canadian Standards Association. (2003). *Engineering design in wood*, Canadian Standards Association. Toronto,ON, Ontario.
23. Canadian Sphagnum Peat Moss Association (CSPMA). (2011). Peat and Peatland, < https://peatmoss.com/what-is-peat-moss/peatland-distribution/ > (accessed 20 December 2019).
24. Carder, D. R., and Temporal, J. (2000). *A review of the use of spaced piles to stabilise embankment and cutting slopes*. TRL REPORT 466, Crowthorne, United Kingdom (UK), 1-34.

25. Chai, J., and Bergado, D. T. (1993). “Some techniques for finite element analysis of embankments on soft ground.” *Canadian Geotechnical Journal*, 30(4), 710–719.
26. Chakrabarti, S., Cheenikal, L., and Singh, G. (2013). “Embankment design and construction for a major rail upgrade project in Western Australia.” *Australian Geomechanics Journal*, 48(2), 2–9.
27. Chang, S., and Zhang, S. (2006). *Geological engineering manual*, 4 th Ed., China Construction and Industry Press, Beijing, China.
28. Chen, R. P., Chen, Y. M., Han, J., and Xu, Z. Z. (2008). “A theoretical solution for pile-supported embankments on soft soils under one-dimensional compression.” *Canadian Geotechnical Journal*, 45(2003), 611–623.
29. Ciotlaus, M., Kollo, G., Moldovan, D., and Muntean, L. (2017). “Slope stability of railway embankment*.” 10th International Conference Interdisciplinarity in Engineering, INTER-ENG 2016, 6-7 October 2016, Tirgu Mures, Romania*, L. Moldovan and A. Gligor, eds., Elsevier Ltd, Tirgu Mures, 52–59.
30. Cowan, D. (2013). *Measure and manage organic soils,* SGS Agri-Food Laboratories Inc., Guelph, Ontario, Canada.
31. CN Engineering Specifications for Industrial Tracks (2019). *CN – Engineering office of design & construction,* Montreal, Canada.
32. Den Haan, E. J. (1997). *An overview of the mechanical behavior of peats and organic soils*. TPN200100, Geodelft Publication, Delft, Netherlands, 1-29.
33. De Guzman, E. M., and Alfaro, M. (2017). “Settlement of embankments on peat foundations: Two case studies.” *Proceedings of the 19th International Conference on Soil Mechanics and Geotechnical Engineering*, International society for soil mechanics and geotechnical engineering, Seoul, S. Korea, 1349–1352.
34. Deboucha, S., Hashim, R., and Alwi, A. (2008). “Engineering properties of stabilized tropical peat soils.” *Electronic Journal of Geotechnical Engineering*, Vol. 13(Bund. E), 1–9.
35. Decker, M. (1982). *Peat as an energy source*, Internal report Ground Engineering, No. 104, Purdue University, West Lafayette, Indiana, IN, USA.
36. Dhowian, A. W., and Edil, T. B. (1980). “Consolidation behavior of peats.” *Geotechnical Testing Journal*, 3(3), 1-11.

37. Dostál, I., and Adamec, V. (2011). "Transport and its role in the Society." *Transactions on Transport Sciences*, 4(2), 43–56.
38. Doyle, N. F. (1980). *Railway track design a review of current practice*, (Economic bureau of transport), Canberra: Australian Government Publishing Service, Melbourne, Victoria, Australia.
39. Drusa, M., Kais, L., Vlček, J., and Mečár, M. (2015). "Piled embankment design comparison." *Civil and Environmental Engineering (Sciendo)*, 11(1), 76–82.
40. Duncan, J. M. (1996). "Soil slope stability." *Landslides: Investigation and Mitigation*, K. A. Turner and R. L. Schuster, eds., Transportation Research Press, Washington DC, USA, 337–371.
41. Dutch Water Sector. (2015). Final countdown for clay-peat levee: slide failure to occur any moment, https://www.dutchwatersector.com/news/final-countdown-for-clay-peat-levee-slide-failure-to-occur-any-moment (accessed 08 August 2020).
42. Eberhardt, E. (2003). "Rock slope stability analysis - Utilization of advanced numerical techniques." *University of British Columbia, Vancouver*, (Department of Earth, Ocean and Atmospheric Sciences), 1-41.
43. Egeli, I., and Usun, H. (2012). "Designing high-speed train railway embankments using finite
44. element analysis." *Arabian Journal for Science and Engineering*., 37, 2127-2126.
45. Esmaeili, M., Nik, M. G., and Khayyer, F. (2013). "Experimental and numerical study of micropiles to reinforce high railway embankments." *International Journal of Geomechanics*, 13(6), 729–744.
46. Esveld, C. (2001). *Modern railway track*, (D. Z. Nieuwenhuize, ed.), MRT -Productions, Delft, The Netherlands.
47. European Commission (EU). (2014). "Commission Regulation." Official Journal of the European Union, 6(1), 228-389.
48. Forde, M., Zimele, L., De Bold, R., and Ho, C. (2017). *Evaluating the dynamic behavior of concrete slab*. (M. Forde, ed.), Engineering Technics Press, Edinburgh, Scotland.
49. Freitas de Cunha, J. P. (2013). "Modelling of ballasted railway tracks for high-speed trains." PhD Thesis, University of Minho, Braga, Portugal.

50. Galloway, D., Jones, D. R., and Ingebritsen, S. (1999). *Land subsidence in the United States*. U.S. Geological Survey, Denver, Colorado, USA.
51. Gedney, D. S., and Weber Jr, W. (1978). "Design and construction of soil slopes." *Landslides: analysis and control*, R. l. Schuster and R. J. Krizek, eds., Transportation Research Board, Washington DC, USA, 172–191.
52. Gharpure, A. D., Korulla, M., Jayakrishnan, P. V, Scotto, M., and Naughton, P. (2008). "Design methods for pile supported basal reinforced embankments over soft clay." *Proceedings of the 4th Asian Regional Conference on Geosynthetics*, Shanghai, China, 703–708.
53. Giannakos, K. (2010). "Interaction between superstructure and substructure in railways." 2010 - *Fifth International Conference on Recent Advances in Geotechnical Earthquake Engineering and Soil Dynamics*, Missouri University of Science and Technology, San Diego, California, USA, 1–9.
54. Grand, B. A. (1970). "Types of piles: Their characteristics and general use." *49th Annual Meeting of the Highway Research Board*, Washington DC, USA, 3–15.
55. Gruen Jr, H., and Lovell, C. (1983). *Uses of Peats as embankment foundations*, Edward Arnold (Publishers) Ltd, West Lafayette, Indiana, USA.
56. Gustafsson, P., and Tian, T. (2011). "Numerical study of different creep models used for soft soils." Master of Science Thesis in the Master's Programme Geo and Water Engineering Chalmers university of technology, Gothenburg, Sweden.
57. Gupta, V., Bhasin, R. K., Kaynia, A. M., Chauhan, V. K., Saini, A. S., Tandon, R., and Pabst, T. (2016). "Finite element analysis of failed slope by shear strength reduction technique: a case study for Surabhi Resort Landslide, Mussoorie township, Garhwal Himalaya." *Geomatics, natural hazards and risk*, 7(5), 1–14.
58. Hammah, R. E., Curran, J. H., and Corkum, B. (2004). "Stability analysis of rock slopes using the finite element method." *EUROCK 2004 & 53rd Geomechanics Colloquium*, Schubert, ed., rocscience Inc., Toronto, Canada, 1–6.
59. Hammah, R., Yacoub, T., Corkum, B. T., and Curran, J.H. (2005). "A comparison of finite element slope stability analysis with conventional limit-equilibrium investigation." *58th Canadian Geotechnical and 6th Joint IAH-CNC and CGS Groundwater Specialty Conferences, rocscience Inc*., Toronto, Canada, Saskatoon, 1–8.

60. Hammah, R., Yacoub, T., and Curran, J. (2006). “Investigating the performance of the shear strength reduction (SSR) method on the analysis of reinforced.” *Proceedings of the 59th Canadian Geotechnical and 7th Joint CGS/IAH-CNC Groundwater Specialty Conference, Vancouver, British Columbia*, Rocscience Inc, Toronto, Canada, 2–6.
61. Hashim, R., and Islam, M.S. (2008). “A model study to determine engineering properties of peat soil and effect on strength after stabilization.” *European Journal of Scientific Research*, 22 (2), 205-215.
62. Hayashi, H., Nishimoto, S., and Yamanashi, T. (2016). “Applicability of settlement prediction method to peaty ground.” *Soils and Foundations Open access (Japanese Geotechnical Society (JGS))*, Elsevier Publishing company, 56(1), 144–151.
63. Hendry, M. T. (2011). “The geomechanical behavior of peat foundations below rail-track structures.” Degree of Doctor of Philosophy in the Department of Civil Engineering, University of Saskatchewan, Saskatoon, Canada.
64. Hannigan, P. J., Rausche, F., Likins, G. E., Robinson, B. R., and Becker, M. L. (1997). *Design and construction of driven pile foundations*. Federal Highway Administration (FHWA).
65. Huat, B. B. K. (2006). “Deformation and shear strength characteristics of some tropical peat and organic soils.” *Pertanika Journal of Science & Technology (JST),* 14(1&2), 61–74.
66. Ibrahim, A., Huat, B. B., Asadi, A. A., and Nahazanan, H. (2014). “Foundation and embankment construction in peat: An overview.” *Electronic Journal of Geotechnical Engineering*, 19, 10079–10094.
67. International Union of Railways. (1994). *Earthworks and track-bed layers for railway lines: UIC code*, 2nd Ed., International Union of Railways, Paris, 85–100.
68. Islam, S., and Hashim, R. (2009). “Bearing capacity of stabilised tropical peat by deep mixing method.” *Australian Journal of Basic and Applied Sciences*, 3(2), 682–688.
69. Jennings, P., and Johnston, T. (2013). “Permeability of peat: an engineering case study.” E.T. Hanrahan Memorial Symposium, Applied Ground Engineering Consultants (AGEC) Ltd., Bagenalstown County Carlow, Dublin, Republic of Ireland, 1–29.
70. Jiang, Y., and Nimbalkar, S. (2019). “Finite element modeling of ballasted rail track capturing effects of geosynthetic inclusions.” *Frontiers in Built Environment*, 5, 1–

11Jinming, H., and Xue-hui, M. (2011). “Physical and chemical properties of peat.” *Coal, oil shale, natural bitumen, heavy oil and peat*, G. Jinsheng, ed., Encyclopedia of Life Support Systems (EOLSS), Beijing.

71. Johannessen, I. J., and Bjerrum, J. M. (1965). “Measurement of the compression of a steel pile to rock due to settlement of the surrounding clay.” *Proc., 6th ICSMFE Conf.*, Soil Mech & Fdn Eng Conf Proc., Montreal, Canada/, Pittsburgh, pp. 261-264.
72. Johari, N., Bakar, I., Razali, S. N., and Wahab, N. (2016). “Fiber effects on compressibility of peat.” *Soft soil engineering international conference 2015 (SEIC2015),* IOP Publishing, Malaysia, 1-10.
73. Joosteen, H., and Clarke, D. (2002). *Wise use of mires and peatlands – background and principles including a framework for decision – making*, International Mire Conservation Group and International Peat Society, Totnes, Devon, UK.
74. Kalantari, B. (2013). “Civil engineering significant of peat.” *Global Journal of Researches in Engineering Civil and Structural Engineering,* 13(2), 1-6.
75. Kazemian, S. and Mohayedi, H. (2014). " Improvement of settlement problems of fibrous peat." *Geo-Hubei 2014 International Conference on Sustainable Civil Infrastructure*, Geotechnical Special Publication, 125-132.
76. Kazemian, S., and Huat, B. B. K. (2009). “Compressibility characteristics of fibrous tropical peat reinforced with cement column.” *Electronic Journal of Geotechnical Engineering*, 14(Bund. C), 1-13.
77. Kazemian, S., Huat, B. B. K., Prasad, A., and Barghchi, M. (2011). “A state of art review of peat: Geotechnical engineering perspective.” *International Journal of Physical Sciences*, 6(8), 1974–1981.
78. Keller, G., and Sherar, J. (2003). *Low-volume roads engineering: best management practices: Field Guide,* USDA Forest Service/USAID, Virginia, USA.
79. Kim, E., Kim, M. E., Delos, G., and Clark, T. (2019). “Post-construction alignment revision in direct-fixation railroad tracks.” *Sustainable Rail and Metro Systems,* 11(21), 1–14.
80. Koca, T. K., and Koca, Y. M. (2020). “Comparative analyses of finite element and limit-equilibrium methods for heavily fractured rock slopes.” *Indian Academy of Sciences*, 129(49), 1–13.

81. Kolay, P. K., and Taib, S. N. L. (2018). *Physical and geotechnical properties of tropical peat and its stabilization,* IntechOpen, London, UK.
82. Kosthilaire. (2015). Geotechnical portfolio; personal observations and reflections. <https://kosthilaire8162.wordpress.com/author/kosthilaire8162/> (accessed 15 December 2020).
83. Kroetsch, D. J., Geng, X., Chang, S. X., and Saurette, D. D. (2011). "Organic soils of Canada: Part 1. Wetland organic soils." *Canadian Journal of Soil Sciences*, 91(5), 807-822.
84. Labadz, J., Allott, T., Evans, M., Butcher, D., Billett, M., Stainer, S., Yallop, A., Jones, P., Innerdale, M., Harmon, N., Maher, K., Bradbury, R., Mount, D., O'Brien, H., and Hart, R. (2010). *Peatland Hydrology (Draft Scientific Review)*, IUCN UK Peatland Programme'sCommission of Inquiry on Peatlands, Edinburgh United Kingdom (UK).
85. Li, D., Hyslip, J., Sussmann, T., Chrismer, S., Li, D., Hyslip, J., Sussmann, T., and Chrismer, S. (2016). "Substructure." *Railway Geotechnics*, Taylor & Francis Group, LLC, London, UK, 1–56.
86. Likitlersuang, S., Pholkainuwatra, P., Chompoorat, T., and Keawsawasvong, S. (2018). "Numerical modelling of railway embankments for high-speed train constructed on soft soil." *Journal of GeoEngineering*, 13(3), 149–159.
87. Lin, H., Zhong, W., Xiong, W., and Tang, W. (2014). "Slope stability analysis using limit equilibrium method in nonlinear criterion." *The Scientific World Journal*, Hindawi Publishing Corporation, 2014.
88. Lindberg, N. (2020). "Three-dimensional effects in slope stability for shallow excavations." Master of Science Program in civil engineering, Luleå University of Technology, Luleå, Sweden.
89. Long, M. (2005). "Review of peat strength, peat characterisation and constitutive modelling of peat with reference to landslides." *Studia Geotechnica et Mechanica*, XXVII (3), 24.
90. Lu, H. H., Xu, L. M., Fredlund, M. D., and Fredlund, D. (2013). "Comparison of 3D finite element slope stability with 3D limit equilibrium analysis." *Proceedings of the 18th International Conference on Soil Mechanics and Geotechnical Engineering*, Paris, France, 1-4.

91. MacFarlane, I. C. (1969). *Muskeg Engineering Handbook*, National Research Council of Canada, University of Toronto Press, Toronto, Canada.
92. Makusa, G. P. (2013). *A review of geotechnical behavior of stabilized soils: Design and analysis considerations*, Luleå tekniska universitet, Luleå, Sweden, 1-62.
93. Mathew, T. V, and Rao, K. K. (2007). "Role of transportation in society." Introduction to Transportation Engineering, NPTEL, Mumbai, India, 2–6.
94. Matthews, C., Farook, Z., and Helm, P. H. (2014). "Slope stability analysis – limit equilibrium or the finite element method?" *Ground Engineering*, 48(5), 22–28.
95. McAfee, M. (1984). "Drainage of peat soils. A literature review". Master of Science degree. Swedish University of Agricultural Sciences, Department of Soil Sciences Division of Agricultural Hydrotechnics, Uppsala, Sweden.
96. McHenry, T. M., and Rose, J. G. (2012*). Railroad subgrade support and performance indicators: A review of available laboratory and in – situ testing methods*. Kentucky Transportation Center, Lexington, KY, USA.
97. Makusa, G. P. (2013). *A review of geotechnical behavior of stabilized soils: Design and analysis considerations*, Luleå tekniska universitet, Luleå, Sweden, 1-62.
98. Mestat, P., Bourgeois, E., and Riou, Y. (2017). "Numerical modelling of embankments and underground works." *Computers and Geotechnics*, 31(3), 227–236.
99. Mochtar, N., Yulianto, F. E., and Harwadi, F. (2015). "The effect of curing period to the physical and engineering properties of fibrous peat soil stabilized with lime properties of fibrous peat soil stabilized with lime caco3 + pozolon." *Proceedings of the second, Makassar International Conference on Civil Engineering (MICCE 2015), Makassar, Indonesia,* Makassar, Indonesia, 35–40.
100. Morrell, J. J., Helsing, G. uy G., and Graham, R. (1984). *Wood maintenance manual: A guide for proper use of Douglas-fir in marine exposures*. Corvallis, Oregon.
101. Munro, R. (2004). *Dealing with bearing capacity problems on low volume roads constructed on peat including case histories from roads projects within the roadex partner districts*. The Highland Council, Scotland.
102. Murthy, V. N. (2003). *Geotechnical Engineering: Principles and practices of soil mechanics and foundation engineering*, Marcel Dekker Inc, New York, NY, USA,365–418.

103. Nakamura, A., Cai, F., and Ugai, K. (2008). "Embankment basal stability analysis using shear strength reduction finite element method." *Landslide and Engineering Slope. From the past to the future, two volume*, Z. Chen, J.-M. Zhang, K. Ho, F.-Q. Wu, and Z.-K. Li, eds., CRC Press Taylor & Francis Group, Xi'an, P.R. of China, 851–856.
104. National Academies of Sciences, Engineering, and Medicine. (2012). *Track design handbook for light rail transit, Second Edition*. The National Academies Press, Washington DC, 1-647.
105. Osman, K. T. (2017). *Management of soil problems*. Springer International Publishing AG, Chittagong, Bangladesh.
106. Peat Moss Associations in Canada. (2020). Peatland distribution in Canada's provinces and territories. https://www.peatmoss.com/peatlands/ (accessed 09 May 2020).
107. Peck, R. B., Hanson, W. E., and Thornburn, T. H. (1974). *Foundation engineering*, Wiley, New York, NY, USA.
108. Poulos, H.G. (2006). *Methods of Analysis of Piled Raft Foundations: A Report Prepared on Behalf of Technical Committee TC18 on Piled Foundations 2014/15*, International Society of Soil Mechanics and Geotechnical Engineering, The University of Sydney, Sydney, Australia.
109. Prakash, S., and Sharma, H. D. (1990). *Pile foundations in engineering practice*. A wiley-interscience publication-John Wiley & Sons, Inc., Toronto, Canada.
110. Profillidis, V. A. (2014). *Railway management and engineering*, Ashgate Publishing, Farnham, U.K. (United Kingdom)
111. Pyrgidis, N. C. (2016). *Railway transportation systems: Design, construction and operation*. CRC Press Taylor & Francis Group, Boca Raton, Florida, USA.
112. Quigley, P., and Naughton, P. (2007). "Design of piled embankments." *Proceedings of the conference on soft ground engineering, organized by the Geotechnical Society of Ireland*, Educational Publishers, New York, USA, 1–9.
113. Rabie, M. (2014). "Comparison study between traditional and finite element methods for slopes under heavy rainfall." *HBRC Journal*, Housing and Building National Research Center, 10(2), 160–168.

114. Railway Association of Canada. (2016). A Parliamentarian's guide to Canada's railways. https://www.railcan.ca/wp-content/uploads/2016/10/RAC_ParliamentGuide_EN.pdf (accessed 10 June 2020)
115. Raithel, M., Kirchner, A., and Kempfert, H-G. (2008). "Retrofitting distortion-induced fatigue cracking of noncomposite steel girder-floorbeam-stringer bridges." *Proc., 4th Asian Regional Conference on Geosynthetics*, Shanghai, China, 4-7.
116. Rakoczy, A. M., and Nowak, A. S. (2018). "Live load spectra for railway bridges in USA." *4 Scientific Conference, Railway engineering – challenges and opportunities*, Krynica Zdroj, Poland.
117. Razali, M. N. S., Bakar, I. bin, and Zainorabidin, A. (2013). "Behaviour of peat soil in instrumented physical model studies." *Malaysian Technical Universities Conference on Engineering & Technology 2012, MUCET 2012 Part 3 - Civil and Chemical Engineering, Elsevier B.V.,* Perlis, Malaysia, 145–155.
118. Rezanezhad, F., Price, J. S., Quinton, W. L., Lennartz, B., Milojevic, T., and Cappellen, P. Van. (2016). "Structure of peat soils and implications for water storage, flow and solute transport: A review update for geochemists." *Chemical Geology*, 429, 75–84.
119. Rocscience. (n.d). Constitutive Models Manual; Soft Soil Creep Model- PLAXIS, <https://www.rocscience.com/help/rs3/pdf_files/theory/Constitutive_models_Manual/18-Soft_Soil_Creep_Model_-_PLAXIS.pdf> (accessed 08 November 2020).
120. Rocscience Inc. (2004). *Application of the finite element method to slope stability,* Rocscience Inc. Toronto, Canada.
121. Rocscience Inc. (2019). RS2 Excavation & Design support software. Specification sheet.
122. Rollins, M. (2012). *Timber Piling Design*, The Wood Products Council, Washington DC, USA.
123. Rowe, R. K. (2012). *Geotechnical and geoenvironmental engineering handbook*, Springer Science & Business Media, Berlin, Germany.
124. Salunkhe, D. P., and Bartakke, R. N. (2017). "An overview on methods for slope stability analysis." *International Journal of Engineering Research & Technology (IJERT)*, 6(03), 528–535.

125. Satibi, S., Meij, R. Van Der, and Leoni, M. (2007). *Piled embankments: literature review and required further research using numerical analysis*. Institutsbericht 34 Institute for Geotechnical Engineering University of Stuttgart, Stuttgart, Germany.
126. Seyedan, S., and Sołowski, W. T. (2019). "Enhancing constitutive models for soils: Adding the capability to model nonlinear small strain in shear." *Advances in Civil Engineering*, 2019(6016350), 1–11
127. Sayeed, A. M., and Shahin, A. M. (2017). "Design of ballasted railway track foundations using numerical modelling Part I: Development." *Canadian Geotechnical Journal*, 55(3), 369–396.
128. Selig, E. T., and Waters, J. M. (1994). *Track technology and substructure management*, Thomas Telford, London, United Kingdom (UK).
129. Sing, W. L., Hashim, R., and Ali, F. H. (2008). "Compression rates of untreated and stabilized peat soils." *Electronic Journal of Geotechnical Engineering*, 13 (Bund F), 1-13.
130. State of New York Department of Transportation. (2015). *Geotechnical engineering manual: guidelines for embankment construction.* State of New York Department of Transportation, New York, USA.
131. Susanti, R. D., Maulana, and Waruwu, A. (2017). "Bearing capacity improvement of peat soil by preloading." *ARPN Journal of Engineering and Applied Sciences*, 12(1), 121–124.
132. Sutejo, Y., Saggaff, A., Rahayu, W., and Hanafiah. (2019). "Hydraulic conductivity and compressibility characteristics of fibrous peat hydraulic conductivity and compressibility characteristics of fibrous peat." *Sriwijaya International Conference on Science, Engineering, and Technology,* IOP Publishing, Bristol, United Kingdom, 1-12.
133. Tan, Y. (2008). "Finite element analysis of highway construction in peat bog." *Canadian Geotechnical Journal*, 45(2), 147–160.
134. Ti, K.S., Bujang B. K.Huat,J. Noorzaei, M. S. Jaafar, and G.S.Sew.2009. "A review of basic soil constitutive models for geotechnical application." *Electron.J.Geotech.Eng.*, 14, 1-18.
135. Tien, N.T. (1981). *Design of piles in cohesive soil*, Varia 65, SGI, Linköping, Sweden.
136. Toprak, B., Sevim, O., and Kalkan, I. (2018). "The functions of pile types and piles used in construction." *International Journal of Advances in Mechanical and Civil Engineering*, 5(2), 4.

137. Thompson, K. (2010). *Railway noise and vibration: mechanisms, modeling and means of control*. Southampton, UK: Elsevier.
138. Timber Piling Council. (2016). *Timber Pile Design and Construction Manual*. (J. G. Collin, ed.), American Wood Preservers Institute, Fairfax, Virginia, VA, USA.
139. Transportation Research Board of National Research Council. (1977). *Design of pile foundations*: *national cooperative highway research program synthesis of highway practice 42*, Transportation Research Board, Washington DC, USA.
140. Transportation Safety Board of Canada (2007). *Railway investigation report r04q0040 main-track derailment, Canadian national train u-781-21-17 mile 3.87*, Transportation Safety Board of Canada, Montreal, QC, Canada.
141. Uthayakumar, M. and Oliver, M. (2018). "Case history of pile supported highway embankments on very soft and compressible soils." *Proceedings of the Canadian Geotechnical Conference*, September 23 - 26, 2017, Edmonton, Alberta.
142. Verry, E. S., Boelter, D. H., Päivänen, J., Nichols, D. S., Malterer, T., and Gafni, A. (2011). "Physical properties of organic soils." *Peatland biogeochemistry and watershed hydrology at the Marcell Experimental Forest.*, CRC Press, Boca Raton, Florida, United States, 135–176.
143. Wang, C., Zhou, S., Guo, P., and Wang, B. (2014). "Experimental analysis on settlement controlling of geogrid-reinforced pile-supported embankments on collapsible loess in high-speed railway." *International Journal of Pavement Engineering*, Taylor & Francis, 15(9), 867–878.
144. Wang, J. G., Liu, G. R., and Lin, P. (2002). "Numerical analysis of Biot's consolidation process by radial point interpolation method." *International Journal of Solids and Structures*, 39(6), 1557–1573.
145. Wong, R. C. K., Thomson, P. R., and Choi, E. S. C. (2006). "In situ pore pressure responses of native peat and soil under train load: A Case Study." *Journal of Geotechnical and Geoenvironmental Engineering*, 132(10), 1360–1369.
146. Xue, F.-C., and Zhang, J.-M. (2014). "Dynamic responses of rail-embankment-foundation on high-speed railways under moving loads." *10th Asia Pacific Transportation Development Conference* ASCE (American Society of Civil Engineers) Library, Beijing, China, 655-662

147. Yang, M., and Liu, K. (2016). “Deformation behaviors of peat with influence of organic matter.” Creative Commons Attribution 4.0 International License*,* Springer International Publishing, 18.
148. You, G., Mandalawi, M. Al, Soliman, A., Dowling, K., and Dahlhaus, P. (2018). “Finite element analysis of rock slope stability using shear strength reduction method.” *International Congress and Exhibition “Sustainable Civil Infrastructures: Innovative Infrastructure Geotechnology*,” W. Frikha, S. Varaksin, and A. Viana da Fonseca, eds., Springer International Publishing, New York, NY, USA,227–235.
149. Yu, H., and Sloan, S. (1994). “A note on bearing capacity of soft clays under embankments.” *Journal of Geotechnical Engineering,* 120(1), 246–255.
150. Zainorabidin, A., and Wijeyesekera, D. C. (2008). “Geotechnical characteristics of peat.” *Proceedings of Advances in Computing and Technology, (AC&T) The School of Computing and Technology 5th Annual Conference*, University of East London, London, UK, 71–78.
151. Zaytsev, A. A. (2014). “Physical modeling embankment on peat foundation with reinforcing of the wooden piles.” *Proceedings of the 8th International Conference on Physical Modelling in Geotechnics 2014 (ICPMG 2014), Perth, Australia*, C. Gaudin and D. White, eds., CRC Press Taylor & Francis Group, London, UK, 877–881.
152. Zaytsev, A.A., Frolovsky, Y.K., Gorlov, A.V., Petryaev, A. V., Ganchits, V.V., (2018). “Physical modelling and monitoring of the subgrade and weak foundation and its reinforcing with geosynthetics.” *Preceedings of the 9th International conference on physical modeling in geotechnics,* London, United Kingdom (UK), pp 1277- 1282.
153. Zhao, J., Zhou, T., and Wang, G. (2015). “Numerical analysis of consolidation settlement and creep deformation of artificial island revetment structure in a large-scale marine reclamation land.” *Polish Maritime Research*, 22(86), 35–42.
154. Zhang, L., and O’Kelly, B. (2013). “Constitutive models for peat - A review.” *Proceedings of the 12th International Conference on Computational Plasticity – Fundamentals and Applications (COMPLAS XII),* E. Oñate, D. R. Owen, D. Peric, and B. Suárez, eds., International Center for Numerical Methods in Engineering (CIMNE), Barcelona, Spain, 1294–1304.

155. Zhang, C., Zhao, M., Zhou, S., and Xu, Z. (2019). “A theoretical solution for pile-supported embankment with a conical pile-head.” MDPI *open access journals (Applied Sciences)*, 9(13), 1-19.
156. Zhang, T., Cui, Y., Lamas-Lopez, F., Calon, N., and D’Aguiar, S. C. (2016). “Modelling stress distribution in substructure of French conventional railway tracks.” *Construction and Building Materials*, 116, 326-334.
157. Zhao, J., Zhou, T., and Wang, G. (2015). “Numerical analysis of consolidation settlement and creep deformation of artificial island revetment structure in a large-scale marine reclamation land.” *Polish Maritime Research*, 22(86), 35–42.
158. Zhou, S., Wang, B., and Shan, Y. (2020). “Review of research on high-speed railway subgrade settlement in soft soil area.” *Railway Engineering Science,* Springer Singapore, 28(2), 129–145.

Appendix

Table 1. Available timber pile sizes per CAN/CSA 056 -M79.

Size Designation	36	33	30	27	24
Diameter at Extreme Butt or Large End (cm)	36	33	30	27	24
Length (m)	Diameter at Tip Small End (cm)				
Up to 6	25	25	23	20	18
6 to 11	25	23	20	18	15
12 to 14	23	20	18	15	-
15 to 18	20	18	18	-	-
19 to 21	20	18	15	-	-
22 to 27	18	15	-	-	-
28 to 32	15	13	-	-	-

*Guide to the selection of pile sizes.

The equation used in estimating pile length according to Wang and Chen (2011)

$$l_e = d\sqrt{\frac{5E_P(3-2\mu)(1+\mu)}{4E_S}}$$

Where μ is the Poisson ratio of soil, d is pile diameter. E_P and E_S is the elastic modulus of pile and compression modulus of soil respectively. l_e is the effective pile length defined as the bearing capacity of a single pile during the transfer and spreading of load to the surrounding soil (Zhou et al. 2015).

Table 2. Table of results for designated pile size for module creation.

	Embankment Height (m)				
	5	4	3	2	1
Pile Size (m)					
Diameter	0.36	0.33	0.3	0.27	0.24
Length	22.70	20.88	18.92	17.23	15.14
Pile Spacing	1.62	1.49	1.35	1.22	1.08

*Pile Spacing = 4.5 (D); D is pile diameter

Table 3. Maximum Vertical displacement of 1m embankment under long term load settlement (slope ratio = 3:1)

D_{bs} (m)	Train speed (km/h)					
	0	24	48	72	96	120
	Vertical displacement (m)					
-20	-0.17	-0.18	-0.20	-0.22	-0.24	-0.27
-15	-0.20	-0.22	-0.23	-0.26	-0.28	-0.30
-10	-0.24	-0.25	-0.27	-0.30	-0.32	-0.35
-5	-0.26	-0.28	-0.31	-0.36	-0.37	-0.39
0	-0.29	-0.31	-0.35	-0.39	-0.41	-0.44
5	-0.26	-0.28	-0.31	-0.36	-0.37	-0.39
10	-0.24	-0.25	-0.27	-0.30	-0.32	-0.35
15	-0.20	-0.22	-0.23	-0.26	-0.28	-0.30
20	-0.17	-0.18	-0.20	-0.22	-0.24	-0.27

*D_{bs} = Distance along ballast surface from center line (m)

Table 4. Maximum Vertical displacement of 2 m embankment under long term load settlement (slope ratio = 3:1)

Dbs (m)	Train speed (km/h)					
	0	24	48	72	96	120
	Vertical displacement (m)					
-20	-0.22	-0.26	-0.27	-0.3	-0.33	-0.35
-15	-0.22	-0.26	-0.27	-0.3	-0.33	-0.35
-10	-0.28	-0.29	-0.31	-0.34	-0.37	-0.40
-5	-0.3	-0.33	-0.35	-0.39	-0.43	-0.47
0	-0.34	-0.38	-0.41	-0.45	-0.48	-0.51
5	-0.30	-0.33	-0.35	-0.39	-0.43	-0.47
10	-0.28	-0.29	-0.31	-0.34	-0.37	-0.40
15	-0.22	-0.26	-0.27	-0.3	-0.33	-0.35
20	-0.22	-0.26	-0.27	-0.3	-0.33	-0.35

*D_{bs} = Distance along ballast surface from center line (m)

Table 5. Maximum Vertical displacement of 3 m embankment under long term load settlement (slope ratio = 3:1)

D_{bs} (m)	Train speed (km/h)					
	0	24	48	72	96	120
	Vertical displacement (m)					
-20	-0.19	-0.22	-0.24	-0.26	-0.30	-0.32
-15	-0.23	-0.25	-0.27	-0.30	-0.32	-0.36
-10	-0.29	-0.3	-0.35	-0.38	-0.39	-0.41
-5	-0.32	-0.36	-0.38	-0.42	-0.48	-0.50
0	-0.37	-0.40	-0.46	-0.50	-0.54	-0.59
5	-0.32	-0.36	-0.38	-0.42	-0.48	-0.50
10	-0.29	-0.30	-0.35	-0.38	-0.39	-0.41
15	-0.23	-0.25	-0.27	-0.30	-0.32	-0.36
20	-0.19	-0.22	-0.24	-0.26	-0.30	-0.32

***D_{bs}** = Distance along ballast surface from center line (m)

Table 6. Maximum Vertical displacement of 1 m embankment under short term load settlement (slope ratio = 3:1)

D_{bs} (m)	Train speed (km/h)					
	0	24	48	72	96	120
	Vertical displacement (m)					
-20	-0.14	-0.15	-0.19	-0.21	-0.22	-0.23
-15	-0.17	-0.19	-0.22	-0.26	-0.27	-0.29
-10	-0.21	-0.24	-0.28	-0.30	-0.31	-0.33
-5	-0.23	-0.25	-0.30	-0.32	-0.35	-0.38
0	-0.26	-0.29	-0.33	-0.37	-0.39	-0.40
5	-0.23	-0.25	-0.30	-0.32	-0.35	-0.38
10	-0.21	-0.24	-0.28	-0.30	-0.31	-0.33
15	-0.17	-0.19	-0.22	-0.26	-0.27	-0.29
20	-0.14	-0.15	-0.19	-0.21	-0.22	-0.23

***D_{bs}** = Distance along ballast surface from center line (m)

Table 7. Maximum Vertical displacement of 2 m embankment under short term load settlement (slope ratio = 3:1)

D_{bs} (m)	Train speed (km/h)					
	0	24	48	72	96	120
	Vertical displacement (m)					
-20	-0.15	-0.17	-0.20	-0.22	-0.22	-0.24
-15	-0.17	-0.21	-0.22	-0.25	-0.27	-0.29
-10	-0.23	-0.24	-0.27	-0.29	-0.31	-0.33
-5	-0.25	-0.27	-0.3	-0.32	-0.37	-0.4
0	-0.29	-0.32	-0.35	-0.39	-0.45	-0.47
5	-0.25	-0.27	-0.3	-0.32	-0.37	-0.4
10	-0.23	-0.24	-0.27	-0.29	-0.31	-0.33
15	-0.17	-0.21	-0.22	-0.25	-0.27	-0.29
20	-0.15	-0.17	-0.2	-0.22	-0.22	-0.24

*D_{bs} = Distance along ballast surface from center line (m)

Table 8. Maximum Vertical displacement of 3 m embankment under short term load settlement (slope ratio = 3:1)

D_{bs} (m)	Train speed (km/h)					
	0	24	48	72	96	120
	Vertical displacement (m)					
-20	-0.16	-0.19	-0.21	-0.23	-0.25	-0.29
-15	-0.18	-0.23	-0.24	-0.25	-0.27	-0.32
-10	-0.24	-0.27	-0.29	-0.32	-0.34	-0.38
-5	-0.29	-0.31	-0.33	-0.39	-0.41	-0.47
0	-0.33	-0.36	-0.39	-0.43	-0.48	-0.5
5	-0.29	-0.31	-0.33	-0.39	-0.41	-0.47
10	-0.24	-0.27	-0.29	-0.32	-0.34	-0.38
15	-0.18	-0.23	-0.24	-0.25	-0.27	-0.32
20	-0.16	-0.19	-0.21	-0.23	-0.25	-0.29

*D_{bs} = Distance along ballast surface from center line (m)

Table 9. Maximum Vertical displacement of 1 m embankment under long term load settlement (slope ratio = 2:1)

D_{bs} (m)	Train speed (km/h)					
	0	24	48	72	96	120
	Vertical displacement (m)					
-20	-0.18	-0.2	-0.22	-0.25	-0.28	-0.32
-15	-0.22	-0.24	-0.26	-0.29	-0.31	-0.35
-10	-0.26	-0.27	-0.3	-0.32	-0.34	-0.38
-5	-0.29	-0.33	-0.35	-0.37	-0.39	-0.43
0	-0.32	-0.37	-0.4	-0.42	-0.44	-0.47
5	-0.29	-0.33	-0.35	-0.37	-0.39	-0.43
10	-0.26	-0.27	-0.3	-0.32	-0.34	-0.38
15	-0.22	-0.24	-0.26	-0.29	-0.31	-0.35
20	-0.18	-0.2	-0.22	-0.25	-0.28	-0.32

*D_{bs} = Distance along ballast surface from center line (m)

Table 10. Maximum Vertical displacement of 2 m embankment under long term load settlement (slope ratio = 2:1)

D_{bs} (m)	Train speed (km/h)					
	0	24	48	72	96	120
	Vertical displacement (m)					
-20	-0.19	-0.21	-0.24	-0.27	-0.29	-0.34
-15	-0.23	-0.26	-0.28	-0.31	-0.37	-0.39
-10	-0.28	-0.29	-0.32	-0.36	-0.41	-0.46
-5	-0.32	-0.34	-0.38	-0.42	-0.47	-0.49
0	-0.36	-0.39	-0.43	-0.46	-0.49	-0.52
5	-0.32	-0.34	-0.38	-0.42	-0.47	-0.49
10	-0.28	-0.29	-0.32	-0.36	-0.41	-0.46
15	-0.23	-0.26	-0.28	-0.31	-0.37	-0.39
20	-0.19	-0.21	-0.24	-0.27	-0.29	-0.34

*D_{bs} = Distance along ballast surface from center line (m)

Table 11. Maximum Vertical displacement of 3 m embankment under long term load settlement (slope ratio = 2:1)

D_{bs} (m)	Train speed (km/h)					
	0	24	48	72	96	120
	Vertical displacement (m)					
-20	-0.20	-0.23	-0.26	-0.27	-0.33	-0.39
-15	-0.23	-0.27	-0.30	-0.33	-0.37	-0.42
-10	-0.29	-0.31	-0.37	-0.44	-0.47	-0.50
-5	-0.34	-0.35	-0.40	-0.48	-0.51	-0.55
0	-0.38	-0.42	-0.46	-0.51	-0.56	-0.61
5	-0.34	-0.35	-0.40	-0.48	-0.51	-0.55
10	-0.29	-0.31	-0.37	-0.44	-0.47	-0.50
15	-0.23	-0.27	-0.30	-0.33	-0.37	-0.42
20	-0.20	-0.23	-0.26	-0.27	-0.33	-0.39

*D_{bs} = Distance along ballast surface from center line (m)

Table 12. Maximum Vertical displacement of 1 m embankment under short term load settlement (slope ratio = 2:1)

D_{bs} (m)	Train speed (km/h)					
	0	24	48	72	96	120
	Vertical displacement (m)					
-20	-0.15	-0.19	-0.20	-0.21	-0.23	-0.24
-15	-0.17	-0.20	-0.23	-0.25	-0.28	-0.30
-10	-0.21	-0.24	-0.27	-0.30	-0.32	-0.35
-5	-0.25	-0.28	-0.29	-0.32	-0.37	-0.40
0	-0.28	-0.31	-0.33	-0.36	-0.39	-0.42
5	-0.25	-0.28	-0.29	-0.32	-0.37	-0.40
10	-0.21	-0.24	-0.27	-0.30	-0.32	-0.35
15	-0.17	-0.20	-0.23	-0.25	-0.28	-0.30
20	-0.15	-0.19	-0.20	-0.21	-0.23	-0.24

*D_{bs} = Distance along ballast surface from center line (m)

Table 13. Maximum Vertical displacement of 2 m embankment under short term load settlement (slope ratio = 2:1)

D_{bs} (m)	Train speed (km/h)					
	0	24	48	72	96	120
	Vertical displacement (m)					
-20	-0.16	-0.19	-0.22	-0.24	-0.26	-0.28
-15	-0.19	-0.21	-0.26	-0.28	-0.29	-0.31
-10	-0.23	-0.25	-0.31	-0.34	-0.36	-0.37
-5	-0.27	-0.30	-0.33	-0.39	-0.40	-0.43
0	-0.32	-0.37	-0.41	-0.44	-0.48	-0.51
5	-0.27	-0.30	-0.33	-0.39	-0.40	-0.43
10	-0.23	-0.25	-0.31	-0.34	-0.36	-0.37
15	-0.19	-0.21	-0.26	-0.28	-0.29	-0.31
20	-0.16	-0.19	-0.22	-0.24	-0.26	-0.28

*D_{bs} = Distance along ballast surface from center line (m)

Table 14. Maximum Vertical displacement of 3 m embankment under short term load settlement (slope ratio = 2:1)

D_{bs} (m)	Train speed (km/h)					
	0	24	48	72	96	120
	Vertical displacement (m)					
-20	-0.21	-0.24	-0.27	-0.29	-0.31	-0.32
-15	-0.23	-0.26	-0.30	-0.32	-0.34	-0.37
-10	-0.27	-0.29	-0.33	-0.36	-0.39	-0.41
-5	-0.30	-0.32	-0.37	-0.40	-0.43	-0.49
0	-0.35	-0.39	-0.42	-0.48	-0.53	-0.57
5	-0.30	-0.32	-0.37	-0.40	-0.43	-0.49
10	-0.27	-0.29	-0.33	-0.36	-0.39	-0.41
15	-0.23	-0.26	-0.30	-0.32	-0.34	-0.37
20	-0.21	-0.24	-0.27	-0.29	-0.31	-0.32

*D_{bs} = Distance along ballast surface from center line (m)